
BIOLOGICAL NEURONS COMPETE WITH DEEP REINFORCEMENT LEARNING IN SAMPLE EFFICIENCY IN A SIMULATED GAMEWORLD

Moein Khajehnejad *
Turner Institute for Brain and Mental Health,
Monash University, Clayton, Australia

Forough Habibollahi *
Cortical Labs,
Melbourne, Australia

Aswin Paul
Turner Institute for Brain and Mental Health,
Monash University, Clayton, Australia
IITB-Monash Research Academy,
Mumbai, India

Adeel Razi
Turner Institute for Brain and Mental Health,
Monash University, Clayton, Australia
Wellcome Centre for Human Neuroimaging,
University College London, United Kingdom

Brett J. Kagan †
Cortical Labs,
Melbourne, Australia

ABSTRACT

How do biological systems and machine learning algorithms compare in the number of samples required to show significant improvements in completing a task? We compared the learning efficiency of *in vitro* biological neural networks to the state-of-the-art deep reinforcement learning (RL) algorithms in a simplified simulation of the game ‘Pong’. Using *DishBrain*, a system that embodies *in vitro* neural networks with *in silico* computation using a high-density multi-electrode array, we contrasted the learning rate and the performance of these biological systems against time-matched learning from three state of the art deep RL algorithms (i.e., DQN, A2C, and PPO) in the same game environment. This allowed a meaningful comparison between biological neural systems and deep RL. We find that when samples are limited to a real-world time course, even these very simple biological cultures outperformed deep RL algorithms across various game performance characteristics, implying a higher sample efficiency. Ultimately, even when tested across multiple types of information input to assess the impact of higher dimensional data input, biological neurons showcased faster learning than all deep reinforcement learning agents.

Keywords In Vitro · Neural Cultures · Deep Reinforcement Learning · Synthetic Biological Intelligence · Sample Efficiency · Electrophysiology · Biocomputing · Learning · Intelligence

1 Introduction

Both biological and machine intelligence systems demonstrate the ability to learn and achieve goals. Although the complexity of, and drivers behind, these tasks may differ, comparisons between these types of systems can yield valuable insights (Nefci and Averbeck). Even definitions of what traits artificial intelligence should demonstrate are heavily informed by traits observed in biological intelligence (Lake et al.; Hassabis et al.). Yet comparisons between biological and machine intelligence have been notoriously difficult, as the scale of connections in even simple biological organisms far exceeds that found in artificial neural networks or comparable Machine Learning (ML) algorithms (Richards et al.;

*Equal contribution.

†Corresponding author: brett@corticallabs.com

Hasson et al.). However, by taking a system-based approach, we aimed to compare data gathered from a biological neural network (BNN) using the recently validated *DishBrain* system (Kagan et al., 2022) against time-matched learning from deep reinforcement learning (RL) algorithms - DQN, A2C and PPO. Despite the inherent differences between silicon and biological systems - such as power consumption and network size - this approach makes it possible to explore learning performance and sample efficiency in these different systems. Should compelling differences be found, it would further support extended efforts to understand key differences in the information processing dynamics unique to each system.

RL has become increasingly popular in the fields of ML and artificial intelligence by offering a way of programming agents through reward and punishment cues without having to specify how the task is to be accomplished. However, to deliver on this promise, formidable computational obstacles must be overcome. RL implies learning the best policy to maximize an expected cumulative long-term reward throughout many steps in order to achieve objectives (goals) (Sutton and Barto, 2018). A deep RL approach integrates artificial neural networks with an RL framework that helps the system to achieve its goals (Hessel et al., 2017). It maps states and actions to the rewards they bring, combining function approximation and target optimization. Reinforcement algorithms that incorporate deep neural networks have been developed to beat human experts in multiple game settings including: poker (Moravčík et al., 2017), multiplayer contests (Jaderberg et al., 2018), complex board games, including go and chess (Silver et al., 2017a,b, 2018) and numerous Atari video games (Mnih et al., 2015). Nevertheless, RL still faces real challenges including but not limited to: complexities in the selection of hyper-parameters and reward structure, sample inefficiency (Tsividis et al., 2017; Marcus, 2018), reproducibility issues (Gibney et al., 2020), and catastrophic forgetfulness (Kirkpatrick et al.; Fan and Glynn). Furthermore, to allow RL algorithms to train quickly requires considerable levels of computing power (Mousavi et al., 2018) with notable associated environmental impacts (Freitag et al.). Finally, RL algorithms are typically trained for narrow tasks in static environments; where training and performance phases are separate (Neftci and Averbek; Fan and Glynn).

Holistically, these traits suggest that although deep RL algorithms are highly functional, their learning mechanisms almost certainly differ fundamentally from biological learning (Marcus, 2018; Neftci and Averbek; Whittington and Bogacz). It is noted that RL as a mechanism has been found to elicit rapid and adaptable learning in animals (Hamid et al.; Costa et al.). Yet it seems unlikely that similar underlying statistical mechanisms that support RL, such as back-propagation and gradient descent, have biological parallels in the brain (Whittington and Bogacz; Friston et al.). Ultimately, these mechanisms are likely too inefficient to be accepted as plausible models of human learning (Tsividis et al., 2017; Song et al., 2022; Whittington and Bogacz, 2017). This is especially true when considering how intelligence may arise from cells without established pathways of motivation. Early work investigating how cells respond to stimulation that can be modified through their own activity showed rapid adaptation displayed through synaptic plasticity (Tessadori et al.; Bakkum et al.; Müller et al., 2013). Furthermore, it was recently demonstrated that by using electrophysiological stimulation and recording in a real-time closed-loop system with a monolayer of living biological neurons, biological neural cells could be trained to significantly improve performance in a simulated 'pong' game-world (Kagan et al., 2022). The question arises as to whether the observed performance in these simple BNNs is notable compared to that of RL at the same task, especially regarding sample efficiency.

DishBrain is a novel system shown to display simple biological intelligence by harnessing inherent adaptive properties of neurons. In *DishBrain*, *in vitro* neuronal networks are integrated with *in silico* computing via high-density multi-electrode arrays (HD-MEAs). These cultured neuronal networks showcase biologically-based adaptive intelligence within a simulated gameplay environment in real-time through closed-loop stimulation and recordings (Kagan et al., 2022). Specifically, BNNs exhibited self-organised adaptive electrophysiological activity that was consistent with an innate ability to learn and showcase an intelligent response to limited - although biologically plausible (Harrell et al.) - structured external information. Data was generated from cortical cells obtained from either embryonic rodent or human induced pluripotent stem cell (hiPSC) sources. These cell types were compared to assess reproducibility of learning effects across species and preparations. Here, we investigate whether these elementary learning systems achieve performance levels that can compete with state-of-the-art deep RL algorithms. Additionally, by varying the input information density presented during training of the RL algorithms, we can determine the impact of information sparsity and ensure suitable comparisons to the biological system. This is the first comparison between a Synthetic Biological Intelligence (SBI) system (Kagan et al., 2023) and state-of-the-art RL algorithms. Figure 1.a,b illustrate the input information, feedback loop setup, and electrode configurations in the *DishBrain* system. This research aims to investigate whether simple biological systems can demonstrate characteristics compared to established RL methods to justify further research in this area, either where SBI systems are standalone learning devices, or inform further algorithm development in the ML space. We anticipate that SBI systems will exhibit greater sample efficiency than RL models, as suggested by prior research. However, this entails constraining training to a real-time approximate sample count for RL algorithms. Figure 1.c illustrates the comparison between input information in the *DishBrain*

system and deep RL algorithms.

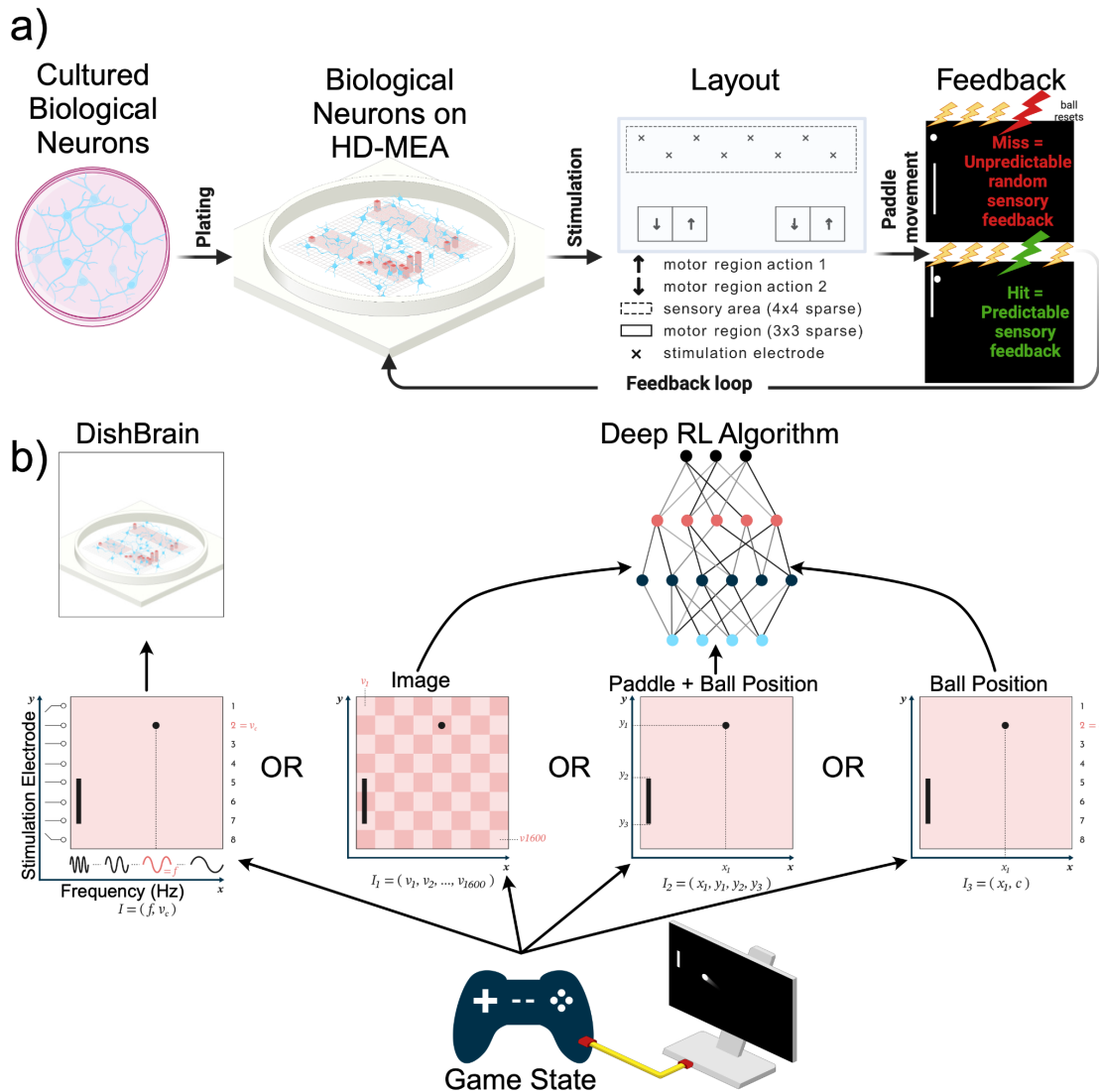


Figure 1: **DishBrain system and Various input designs to RL algorithms.** **a)** *DishBrain* feedback loop setup and Electrode configuration and predefined sensory and motor regions. Figures adapted and modified from (Kagan et al., 2022). **b)** Schematic comparing the information input routes in the *DishBrain* system (left) and the three implementations of the deep RL algorithms (right). In each design, the input information to the computing module (deep RL algorithms or *DishBrain*) is denoted by a vector I .

2 Results

Game performance of human cortical cells (HCCs; 174 sessions) and mouse cortical cells (MCCs; 110 sessions) was compared with three RL baseline methods. To determine how learning arises both in cultures and in baseline methods, three key gameplay characteristics were examined. These include: mean hit-to-miss ratio (average hits-per-rally), number of times the paddle failed to intercept the ball on the initial serve (aces), and number of long rallies or episodes (≥ 3 consecutive hits).

For comparison, every 70-episode run of each RL algorithm was mapped to approximately 20 real-time minutes by normalizing the actual total length of each run in minutes and then multiplying by 20. This approximates the number

of rallies biological cultures would experience in a 20-minute session. Details of the implemented RL algorithms and information about the selected hyper-parameters are included in Supplementary Materials A.4. Figures 2, 3, and 4 represent the main findings for comparisons between biological cultures and the IMAGE INPUT, PADDLE&BALL POSITION INPUT, and BALL POSITION INPUT designs of the RL methods. The intent behind different input designs was to determine whether varying the amount of information input into the algorithm altered sample efficiency and learning characteristics of these systems. In particular, the PADDLE&BALL POSITION INPUT, and BALL POSITION INPUT methods were intended to be more accurate comparisons to the information density presented to the *DishBrain* system. Extended Data Tables S3 and S4 present all multivariate statistical tests performed in relation to the following results. All *post-hoc* follow-up tests are presented in Extended Data Table S2.

2.1 Comparison in performance between *DishBrain* and three RL algorithms with various information densities

In all three designs, biological cultures (i.e. HCC and MCC) outperform all RL baseline algorithms (see Subfigures 2.b, 3.b, and 4.b) in terms of the highest level of average hits-per-rally achieved. The cultures demonstrate faster learning rates over time. Subfigures 2.c, 3.c, and 4.c compare the % of aces among the biological cultures and the RL groups given the three different designs. HCC and MCC achieve the lowest percentage of aces compared to the deep RL algorithms in Subfigure 2.c and the other RL baseline designs in Subfigures 3.c, and 4.c. The increasing trend in % of long rallies is observed in all groups and among all designs except the DQN and PPO groups in the IMAGE INPUT design and PPO in the PADDLE&BALL POSITION INPUT design, as illustrated in Subfigures 2.d, 3.d, and 4.d. Average % of long rallies was highest for MCC and HCC compared to RL baselines.

Key activity metrics in the first 5 minutes versus the last 15 minutes in each session were compared to identify any significant improvement occurring in the learning process within each group.

Panel (e) in Figures 2, 3, and 4 compares average rally length between the two defined time intervals within groups. The results imply that the within-group increasing trend in rally length is significant only in the biological groups.

Panel (f) in Figures 2, 3, and 4 represents the change in average percentage of aces over time. A significant decrease in number of aces (where the ball was missed immediately in an episode with no accurate hits) implies an improved game performance. Only MCC and HCC had a significant decrease in average ace percentage as opposed to the rest of RL based algorithms with different input designs.

Panel (g) in Figures 2, 3, and 4, shows that the percentage of long rallies in the first 5 minutes versus the last 15 minutes only significantly increased for biological cultures and A2C with the IMAGE INPUT and BALL POSITION INPUT designs.

Inter-group comparison was carried out for both time intervals (0-5 and 6-20 minutes) and all three metrics using Tukey's post-hoc test as represented in panels (h), (i), and (j) in Figures 2, 3, and 4 for rally length (i.e. hit counts), % of aces, and % of long rallies respectively.

Note, in the IMAGE INPUT design, where average rally length of deep RL methods comes closest to the biological cultures, the input information density is starkly different between the two groups. While RL agents received pixel data with a density of 40×40 pixels, biological cultures only receive input from 8 stimulation points with a given integer rate code of 4Hz–40Hz, highlighting important efficiency differences in informational input between these learning systems. The possibility of higher input information dimensionality having adverse effects on overall sample efficiency of RL algorithms is further nullified by evaluating two alternative input structures (PADDLE&BALL POSITION INPUT and BALL POSITION INPUT designs).

2.2 Examining impact of paddle movement speed on learning rates

To account for potential effects of paddle movement speed and whether it plays an important role in determining the success rate of paddle control, we derived the average paddle movement (in pixels) for all groups. Subfigures 5.a,c, and e represent these results for the IMAGE INPUT, PADDLE&BALL POSITION INPUT, and BALL POSITION INPUT designs, respectively. Using Tukey's post-hoc tests, a consistently significant difference between pairs of DQN, PPO or A2C with MCC or HCC was found in terms of average paddle movement, with RL algorithms having the higher average. This occurs when all the RL algorithms with different input designs have significantly higher average paddle movement compared to both groups of biological cultures. As per previous findings (Kagan et al., 2022), increased paddle movement speed in RL algorithms does not translate to improved game performance, likely suggesting a more stochastic paddle control.

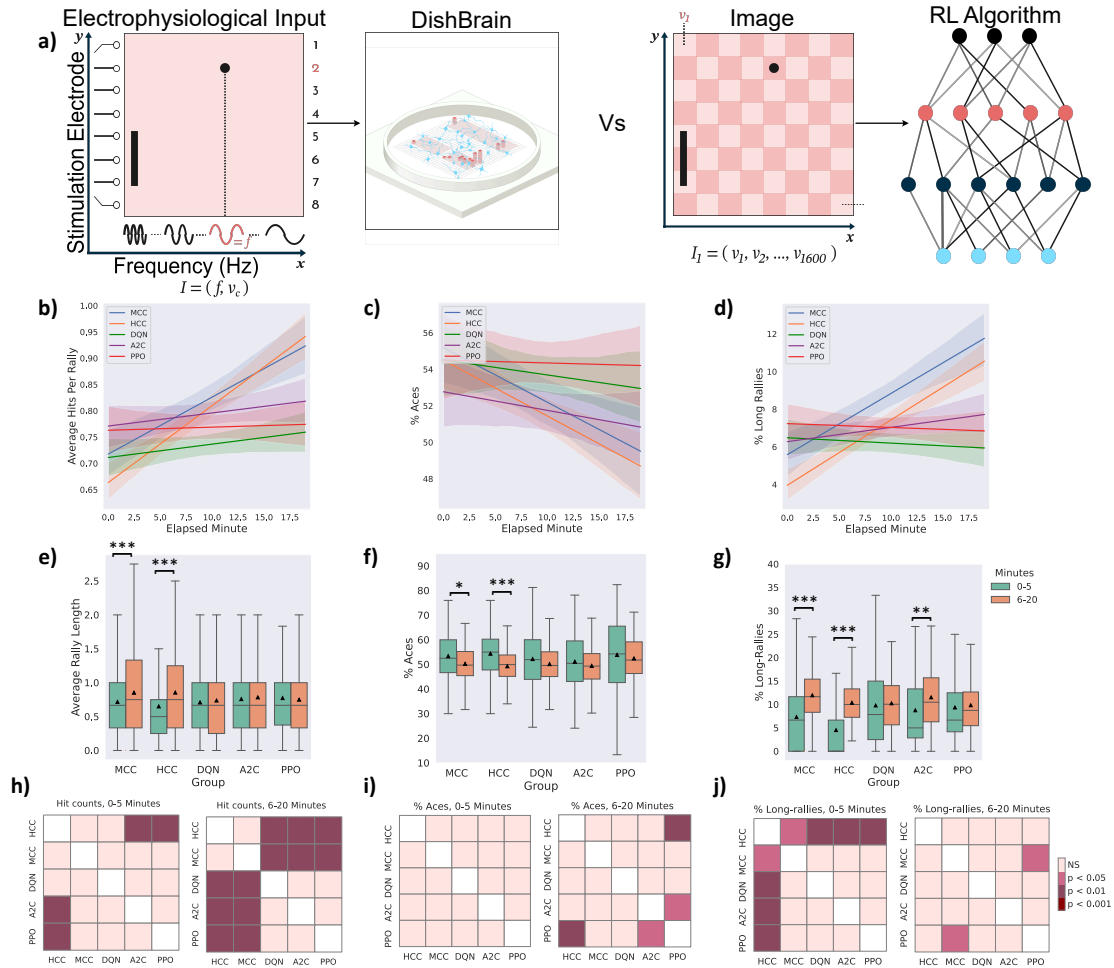


Figure 2: IMAGE INPUT to the deep RL algorithms. a) Schematic highlighting figure comparisons are between biological DishBrain system and an pixel-based information input to the RL algorithms. Average number of b) hits-per-rally, c) % of aces, and d) % of long rallies over 20 minutes real-time equivalent of training DQN, A2C, PPO, and MCC, HCC cultures. A regressor line on the mean values with a 95% confidence interval highlights the learning trends. Comparing the performance amongst all groups, the highest level of average hits-per-rally is achieved by the neuronal MCC and HCC cultures while PPO is outperformed by all the opponents. The average % of aces is lowest for the neuronal cultures compared to all deep RL baseline methods. The average % of long rallies reaches its highest levels for MCC and HCC. e) Average performance of groups over time. Only biological cultures have significant within-group improvement and increase in their performance at the second time interval (One-way ANOVA test, $p = 5.854e-6$, $p = 7.936e-17$, for MCC and HCC respectively; $p = 0.231$, $p = 0.318$, and $p = 0.400$ for DQN, A2C, and PPO respectively). f) Average % of aces within groups and over time. Only MCC and HCC (One-way ANOVA test, $p = 0.014$, $p = 2.907e-08$, respectively) differed significantly over time. No significant change was detected within the DQN, A2C, or PPO groups (One-way ANOVA test, $p = 0.080$, $p = 0.195$, and $p = 0.308$, respectively). g) Average % of long-rallies (≥ 3) performed in a session. All groups showed an increase in the average number of long rallies where this within-group increase was significant only for MCC, HCC, and A2C (One-way ANOVA test, $p = 1.172e-7$, $p = 1.525e-24$ for MCC and HCC, respectively and $p = 0.605$, $p = 0.002$, and $p = 0.684$ for DQN, A2C, and PPO, respectively). * $p < 0.05$, ** $p < 0.01$, and *** $p < 0.001$. h) Pairwise Tukey's post-hoc test shows that HCC and MCC groups significantly outperform PPO, A2C, and DQN in the last 15 minutes interval. i) Using pairwise Tukey's post-hoc test, the HCC group significantly outperforms the PPO in the last 15 minutes interval with a lower average of % Aces. A2C also outperforms PPO in this time interval. j) Pairwise comparison using Tukey's test only shows a significant difference in the percentage of long rallies between HCC and the rest of the groups in the first 5 minutes. However, this is later altered in the direction of all groups having an increased % of long rallies with MCC outperforming PPO in the last 15 minutes of the game. Box plots show interquartile range, with bars demonstrating 1.5X interquartile range, the line marks the median and the black triangle marks the mean. Error bands = 1 SE

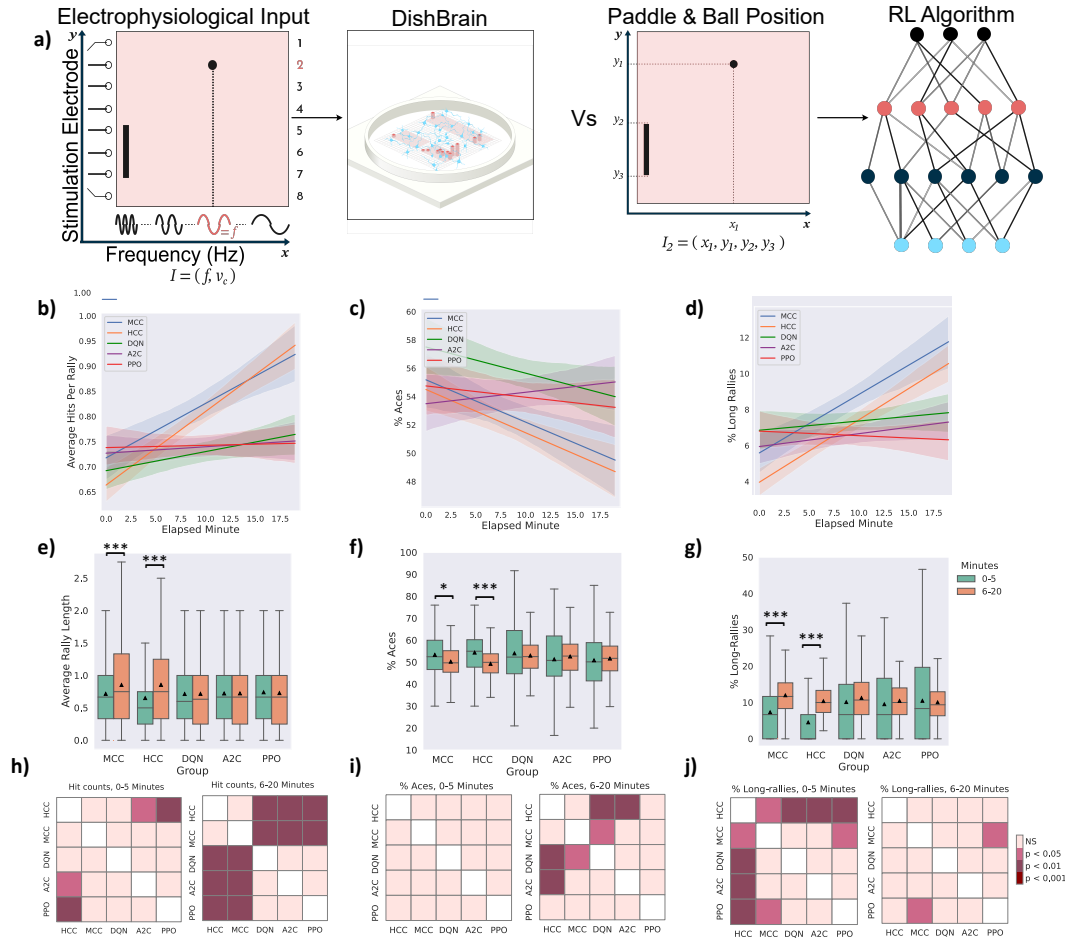


Figure 3: PADDLE&BALL POSITION INPUT to the deep RL algorithms. a) Schematic highlighting figure comparisons are between biological DishBrain system and PADDLE&BALL POSITION INPUT to RL algorithms. Average number of b) hits-per-rally, c) % of aces, and d) % of long rallies over 20 minutes real-time equivalent of training DQN, A2C, PPO, and MCC, HCC cultures. A regressor line on the mean values with a 95% confidence interval highlights the learning trends. The highest level of average hits-per-rally is achieved by the MCC and HCC cultures. The average % of aces is lowest for the neuronal cultures compared to all deep RL baseline methods. The average % of long rallies reaches its highest levels for MCC and HCC. e) Average rally length over time only showed a significant increase in the biological cultures between the two time intervals (One-way ANOVA test, $p = 0.913$, $p = 0.958$, and $p = 0.610$ for DQN, A2C, and PPO respectively). f) Average % of aces within groups and over time only showed a significant difference in the MCC and HCC groups. No significant change was detected within the DQN, A2C, or PPO groups (One-way ANOVA test, $p = 0.463$, $p = 0.338$, and $p = 0.544$ respectively). g) Average % of long-rallies (≥ 3) performed in a session increased in the second time interval in all groups. This within-group difference was only significant for the MCC and HCC groups (One-way ANOVA test, $p = 1.172e-7$, $p = 1.525e-24$, $p = 0.233$, $p = 0.320$, and $p = 0.650$ for MCC, HCC, DQN, A2C, and PPO, respectively). * $p < 0.05$, ** $p < 0.01$, and *** $p < 0.001$. h) Pairwise Tukey's post-hoc test shows that the HCC group is significantly outperformed by A2C and PPO in the first 5 minutes in terms of the hit counts. Biological cultures, however, do significantly better compared to all deep RL opponents in the 15 minutes interval. i) Using pairwise Tukey's post-hoc test, HCC group significantly outperforms the DQN and A2C groups in the last 15 minutes interval with a lower average of % Aces. DQN is also outperformed by the MCC group in this time interval. j) Pairwise comparison using Tukey's test shows a significant difference in the percentage of long rallies between HCC and the rest of the groups in the first 5 minutes all outperforming the HCC. However, this is later altered in the last 15 minutes with only MCC outperforming PPO significantly having an increased % of long rallies. Box plots show interquartile range, with bars demonstrating 1.5X interquartile range, the line marks the median, and the black triangle marks the mean. Error bands = 1 SE

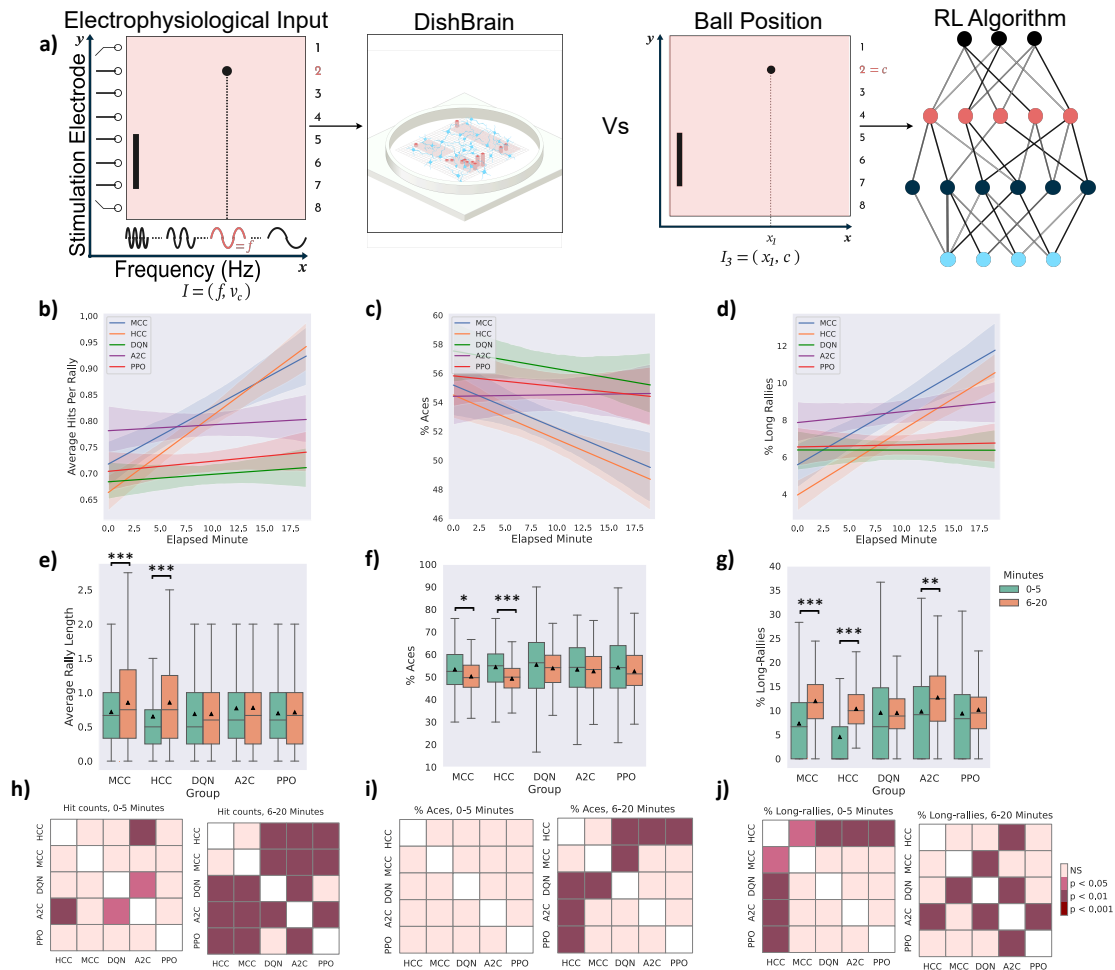


Figure 4: BALL POSITION INPUT to the deep RL algorithms. a) Schematic highlighting figure comparisons are between biological DishBrain system and BALL POSITION INPUT to RL algorithms. Average number of b) hits-per-rally, c) % of aces, and d) % of long rallies over 20 minutes real-time equivalent of training DQN, A2C, PPO, and MCC, HCC cultures. A regressor line on the mean values with a 95% confidence interval highlights the learning trends. The highest level of average hits-per-rally is achieved by the neuronal MCC and HCC cultures. The average % of aces is lowest for the neuronal cultures compared to all deep RL baseline methods. The average % of long rallies reaches its highest levels for MCC and HCC. Comparing to the same findings for the HCC and MCC groups, e) average rally length over time only showed a significant increase in the biological cultures between the two time intervals (One-way ANOVA test, $p = 0.995$, $p = 0.812$, and $p = 0.547$ for DQN, A2C, and PPO respectively). f) Average % of aces within groups and over time only showed a significant difference in the MCC and HCC groups. No significant change was detected within the DQN, A2C, or PPO groups (One-way ANOVA test, $p = 0.241$, $p = 0.581$, and $p = 0.216$ respectively). g) Average % of long-rallies (≥ 3) performed in a session increased in the second time interval in all groups except DQN. This within-group difference was only significant for MCC, HCC, and A2C groups with $p = 0.002$ for the A2C group. $*p < 0.05$, $**p < 0.01$, and $***p < 0.001$. h) Pairwise Tukey's post-hoc test shows that biological cultures significantly outperform all deep RL groups in the last 15 minutes in terms of the hit counts or rally length. i) Using pairwise Tukey's post-hoc test, the HCC group significantly outperforms all the deep RL groups in the last 15 minutes interval while MCC also outperforms DQN with a lower average of % Aces. j) Pairwise comparison using Tukey's test shows a significant out-performance of all groups over HCC in the percentage of long rallies in the first 5 minutes. In the second time interval, MCC shows a significantly higher % of long rallies compared to DQN with HCC now being outperformed only by A2C. Box plots show interquartile range, with bars demonstrating 1.5X interquartile range, the line marks the median and the black triangle marks the mean. Error bands = 1 SE

Subfigures 5.b, d, and f compare relative improvement in performance between biological cultures and RL algorithms for IMAGE INPUT, PADDLE&BALL POSITION INPUT, and BALL POSITION INPUT, respectively. This measure identifies the relative increase in average accurate hit counts in the second 15 minutes of the game compared to the first 5 minutes. The HCC group shows the highest improvement in time. Post-hoc tests showed significant differences between HCC and all the RL methods across all of the three different input designs. The MCC group also outperforms PPO in both IMAGE INPUT and PADDLE&BALL POSITION INPUT designs as well as DQN and A2C in the IMAGE INPUT and PADDLE&BALL POSITION INPUT designs, respectively.

Subfigures 5.g, h, i, and j compare frequency tables for distributions of mean summed hits per minute amongst groups for the IMAGE INPUT, PADDLE&BALL POSITION INPUT, and BALL POSITION INPUT designs respectively. These tables were not significantly different (Two-sample *t*-test).

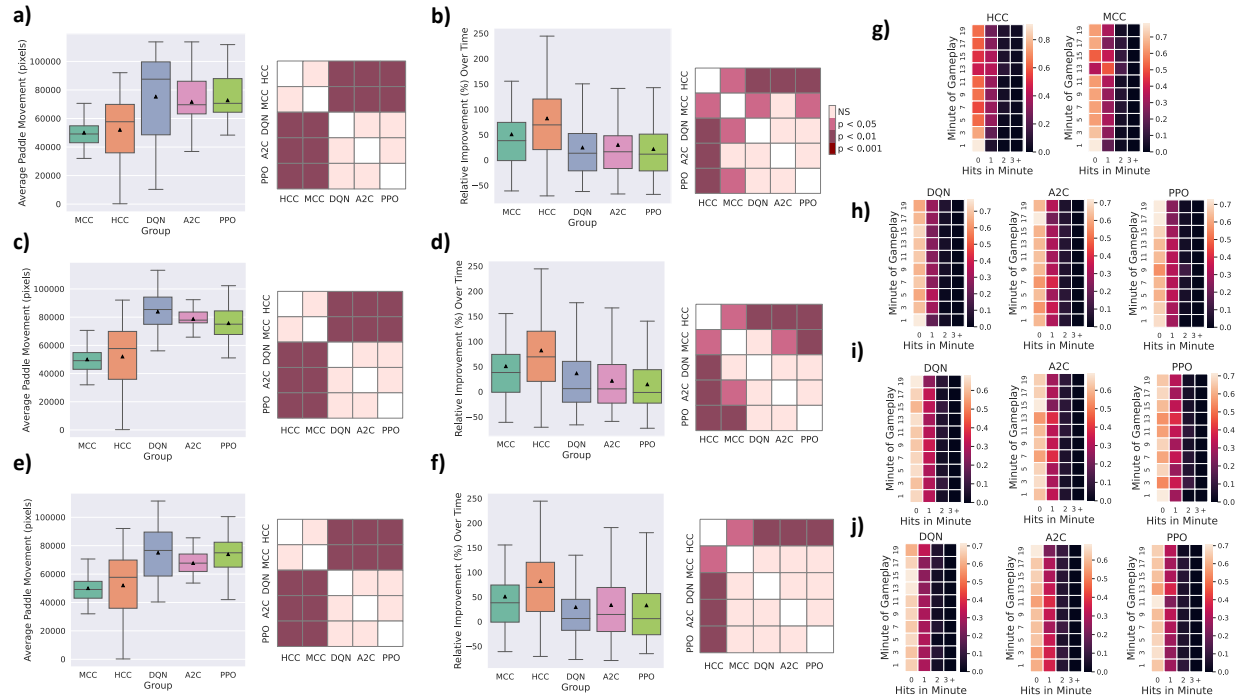


Figure 5: Paddle movement and relative improvement. The average paddle movement in pixels in all the different groups for the **a)** IMAGE INPUT, **c)** PADDLE&BALL POSITION INPUT, and **e)** BALL POSITION INPUT to the deep RL algorithms. Tukey’s post-hoc test was conducted showing that DQN, PPO, and A2C had a significantly higher average paddle movement compared to HCC and MCC in all scenarios. Relative improvement (%) in the average hit counts between the first 5 minutes and the last 15 minutes of all sessions in each separate group for the **b)** IMAGE INPUT, **d)** PADDLE&BALL POSITION INPUT, and **f)** BALL POSITION INPUT to the deep RL algorithms. The biological groups show higher improvements with HCC outperforming all. **b)** Using Games Howell post-hoc test, the inter-group differences were significant with HCC outperforming all other groups, as well as MCC significantly outperforming PPO. **d)** HCC showed a significantly higher relative improvement over time compared to all the other groups while MCC also outperformed A2C and PPO in terms of relative improvement over time. **f)** Finally, HCC could still perform significantly better than all the deep RL groups with the BALL POSITION INPUT design to the deep RL algorithms with MCC outperforming PPO and DQN in this design. Distribution of frequency of mean summed hits per minute amongst groups for **g)** biological cultures and deep RL algorithms with **h)** IMAGE INPUT, **i)** PADDLE&BALL POSITION INPUT, and **j)** BALL POSITION INPUT.

Details of the implemented RL algorithms and hyper-parameters can be found in the data repository provided in Section 4.4. In summary, a comprehensive grid search was conducted within the parameter space of *learning rate*, *replay buffer size*, and the training *batch size* aiming to identify the optimal parameter configuration and it was found that similar results were obtained across a variety of hyper-parameters, strongly supporting the initial conclusions of this work. Here, we include the example of how increasing the *batch size* affects the overall performance of the RL algorithms, while keeping the rest of the parameters set to their initial values in the search space (For further details and exploration of selected hyper-parameters, see Supplementary Materials A.5, A.4 and Extended Data Figures S2, S3, S4, S5, S6,

and S7). In general, we observed some quantitative changes in outcome metrics when varying the batch size for these algorithms, but these adjustments did not alter the ultimate conclusions of our work. Focusing on the quality of learning in each group and the comparison of sample efficiency, both of these were unaffected or in some cases worsened by increasing the batch size. Specifically, when examining the changes in average accurate hit counts during the first 5 minutes versus the last 15 minutes of training and the overall relative improvement, the increased batch size did not appear to significantly impact the resulting sample efficiency in any of the algorithms as seen in Figure 6.a-c. Finally, Figure 6.d illustrates the mean total reward of the RL algorithms with the IMAGE INPUT using the same hyper-parameter sets as in Figure 2 for an extended training period of 11000 game episodes. These results reveal that all three algorithms successfully learned and showed improved performance across an extended number of training episodes. Training the implemented deep RL algorithms for 11,000 game episodes using the same set of hyper-parameters as in Section 2.1 illustrates an increasing trend in their performance and high levels of total reward, measured as episode duration in terms of the number of frames to complete the episode. However, as anticipated, 70 game episodes—the same number used to train the biological cultures—were not sufficient for any of the algorithms.

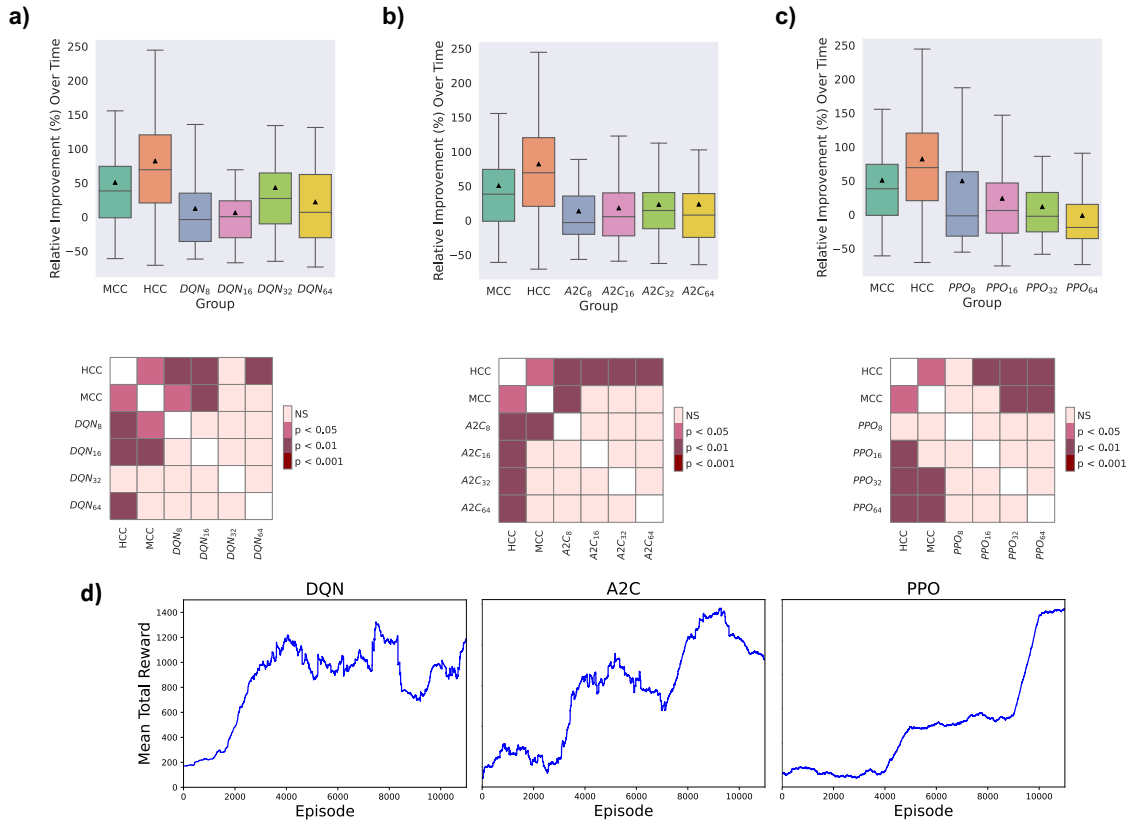


Figure 6: Batch size effect and extended training epochs for the RL algorithms with IMAGE INPUT. Relative improvement (%) in the average hit counts between the first 5 minutes and the last 15 minutes of all sessions as well as the post-hoc tests in each separate group for batch sizes of 8, 16, 32, and 64 in the **a)** DQN, **b)** A2C, and **c)** PPO groups compared to biological cultures. Games Howell post-hoc tests show the inter-group differences which were not significant between any pair of different batch sizes for any of the DQN, A2C, or PPO groups. **d)** Extended training episodes for the deep RL algorithms. The plots show a moving average of the total episode reward with a window size of 100.

3 Discussion

The advantages and disadvantages of biological versus machine intelligence are often discussed, yet technical limitations have prevented meaningful comparisons in terms of performance. In this work, we compare performance of biological neuronal networks with that of state-of-the-art deep reinforcement algorithms (deep RL). Using a controllable game environment of a simplified *pong* simulation, it was possible to compare key traits between these different learning systems, with a focus on sample efficiency. Human or mouse cortical cells (HCC or MCC) along with three deep RL

algorithms (DQN, A2C, and PPO), were compared in sessions with an average episode number of 70 games played. While direct comparisons between these systems are naturally constrained (even what is referred to as a "neuron" is inconsistent between fields of research), the aim of this work was to determine whether meaningful performance differences would arise between learning systems (as contained systems) that may merit further exploration of BNNs as information processing machines. This approach allowed an examination of the overall performance of each group with respect to various gameplay characteristics and, for the RL methods, in response to varying information input.

Across all types of information input, BNN outperformed all RL baselines in terms of average hit-per-rally (Subfigure 2.a), % of aces (Subfigure 2.b), and % of long rallies achieved (Subfigure 2.c). Moreover, the increase in average rally length, decrease in number of aces, and increase in number of long rallies were significant only within the HCC and MCC groups and the A2C algorithm with the IMAGE INPUT and BALL POSITION INPUT designs in terms of the increase in the percentage of long rallies, when comparing the first 5 and the last 15 minutes during gameplay (see Subfigures 2.d, e, and f). Additionally, we found that the HCC group had the highest relative improvement in average number of hits between the first 5 minutes and last 15 minutes of the game as depicted in Subfigures 5.b, d, and f.

Results show that the game performance of deep RL algorithms in terms of relative learning improvement in time and average hits-per-rally is outperformed by biological cultures when number of allowable samples are fixed. This supports the conclusion that RL algorithms showed significantly lower sample efficiency compared to BNN, having lower improvements in learning over an episode-matched training duration provided for all groups. This matches theoretical expectations previously outlined where it was proposed that biological learning is inherently more sample efficient (Neftci and Averbeck; Whittington and Bogacz). Given how rapidly synaptic plasticity or behaviour changes have occurred for both *in vitro* and *in vivo* models, this finding is consistent with such observations (Tessadori et al.; Bakkum et al.; Hamid et al.; Costa et al.; Habibollahi et al., 2023). Furthermore, although difficult to directly compare energy consumption, it should be noted that biological systems use magnitudes less than traditional computing systems used for ML (Jouppi et al.).

Moreover, the comparison between the various machine learning algorithms is also consistent with past research. A2C and PPO often achieve better results compared to DQN which is in line with previous studies proposing that algorithms optimizing a stochastic policy generally perform better than DQN (Siddique et al., 2020; El Mazgualdi et al., 2022) which is known to suffer more from low sample efficiency (Lee et al., 2019). This can best be seen in the relative performance between different levels of information input. When a CNN was integrated into the RL models, some degree of learning (that did not reach statistical significance) was observed for these systems. BNN received only a fraction of the input information density compared to their RL opponents in this condition (8-pixel combination of rate coded and place coded stimulation compared to 40×40 pixels of the input image). Moreover, it was reasonable to consider whether the curse of dimensionality (where higher dimension input can require additional episodes to converge to a minima) may be adversely impacting the RL agents under the IMAGE INPUT condition. To account for potential disadvantages occurring as a result of increased input dimensionality, we also examined two alternative designs for input structure to the RL algorithms (i.e. PADDLE&BALL POSITION INPUT and BALL POSITION INPUT designs). In-depth comparison between BNN performance and these alternative RL algorithms did not provide any significantly different outcome in favour of the RL baselines' sample efficiency (see Figures 3 and 4).

That BNN could perform with such sparsely coded informational input conforms to coding mechanisms known to be used in biological intelligence (Harrell et al.; Buchanan, 2018; Bastos et al.). While RL algorithms use back-propagation, it has been argued that this method is likely too inefficient to function within biological systems (Whittington and Bogacz; Friston et al.; Tsivdis et al., 2017; Song et al., 2022; Whittington and Bogacz, 2017; Hinton, 2022). A more dynamic reconfiguration of network activity has been proposed to be necessary for the learning rates observed in biological cultures (Song et al., 2022; Felleman and Van Essen, 1991; Tsivdis et al., 2017; Whittington and Bogacz, 2017). Theories of how this learning may occur include predictive coding, active inference, prospective configurations, and Hopfield networks, which have been used to describe how neural systems may reorganise activity for learning tasks (Hopfield, 1982; Song et al., 2022; Rao and Ballard, 1999; Friston, 2005; de Wit et al., 2010). While nuances amongst these different theories exist, the general notion supports the idea of a more biological consistent forward-based learning process compared to backpropagation.

To explore this, we explored a biologically inspired algorithm, implementing an active inference agent that uses counterfactual learning and reported the comparison results in Supplementary Materials A.6 and Extended Data Figure S8. Improved learning rates observed in the biological inspired learning protocol supports the potential of active inference agents to provide valuable insights into optimized learning strategies, thereby enhancing our understanding of these dynamics. However, these active inference algorithms are still highly dependent on the chosen hyper-parameters and require relatively higher power consumption compared to biological systems. Nonetheless, these results highlight the value of further exploring biologically-inspired systems of learning and support the notion that SBI systems may offer a useful pathway to do this in the future.

Interplay between individual neuronal activity and population level activity adds further complexity to determining the mechanisms of learning within biological cultures. While limitations in study design (specifically the use of opaque chips) prevent a robust assessment of the specific learning processes within the cultures used in this study beyond that previously reported (Kagan et al., 2022; Habibollahi et al., 2023), findings endorse this approach for future exploration of these dynamics with altered study designs. Future work has potential to not only understand how biological intelligence arises, but also how one may implement more advanced biologically inspired learning protocols that may surpass current performance.

This work acts as the first direct comparison (to our knowledge) between an SBI system and state-of-the-art RL algorithms on a comparable task. A potential limitation of the work results from the fact that the space of hyper-parameters is too large for an exhaustive search in each algorithm. However to explore a significant number of hyper-parameters we used values utilized in the original paper that introduced each algorithm. We tuned the hyper-parameters that were most sensitive by a grid search in a limited space of those parameters. As a result of their sensitivity to hyper-parameter selection, state-of-the-art deep RL algorithms remain challenging to apply. The use of model-based RL is proposed for achieving higher sample efficiencies. Model-free algorithms, however, often perform significantly better asymptotically than these algorithms (Chua et al., 2018). Recently, different accelerated approaches have also been proposed for deep RL (Lee et al., 2019; Chua et al., 2018; Franke et al., 2020). Nonetheless, many still lag behind the performance of the original algorithms or require modern computers and a combination of CPUs and GPUs prompting even higher computational costs (Stooke and Abbeel, 2018). As a future pathway, these modified algorithms may be utilized for further comparisons. Arguably, biological cultures operating with the *DishBrain* system do not require such fine-tuning of parameters or manipulation of the architecture. Nonetheless, the results of this work supports that even rudimentary SBI systems with limited informational input are viable learning systems that can compete and even outperform established RL algorithms on sample efficiency. Coupled with the promise of significant gains in power efficiencies, flexibility of tasks, and upcoming improvements in the associated technologies (Smirnova et al., 2023), these biological-based intelligence systems present a compelling pathway for realizing real-time learning unachievable by current silicon-based approaches alone.

4 Methods

4.1 *DishBrain* System

The initial validation of the *DishBrain* system was previously presented in (Kagan et al., 2022). Briefly, cortical cells were either differentiated from human induced pluripotent stem cells (hiPSC) using a modified Dual SMAD inhibition protocol or surgically extracted from E15 mouse embryos. By setting up cultures from multiple cell sources this helped ensure that results would generalize across different species and preparations. Ethical approvals for animal work were obtained (E/1876/2019/M: Alfred Research Alliance Animal Ethics Committee B) for animal work with all cell culture work according to relevant ethical guidelines. Cell line characterisation and approvals are reported in (Kagan et al., 2022).

Approximately 10^6 cells were plated and integrated onto a high-density multi-electrode array (HD-MEA; Maxwell Biosystems, AG, Switzerland). Cell cultures were maintained in BrainPhys™ Neuronal Medium (Stemcell Technologies Australia, Melbourne, Australia) supplemented with 1% penicillin-streptomycin during testing. The *DishBrain* system was developed as a low latency, real-time system which interacts with the HD-MEA software to allow closed-loop stimulation and recording which has previously been described in detail (Kagan et al., 2022). Using this method, activity from a neuronal culture can be read, along with providing structured stimulation to the same culture in real-time. *DishBrain* was then utilized to embody neural cultures in a virtual game-world, to simulate the classic arcade game ‘Pong’. Biphasic electrical stimulation was used to stimulate neurons consistent with previous attempts to elicit action potentials in comparable cultures (Ruaro et al., 2005). Electrical stimulation was arranged to transmit a variety of task-related information between the cells and the simulated virtual environment using appropriate coding schemes via routed electrodes on the MEA that were divided into discrete regions as in Figure 1.b.

Specifically, stimulation was applied using a combination of rate coding (4Hz - 40Hz) electrical pulses to communicate the position on the x -axis and place coding (on a given electrode that was arranged topographically from an egocentric representation for the culture) to communicate information on the y -axis into a predefined bounded two-dimensional sensory area consisting of 8 sensory electrodes to deliver this input information. Three types of input were provided: the sensory stimulation as explained above, or stimulation in response to activity designated as either ‘Predictable’ or ‘Unpredictable’ feedback (see Figure 1.a). Cultures received Unpredictable stimulation when they missed connecting the paddle with the ‘ball’, i.e. when a ‘miss’ occurred. Using a feedback stimulus at a voltage of 150 mV and a frequency of 5 Hz, an unpredictable external stimulus could be added to the system. Random stimulation took place at random sites over the 8 predefined sensory electrodes at random timescales for a period of four seconds, followed by a

configurable rest period of four seconds where stimulation paused, then the next rally began. Should no miss occur, the game would continue until either a miss occurred or the timer of 20 minutes expired, which would end the session. In contrast, cultures were exposed to Predictable stimulation when a ‘hit’ was registered - that is, when the ‘paddle’ connected successfully with the ‘ball’. This was delivered across all 8 stimulation electrodes simultaneously at 75mV at 100Hz over 100ms and replaced other sensory information for 100 ms.

The movement of the paddle was controlled by the level of electrophysiological activity measured in a predefined ‘motor area’ of the cultured network as shown in Figure 1.b. , which was collected in real-time. Incoming samples were filtered with a 2nd order high-pass Bessel filter with 100Hz cut-off. The absolute value was smoothed using a 1st order low-pass Bessel filter with a 1 Hz cut-off and the spike threshold is proportional to this smoothed absolute value. A relative activity spike of 6 sigma greater than background noise was then used to define an action potential. Detected action potentials from counterbalanced motor regions were then summed together, where higher activity in a given pair of regions would cause the virtual paddle to move in one direction, while activity in the other regions would result in the inverse movement. Information about ball position relative to the paddle was adjusted in a closed-loop manner with a spike-to-stim latency of approximately 5ms. Figure 1.a,b illustrate the input information, feedback loop setup, and electrode configurations in the *DishBrain* system.

The gameplay performance of cell cultures subjected to the simplified pong environment via the *DishBrain* system was assessed. In each episode of the game, the average number of rallies before the ball was missed for the first time was then compared with different deep RL baseline methods. Each recording session of the cultures during gameplay was 20 minutes. During a gameplay session, the average number of rallies (i.e., episodes) an average biological culture would perform was 69.04 ± 7.95 rallies/episodes. Therefore, to compare sample efficiency in a matched comparison, a total of 70 training episodes were provided to deep reinforcement learning algorithms during training.

More details of this system are introduced in Supplementary Materials A.1, A.2, and A.3 as well as Extended Data Figure S1.

4.2 Deep Reinforcement Learning Algorithms

In this work, we use three state-of-the-art deep reinforcement learning algorithms: Deep Q Network (DQN) (Mnih et al., 2015), Advantage Actor-Critic (A2C) (Arulkumaran et al., 2017) and Proximal Policy Optimization (PPO) (Schulman et al., 2017), established to have good performance in Atari games. Benefiting from deep learning advantages in automated feature extraction, specifically exploiting Convolutional Neural Networks (CNN) in their structures, these methods are robust tools in reinforcement tasks, particularly in games where the system’s input is an image. In this work, aiming to account for potential detriments to sample efficiency resulting from the increased dimensionality of the image input to the deep RL algorithms (Bellman and Kalaba, 1957), we designed two additional types of input information to the RL algorithms. We compare all three different designs with the performance of biological cultures. We attempt to study whether the curse of dimensionality and increased size of the feature vectors when directly utilizing image inputs affect the comparison between biological cultures and RL algorithms in terms of their sample efficiency. All the algorithms follow a common strategy although they are different in structure. The three different input categories and RL algorithm designs are introduced below:

- **IMAGE INPUT:** The current state is a tensor of the difference of pixel values from the two most recent frames (i.e. another 40×40 grayscale pixel image)³. This current state is then input into the CNN to obtain the selected action. Next, based on the action taken, a reward is received, and a new state is formed. The ultimate goal is to find a policy that indicates the best action in each state to maximize the reward function.
- **PADDLE&BALL POSITION INPUT:** Instead of the grayscale image, a 4-dimensional vector encoding the x and y coordinates of the ball (distance to the paddle/wall and distance to the floor in pixels) and the y coordinates of the paddle’s top and the bottom was obtained. All values are integers between $[4, 40]$. The current state which is the input to each algorithm is then a tensor of the difference of values from the two most recent 4-dimensional location vectors. No additional CNN layer is utilized in this case.
- **BALL POSITION INPUT:** A design as similar to the *DishBrain* system’s input structure as possible was also examined. For this case, the y -axis of the gameplay environment was divided into 8 equal segments each mimicking one of the sensory electrodes in the biological cultures, and place coding the information about the ball’s y -axis position as an integer in the $[1, 8]$ interval. Then, the ball’s x -axis position is used as the second element of this input vector being an integer value in $[4, 40]$ similar to the rate coded component of the stimulation applied to the biological cultures. No additional CNN layer is utilized in this design.

³We also experimented with an alternative design where the input consisted of a stack of the four most recent frames for all algorithms. However, this modification led to a noticeable decline in the performance of all the methods because it failed to capture the sense of motion between frames.

The overview of the implemented DQN, A2C, and PPO algorithms are represented in Supplementary Materials A.4 (see Algorithms 1, 2, and 3).

All the deep RL implementations run on a 2.3 GHz Quad-Core Intel Core i5. PyTorch 1.8.1 was used to build neural network blocks and Open AI Gym environment to define our game environment represented by a 40×40 pixel grayscale image. In the training phase of all RL algorithms, every algorithm was run for 150 random seeds and a total number of 70 episodes for each seed. These seeds imply 150 different neural networks trained separately, resembling 150 different recorded cultures. In this work, we report the average value of each metric among all seeds.

4.3 Data Availability

All data generated for or used within this manuscript have been deposited at Open Science Framework (OSF) and are publicly available here: https://osf.io/cnpzf/?view_only=a33b7083f78e4c55a20b6c021a695a4a.

4.4 Code Availability

All code for deep reinforcement learning models or used for data analysis to generate the results in this manuscript have been deposited at Open Science Framework (OSF) and are publicly available via https://osf.io/cnpzf/?view_only=a33b7083f78e4c55a20b6c021a695a4a.

4.5 Supplementary information

Supplementary Materials; Extended Data; Tables S1 - S3

4.6 Acknowledgments

The authors thank and acknowledge Dr Haytham Fayek, Dr Hon Weng Chong and Mr Amitesh Gaurav for their input and advice on the manuscript and experimental design.

4.7 Competing interests

B.J.K., F.H., and M.K. were contracted or employed by Cortical Labs during the course of this research. B.J.K. has shares in Cortical Labs and an interest in patents related to this work. There are no other competing interests to declare.

4.8 Author contributions

B.J.K., M.K., and F.H. conceived and designed the work. M.K. developed the models and performed the experiments under the guidance of B.J.K. F.H. and M.K. analysed the data and conducted method comparisons. M.K., F.H., and B.J.K. contributed to materials and the analysis tool. A.P. and A.R. conducted additional analysis. M.K., F.H., and B.J.K. drafted the initial manuscript. All authors contributed to reviewing the manuscript.

References

- Emre O. Neftci and Bruno B. Averbeck. Reinforcement learning in artificial and biological systems. 1(3):133–143. ISSN 2522-5839. doi:10.1038/s42256-019-0025-4. URL <http://www.nature.com/articles/s42256-019-0025-4>.
- Brenden M. Lake, Tomer D. Ullman, Joshua B. Tenenbaum, and Samuel J. Gershman. Building machines that learn and think like people. 40:e253. ISSN 0140-525X, 1469-1825. doi:10.1017/S0140525X16001837. URL https://www.cambridge.org/core/product/identifier/S0140525X16001837/type/journal_article.
- Demis Hassabis, Dharshan Kumaran, Christopher Summerfield, and Matthew Botvinick. Neuroscience-inspired artificial intelligence. 95(2):245–258. ISSN 08966273. doi:10.1016/j.neuron.2017.06.011. URL <https://linkinghub.elsevier.com/retrieve/pii/S0896627317305093>.
- Blake A. Richards, Timothy P. Lillicrap, Philippe Beaudoin, Yoshua Bengio, Rafal Bogacz, Amelia Christensen, Claudia Clopath, Rui Ponte Costa, Archy de Berker, Surya Ganguli, Colleen J. Gillon, Danijar Hafner, Adam Kepecs, Nikolaus Kriegeskorte, Peter Latham, Grace W. Lindsay, Kenneth D. Miller, Richard Naud, Christopher C. Pack, Panayiota Poirazi, Pieter Roelfsema, João Sacramento, Andrew Saxe, Benjamin Scellier, Anna C. Schapiro, Walter Senn, Greg Wayne, Daniel Yamins, Friedemann Zenke, Joel Zylberberg, Denis Therien, and Konrad P. Kording. A deep learning framework for neuroscience. 22(11):1761–1770. ISSN 1097-6256, 1546-1726. doi:10.1038/s41593-019-0520-2. URL <https://www.nature.com/articles/s41593-019-0520-2>.

- Uri Hasson, Samuel A. Nastase, and Ariel Goldstein. Direct fit to nature: An evolutionary perspective on biological and artificial neural networks. 105(3):416–434. ISSN 08966273. doi:10.1016/j.neuron.2019.12.002. URL <https://linkinghub.elsevier.com/retrieve/pii/S089662731931044X>.
- Brett J Kagan, Andy C Kitchen, Nhi T Tran, Forough Habibollahi, Moein Khajehnejad, Bradyn J Parker, Anjali Bhat, Ben Rollo, Adeel Razi, and Karl J Friston. In vitro neurons learn and exhibit sentience when embodied in a simulated game-world. *Neuron*, 2022.
- Richard S Sutton and Andrew G Barto. *Reinforcement learning: An introduction*. MIT press, 2018.
- Matteo Hessel, Joseph Modayil, H. V. Hasselt, Tom Schaul, Georg Ostrovski, Will Dabney, Dan Horgan, Bilal Piot, Mohammad Gheshlaghi Azar, and David Silver. Rainbow: Combining improvements in deep reinforcement learning. *ArXiv*, abs/1710.02298, 2017.
- Matej Moravčík, Martin Schmid, Neil Burch, Viliam Lisý, Dustin Morrill, Nolan Bard, Trevor Davis, Kevin Waugh, Michael Johanson, and Michael Bowling. Deepstack: Expert-level artificial intelligence in heads-up no-limit poker. *Science*, 356(6337):508–513, 2017.
- M Jaderberg, WM Czarnecki, I Dunning, L Marris, G Lever, AG Castaneda, et al. Human-level performance in first-person multiplayer games with population-based deep reinforcement learning. *arXiv preprint arXiv:1807.01281*, 2018.
- David Silver, Thomas Hubert, Julian Schrittwieser, Ioannis Antonoglou, Matthew Lai, Arthur Guez, Marc Lanctot, Laurent Sifre, Dhharshan Kumaran, Thore Graepel, et al. Mastering chess and shogi by self-play with a general reinforcement learning algorithm. *arXiv preprint arXiv:1712.01815*, 2017a.
- David Silver, Julian Schrittwieser, Karen Simonyan, Ioannis Antonoglou, Aja Huang, Arthur Guez, Thomas Hubert, Lucas Baker, Matthew Lai, Adrian Bolton, et al. Mastering the game of go without human knowledge. *nature*, 550(7676):354–359, 2017b.
- David Silver, Thomas Hubert, Julian Schrittwieser, Ioannis Antonoglou, Matthew Lai, Arthur Guez, Marc Lanctot, Laurent Sifre, Dhharshan Kumaran, Thore Graepel, et al. A general reinforcement learning algorithm that masters chess, shogi, and go through self-play. *Science*, 362(6419):1140–1144, 2018.
- Volodymyr Mnih, Koray Kavukcuoglu, David Silver, Andrei A Rusu, Joel Veness, Marc G Bellemare, Alex Graves, Martin Riedmiller, Andreas K Fidjeland, Georg Ostrovski, et al. Human-level control through deep reinforcement learning. *nature*, 518(7540):529–533, 2015.
- Pedro A Tsividis, Thomas Pouncy, Jacqueline L Xu, Joshua B Tenenbaum, and Samuel J Gershman. Human learning in atari. 2017.
- Gary Marcus. Deep learning: A critical appraisal. *arXiv preprint arXiv:1801.00631*, 2018.
- Elizabeth Gibney et al. This ai researcher is trying to ward off a reproducibility crisis. *Nature*, 577(7788):14–14, 2020.
- James Kirkpatrick, Razvan Pascanu, Neil Rabinowitz, Joel Veness, Guillaume Desjardins, Andrei A. Rusu, Kieran Milan, John Quan, Tiago Ramalho, Agnieszka Grabska-Barwinska, Demis Hassabis, Claudia Clopath, Dhharshan Kumaran, and Raia Hadsell. Overcoming catastrophic forgetting in neural networks. 114(13):3521–3526. ISSN 0027-8424, 1091-6490. doi:10.1073/pnas.1611835114. URL <https://pnas.org/doi/full/10.1073/pnas.1611835114>.
- Lin Fan and Peter W. Glynn. The fragility of optimized bandit algorithms. URL <http://arxiv.org/abs/2109.13595>.
- Seyed Sajad Mousavi, Michael Schukat, and Enda Howley. Deep reinforcement learning: An overview. In Yaxin Bi, Supriya Kapoor, and Rahul Bhatia, editors, *Proceedings of SAI Intelligent Systems Conference (IntelliSys) 2016*, pages 426–440, Cham, 2018. Springer International Publishing. ISBN 978-3-319-56991-8.
- Charlotte Freitag, Mike Berners-Lee, Kelly Widdicks, Bran Knowles, Gordon S. Blair, and Adrian Friday. The real climate and transformative impact of ICT: A critique of estimates, trends, and regulations. 2(9):100340. ISSN 2666-3899. doi:10.1016/j.patter.2021.100340. URL <https://www.sciencedirect.com/science/article/pii/S2666389921001884>.
- James C.R. Whittington and Rafal Bogacz. Theories of error back-propagation in the brain. 23(3):235–250. ISSN 13646613. doi:10.1016/j.tics.2018.12.005. URL <https://linkinghub.elsevier.com/retrieve/pii/S1364661319300129>.
- Arif A Hamid, Jeffrey R Pettibone, Omar S Mabrouk, Vaughn L Hetrick, Robert Schmidt, Caitlin M Vander Weele, Robert T Kennedy, Brandon J Aragona, and Joshua D Berke. Mesolimbic dopamine signals the value of work. 19(1):117–126. ISSN 1097-6256, 1546-1726. doi:10.1038/nm.4173. URL <http://www.nature.com/articles/nm.4173>.

- Vincent D. Costa, Olga Dal Monte, Daniel R. Lucas, Elisabeth A. Murray, and Bruno B. Averbeck. Amygdala and ventral striatum make distinct contributions to reinforcement learning. 92(2):505–517. ISSN 08966273. doi:10.1016/j.neuron.2016.09.025. URL <https://linkinghub.elsevier.com/retrieve/pii/S0896627316305840>.
- Karl J. Friston, Jean Daunizeau, and Stefan J. Kiebel. Reinforcement learning or active inference? 4(7):e6421. ISSN 1932-6203. doi:10.1371/journal.pone.0006421. URL <https://dx.plos.org/10.1371/journal.pone.0006421>.
- Yuhang Song, Beren Millidge, Tommaso Salvatori, Thomas Lukasiewicz, Zhenghua Xu, and Rafal Bogacz. Inferring neural activity before plasticity: A foundation for learning beyond backpropagation. *bioRxiv*, pages 2022–05, 2022.
- James CR Whittington and Rafal Bogacz. An approximation of the error backpropagation algorithm in a predictive coding network with local hebbian synaptic plasticity. *Neural computation*, 29(5):1229–1262, 2017.
- Jacopo Tessadori, Marta Bisio, Sergio Martinoia, and Michela Chiappalone. Modular neuronal assemblies embodied in a closed-loop environment: Toward future integration of brains and machines. 6. ISSN 1662-5110. doi:10.3389/fncir.2012.00099. URL <http://journal.frontiersin.org/article/10.3389/fncir.2012.00099/abstract>.
- Douglas J. Bakkum, Zenas C Chao, and Steve M Potter. Spatio-temporal electrical stimuli shape behavior of an embodied cortical network in a goal-directed learning task. 5(3):310–323. ISSN 1741-2560, 1741-2552. doi:10.1088/1741-2560/5/3/004. URL <http://stacks.iop.org/1741-2552/5/i=3/a=004?key=crossref.2e55c5e1d3b8c9612fd3ab6762195e65>.
- Jan Müller, Douglas J Bakkum, and Andreas Hierlemann. Sub-millisecond closed-loop feedback stimulation between arbitrary sets of individual neurons. *Frontiers in neural circuits*, 6:121, 2013.
- Evan R. Harrell, Matías A. Goldin, Brice Bathellier, and Daniel E. Shulz. An elaborate sweep-stick code in rat barrel cortex. 6(38):eabb7189. ISSN 2375-2548. doi:10.1126/sciadv.abb7189. URL <https://www.science.org/doi/10.1126/sciadv.abb7189>.
- Brett J Kagan, Christopher Gyngell, Tamra Lysaght, Victor M Cole, Tsutomu Sawai, and Julian Savulescu. The technology, opportunities and challenges of synthetic biological intelligence. *Biotechnology Advances*, page 108233, 2023.
- Forough Habibollahi, Brett J Kagan, Anthony N Burkitt, and Chris French. Critical dynamics arise during structured information presentation within embodied in vitro neuronal networks. *Nature Communications*, 14(1):5287, 2023.
- Norman P. Jouppi, Doe Hyun Yoon, George Kurian, Sheng Li, Nishant Patil, James Laudon, Cliff Young, and David Patterson. A domain-specific supercomputer for training deep neural networks. 63(7):67–78. ISSN 0001-0782. doi:10.1145/3360307. URL <https://doi.org/10.1145/3360307>.
- Umer Siddique, Paul Weng, and Matthieu Zimmer. Learning fair policies in multiobjective (deep) reinforcement learning with average and discounted rewards. *arXiv e-prints*, art. arXiv:2008.07773, August 2020. doi:10.48550/arXiv.2008.07773.
- Choumicha El Mazgualdi, Tawfik Masrouf, Nouredine Barka, and Ibtissam El Hassani. A learning-based decision tool towards smart energy optimization in the manufacturing process. *Systems*, 10(5):180, 2022.
- Su Young Lee, Choi Sungik, and Sae-Young Chung. Sample-efficient deep reinforcement learning via episodic backward update. *Advances in Neural Information Processing Systems*, 32, 2019.
- Mark Buchanan. *Organoids of intelligence*. PhD thesis, Nature Publishing Group, 2018.
- André Moraes Bastos, Julien Vezoli, Conrado Arturo Bosman, Jan-Mathijs Schoffelen, Robert Oostenveld, Jarrod Robert Dowdall, Peter De Weerd, Henry Kennedy, and Pascal Fries. Visual areas exert feedforward and feedback influences through distinct frequency channels. 85(2):390–401. ISSN 08966273. doi:10.1016/j.neuron.2014.12.018. URL <https://linkinghub.elsevier.com/retrieve/pii/S089662731401099X>.
- Geoffrey Hinton. The forward-forward algorithm: Some preliminary investigations. *arXiv preprint arXiv:2212.13345*, 2022.
- Daniel J Felleman and David C Van Essen. Distributed hierarchical processing in the primate cerebral cortex. *Cerebral cortex (New York, NY: 1991)*, 1(1):1–47, 1991.
- John J Hopfield. Neural networks and physical systems with emergent collective computational abilities. *Proceedings of the national academy of sciences*, 79(8):2554–2558, 1982.
- Rajesh PN Rao and Dana H Ballard. Predictive coding in the visual cortex: a functional interpretation of some extra-classical receptive-field effects. *Nature neuroscience*, 2(1):79–87, 1999.

- Karl Friston. A theory of cortical responses. *Philosophical transactions of the Royal Society B: Biological sciences*, 360(1456):815–836, 2005.
- Lee de Wit, Bart Machilsen, and Tom Putzeys. Predictive coding and the neural response to predictable stimuli. *Journal of Neuroscience*, 30(26):8702–8703, 2010.
- Kurtland Chua, Roberto Calandra, Rowan McAllister, and Sergey Levine. Deep reinforcement learning in a handful of trials using probabilistic dynamics models. *Advances in neural information processing systems*, 31, 2018.
- Jörg KH Franke, Gregor Köhler, André Biedenkapp, and Frank Hutter. Sample-efficient automated deep reinforcement learning. *arXiv preprint arXiv:2009.01555*, 2020.
- Adam Stooke and Pieter Abbeel. Accelerated methods for deep reinforcement learning. *arXiv preprint arXiv:1803.02811*, 2018.
- Lena Smirnova, Brian S Caffo, David H Gracias, Qi Huang, Itzy E Morales Pantoja, Bohao Tang, Donald J Zack, Cynthia A Berlinicke, J Lomax Boyd, Timothy D Harris, et al. Organoid intelligence (oi): the new frontier in biocomputing and intelligence-in-a-dish. *Frontiers in Science*, 1:1017235, 2023.
- Maria Elisabetta Ruaro, Paolo Bonifazi, and Vincent Torre. Toward the neurocomputer: image processing and pattern recognition with neuronal cultures. *IEEE Transactions on Biomedical Engineering*, 52(3):371–383, 2005.
- Kai Arulkumaran, Marc Peter Deisenroth, Miles Brundage, and Anil Anthony Bharath. Deep reinforcement learning: A brief survey. *IEEE Signal Processing Magazine*, 34(6):26–38, 2017.
- John Schulman, Filip Wolski, Prafulla Dhariwal, Alec Radford, and Oleg Klimov. Proximal policy optimization algorithms. *arXiv preprint arXiv:1707.06347*, 2017.
- Richard Bellman and Robert Kalaba. Dynamic programming and statistical communication theory. *Proceedings of the National Academy of Sciences*, 43(8):749–751, 1957.
- Nitish Shirish Keskar, Dheevatsa Mudigere, Jorge Nocedal, Mikhail Smelyanskiy, and Ping Tak Peter Tang. On large-batch training for deep learning: Generalization gap and sharp minima. *arXiv preprint arXiv:1609.04836*, 2016.
- Takuya Isomura and Karl Friston. Reverse-engineering neural networks to characterize their cost functions. *Neural Computation*, 32(11):2085–2121, 2020.
- Takuya Isomura, Hideaki Shimazaki, and Karl J Friston. Canonical neural networks perform active inference. *Communications Biology*, 5(1):55, 2022.
- Karl Friston, Lancelot Da Costa, Danijar Hafner, Casper Hesp, and Thomas Parr. Sophisticated inference. *Neural Computation*, 33(3):713–763, February 2021. ISSN 0899-7667. doi:10.1162/neco_a_01351. URL https://doi.org/10.1162/neco_a_01351.
- Raphael Kaplan and Karl J. Friston. Planning and navigation as active inference. *Biological Cybernetics*, 112(4):323–343, 2018. ISSN 1432-0770. doi:10.1007/s00422-018-0753-2. URL <https://doi.org/10.1007/s00422-018-0753-2>.
- Franz Kuchling, Karl Friston, Georgi Georgiev, and Michael Levin. Morphogenesis as bayesian inference: A variational approach to pattern formation and control in complex biological systems. *Physics of Life Reviews*, 33:88–108, 2020. ISSN 1571-0645. doi:<https://doi.org/10.1016/j.plrev.2019.06.001>. URL <https://www.sciencedirect.com/science/article/pii/S1571064519300909>.
- Alexander Tschantz, Anil K. Seth, and Christopher L. Buckley. Learning action-oriented models through active inference. *PLOS Computational Biology*, 16(4):1–30, 04 2020. doi:10.1371/journal.pcbi.1007805. URL <https://doi.org/10.1371/journal.pcbi.1007805>.
- Thomas Parr and Karl J. Friston. The discrete and continuous brain: From decisions to movement-and back again. *Neural computation*, 30(29894658):2319–2347, September 2018. ISSN 0899-7667. doi:10.1162/neco_a_01102. URL <https://www.ncbi.nlm.nih.gov/pmc/articles/PMC6115199/>.
- Takuya Isomura. Active inference leads to bayesian neurophysiology. *Neuroscience Research*, 175:38–45, 2022. ISSN 0168-0102. doi:<https://doi.org/10.1016/j.neures.2021.12.003>. URL <https://www.sciencedirect.com/science/article/pii/S0168010221002595>. Constructive Understanding of Multi-scale Dynamism of Neuropsychiatric Disorders.
- William S. Lovejoy. A survey of algorithmic methods for partially observed markov decision processes. *Annals of Operations Research*, 28(1):47–65, 1991. ISSN 1572-9338. doi:10.1007/BF02055574. URL <https://doi.org/10.1007/BF02055574>.
- Guy Shani, Joelle Pineau, and Robert Kaplow. A survey of point-based pomdp solvers. *Autonomous Agents and Multi-Agent Systems*, 27(1):1–51, 2013. ISSN 1573-7454. doi:10.1007/s10458-012-9200-2. URL <https://doi.org/10.1007/s10458-012-9200-2>.

Leslie Pack Kaelbling, Michael L. Littman, and Anthony R. Cassandra. Planning and acting in partially observable stochastic domains. *Artificial Intelligence*, 101(1):99–134, 1998. ISSN 0004-3702. doi:[https://doi.org/10.1016/S0004-3702\(98\)00023-X](https://doi.org/10.1016/S0004-3702(98)00023-X). URL <https://www.sciencedirect.com/science/article/pii/S000437029800023X>.

Aswin Paul, Noor Sajid, Manoj Gopalkrishnan, and Adeel Razi. Active inference for stochastic control. In *Joint European Conference on Machine Learning and Knowledge Discovery in Databases*, pages 669–680. Springer, 2021.

A Supplementary Materials

A.1 Cell Culture

Neural cells were cultured either from the cortices of E15.5 mouse embryos or differentiated from human induced pluripotent stem cells via a dual SMAD inhibition (DSI) protocol as previously described (Kagan et al., 2022). Cells were cultured until plating onto MEA. For primary mouse neurons, this occurred at day-in-vitro (DIV) 0, for DSI cultures this occurred at between DIV 30 - 33 depending on culture development.

A.2 MEA Setup and Plating

MaxOne Multielectrode Arrays (MEA; Maxwell Biosystems, AG, Switzerland) was used and is a high-resolution electrophysiology platform featuring 26,000 platinum electrodes arranged over an 8 mm². The MaxOne system is based on complementary meta-oxide-semiconductor (CMOS) technology and allows recording from up to 1024 channels. MEAs were coated with either polyethylenimine (PEI) in borate buffer for primary culture cells or Poly-D-Lysine for cells from an iPSC background before being coated with either 10 µg/ml mouse laminin or 10 µg/ml human 521 Laminin (Stemcell Technologies Australia, Melbourne, Australia) respectively to facilitate cell adhesion. Approximately 10⁶ cells were plated on MEA after preparation as per (Kagan et al., 2022). Cells were allowed approximately one hour to adhere to the MEA surface before the well was flooded. The day after plating, cell culture media was changed for all culture types to BrainPhys™ Neuronal Medium (Stemcell Technologies Australia, Melbourne, Australia) supplemented with 1% penicillin-streptomycin. Cultures were maintained in a low O₂ incubator kept at 5% CO₂, 5% O₂, 36°C and 80% relative humidity. Every two days, half the media from each well was removed and replaced with free media. Media changes always occurred after all recording sessions.

A.3 DishBrain platform and electrode configuration

The current *DishBrain* platform is configured as a low-latency, real-time MEA control system with on-line spike detection and recording software. The *DishBrain* platform provides on-line spike detection and recording configured as a low-latency, real-time MEA control. The *DishBrain* software runs at 20 kHz and allows recording at an incredibly fine timescale. There is the option of recording spikes in binary files, and regardless of recording, they are counted over a period of 10 milliseconds (200 samples), at which point the game environment is provided with how many spikes are detected in each electrode in each predefined motor region as described below. Based on which motor region the spikes occurred in, they are interpreted as motor activity, moving the ‘paddle’ up or down in the virtual space. As the ball moves around the play area at a fixed speed and bounces off the edge of the play area and the paddle, the pong game is also updated at every 10ms interval. Once the ball hits the edge of the play area behind the paddle, one rally of pong has come to an end at which point a ‘miss’ would be recorded and an unpredictable stimulation would be delivered to the cells. Using a feedback stimulus at a voltage of 150 mV and a frequency of 5 Hz, unpredictable external stimulus could be added to the system. Random stimulation took place at random sites over the 8 predefined input electrodes at random timescales for a period of four seconds, followed by a configurable rest period of four seconds where stimulation paused, then the next rally began.

In contrast, a predictable stimulus feedback is provided when the ball contacts the paddle under the standard stimulus condition. Predictable stimulus feedback involves 75mV stimulation at 100Hz over 100ms occurring when the simulated ball struck the paddle and replaced other sensory information. All 8 stimulation electrodes simultaneously would receive predictable stimulation at this frequency and period. A ‘stimulation sequencer’ module tracks the location of the ball relative to the paddle during each rally and encodes it as stimulation to one of eight stimulation sites. Each time a sample is received from the MEA, the stimulation sequencer is updated 20,000 times a second, while the game itself runs at 100Hz. After the previous lot of MEA commands has completed, the *DishBrain* system constructs a new sequence of MEA commands based on the information it has been configured to transmit based on both place codes and rate codes. The stimulations take the form of a short square bi-phasic pulse that is a positive voltage, then a negative voltage. This pulse sequence is read and applied to the electrode by a Digital to Analog Converter (or DAC) on the MEA. A real-time interactive version of the game visualizer is available at <https://spikestream.corticallabs.com/>. Alternatively, cells could be recorded at ‘rest’ in a gameplay environment where activity was recorded to move the paddle but no stimulation was delivered, with corresponding outcomes still recorded. Using this spontaneous activity alone as a baseline, the gameplay characteristics of a culture were determined. Low level code for interacting with Maxwell API was written in C to minimize processing latencies-so packet processing latency was typically <50 µs. High-level code was written in Python, including configuration setups and general instructions for game settings. A 5 ms spike-to-stim latency was achieved, which was substantially due to MaxOne’s inbuilt hardware buffering. Figure S1 illustrates a schematic view of Software components and data flow in the *DishBrain* closed loop system.

A.4 Deep Reinforcement Learning Algorithms

Deep Q Network (DQN): The utilized DQN algorithm begins by extracting spatiotemporal features from inputs, such as the movement of the ball in the game of ‘Pong’. Multiple fully connected layers are used to process the final feature map, which implicitly encodes the effects of actions. As opposed to traditional controllers that use fixed preprocessing steps, this method can adapt the processing of the state based on changes in the learning signal. An epsilon-greedy algorithm was employed in this work to balance the exploration and exploitation capabilities of the DQN algorithm. For the results represented in this manuscript, a comprehensive grid search was conducted within the parameter space of *learning rate* ([0.0001, 0.004]), *replay buffer size* ([10, 10000]), and the training *batch size* ([5, 128]) with starting point of 0.0001, 32, 10000, respectively, aiming to identify the optimal parameter configuration. The results presented in this paper are derived from the superior set of hyper-parameters obtained through this search process. As the outcome of this search for the DQN algorithm, we selected *learning rate* = 0.002, *replay buffer size* = 10000, and *batch size* = 16 for the results of Figure 2, *learning rate* = 0.001, *replay buffer size* = 10000, and *batch size* = 16 for the results of Figure 3, and *learning rate* = 0.001, *replay buffer size* = 10000, and *batch size* = 32 for the results of Figure 4. Figure S2 illustrates the performance of the DQN algorithm with IMAGE INPUT design in terms of average rally length in several sample points of the mentioned search space. While exploring each hyper-parameter in Figure S2, the remaining pair are set to the same values as the starting point of the search (i.e. *learning rate* = 0.0001, *batch size* = 32, and *replay buffer size* = 10000).

For additional details on the set of explored hyper-parameters and network architectures, see Table S1.

Algorithm 1 Deep Q Network (DQN) with Experience Replay

Require:

- 1: \mathcal{D} : Replay buffer with size N (Default: 10000)
 - 2: θ : Initial network parameters
 - 3: $\tilde{\theta}$: Copy of θ
 - 4: γ : Discount factor (Default: 0.95)
 - 5: N_b : Training batch size (Default: 16)
 - 6: \tilde{N} : Target network update frequency (Default: 10)
 - 7: x_t : Input matrix at time t
 - 8: S : Number of seeds (Default: 150)
 - 9: e_{max} : Maximum number of episodes (Default: 70)
 - 10: **for** seed $\in \{1, \dots, S\}$ **do**
 - 11: **for** episode $e \in \{1, \dots, e_{max}\}$ **do**
 - 12: Set state $s_1 \leftarrow x_1$ and preprocess $\phi_1 = \phi(s_1)$
 - 13: $t = 1$
 - 14: **while** ϕ_t is non-terminal **do**
 - 15: With probability ϵ select a random action a_t
 - 16: otherwise select $a_t = \max_a Q^*(\phi(s_t), a; \theta)$
 - 17: Execute action a_t and observe reward r_t and input x_{t+1}
 - 18: Set new state s_{t+1} and preprocess $\phi_{t+1} = \phi(s_{t+1})$
 - 19: Store transition $(\phi_t, a_t, r_t, \phi_{t+1})$ in \mathcal{D}
 - 20: Sample random minibatch of N_b transitions $(\phi_j, a_j, r_j, \phi_{j+1})$ from \mathcal{D}
 - 21: Set $y_j = \begin{cases} r_j & \text{for terminal } \phi_{j+1} \\ r_j + \gamma \max_{a'} Q(\phi_{j+1}, a'; \theta) & \text{for non-terminal } \phi_{j+1} \end{cases}$
 - 22: Perform a gradient descent step on $(y_j - Q(\phi_j, a_j; \theta))^2$
 - 23: Replace target parameters $\tilde{\theta} \leftarrow \theta$ every \tilde{N} steps
 - 24: $t = t + 1$
 - 25: **end while**
 - 26: **end for**
 - 27: **end for**
-

Advantage Actor-Critic (A2C): In an A2C model, the total reward itself could be represented as a *value* of the state plus the advantage of the action. The *value* of each policy is learned while following it. The policy gradient can be calculated by knowing the *value* for any state. The policy network is then updated such that the probability of actions with a higher advantage value is increased. Here, the policy network (which returns a probability distribution of actions) is called the *actor*, as it tells the agents what to do. *Critic* is another network that enables the evaluation of the actions to decide whether they were good or not. In this case, policy and value are implemented as separate heads of the network, which transform the output from the common body into either probability distributions or single numbers representing the state’s value. Thus, low-level features can be shared between the two networks.

For the results represented in the main paper, a comprehensive grid search was conducted within the parameter space of actor learning rate ($[0.0001, 0.004]$), critic learning rate ($[0.0001, 0.004]$), and the training batch size ($[5, 128]$), to identify the optimal parameter configuration. As the outcome of this search for A2C, we selected *actor learning rate* = 0.001, 0.0001, 0.003, *critic learning rate* = 0.001, 0.001, 0.001, and *batch size* = 32, 32, 5 for the results of Figure 2, 3, and 4, respectively. Figure S2 contains the results of this hyper-parameter search for the A2C algorithm with the IMAGE INPUT design in terms of average rally length in several sample points of the mentioned search space. While exploring each hyper-parameter in Figure S2, the remaining pair are set to the same values as the starting point of the search (i.e. *actor learning rate* = 0.0001, *batch size* = 32, and *critic learning rate* = 0.001).

Algorithm 2 Advantage Actor-Critic (A2C)

Require:

```

1:  $\theta_v$ : Initial parameter vector for the value net (critic)
2:  $\theta_\pi$ : Initial parameter vector for the policy net (actor)
3:  $\gamma$ : Discount factor (Default: 0.95)
4:  $N$ : Number of consecutive steps to play current policy in the environment (Default: 5)
5:  $x_t$ : Input matrix at time  $t$ 
6:  $S$ : Number of seeds (Default: 150)
7:  $e_{max}$ : Maximum number of episodes (Default: 70)
8: for seed  $\in \{1, \dots, S\}$  do
9:    $t = 1$ 
10:   $e = 1$ 
11:  repeat
12:     $\partial\theta_\pi \leftarrow 0$  and  $\partial\theta_v \leftarrow 0$ 
13:     $t_{start} = t$ 
14:    Set state  $s_t \leftarrow x_t$  and preprocess  $\phi_t = \phi(s_t)$ 
15:    repeat
16:      Select  $a_t$  according to  $\pi(a_t | \phi_t; \theta)$ 
17:      Execute action  $a_t$  and observe reward  $r_t$  and input  $x_{t+1}$ 
18:      Set new state  $s_{t+1}$  and preprocess  $\phi_{t+1} = \phi(s_{t+1})$ 
19:       $t \leftarrow t + 1$ 
20:    until  $\phi_t$  is terminal or  $t - t_{start} = N$ 
21:     $R = \begin{cases} 0 & \text{for terminal } \phi_t \\ V(\phi_t; \theta_v) & \text{for non-terminal } \phi_t \end{cases}$ 
22:    for  $i \in \{t - 1, \dots, t_{start}\}$  do
23:       $R \leftarrow r_i + \gamma R$ 
24:      Accumulate the policy gradients:  $\partial\theta_\pi \leftarrow \partial\theta_\pi + \nabla_{\theta} \log \pi(a_i | \phi_i; \theta) (R - V(\phi_i, \theta_v))$ 
25:      Accumulate the value gradients:  $\partial\theta_v \leftarrow \partial\theta_v + \frac{\partial(R - V(\phi_i, \theta_v))^2}{\partial\theta_v}$ 
26:    end for
27:    Update  $\theta_\pi$  and  $\theta_v$  using  $\partial\theta_\pi$  and  $\partial\theta_v$ , respectively.
28:    if  $\phi_t$  is terminal then
29:       $e \leftarrow e + 1$ 
30:    end if
31:  until  $e > e_{max}$ 
32: end for
    
```

Proximal Policy Optimization (PPO): PPO models are a family of policy gradient methods for reinforcement learning. The PPO method uses a slightly different training procedure: An extended set of samples is taken from the environment, and then the advantage is estimated for the whole set or sequence of samples before several epochs of training are performed. To estimate policy gradients, instead of using the gradient of action probabilities, the PPO method uses a different objective: the ratio between the new and the old policy scaled by the advantages.

Once more, for the results represented in the main paper, we used the outcome of a grid search for the PPO algorithm in the same space as A2C above and utilized *actor learning rate* = 0.003, 0.0001, 0.001, *critic learning rate* = 0.003, 0.001, 0.001, and *batch size* = 16, 16, 32 to generate the results of Figure 2, 3, and 4, respectively.

Figure S2 represents the performance of the PPO algorithm with the IMAGE INPUT design in terms of average rally length in several sample points of the mentioned search space. While exploring each hyper-parameter in Figure S2, the remaining pair are set to the same values as the starting point of the search (i.e. *actor learning rate* = 0.0001, *batch size* = 32, and *critic learning rate* = 0.001).

Algorithm 3 Proximal Policy Optimization (PPO)

Require:

```

1:  $\theta$ : Initial policy parameter vector
2:  $\epsilon$ : Clipping threshold (Default: 0.2)
3:  $\gamma$ : Discount factor (Default: 0.95)
4:  $\lambda$ : GAE parameter (Default: 1)
5:  $N$ : Number of consecutive steps to play current policy in the environment (Default: 32)
6:  $x_t$ : Input matrix at time  $t$ 
7:  $S$ : Number of seeds (Default: 150)
8:  $e_{max}$ : Maximum number of episodes (Default: 70)
9: for seed  $\in \{1, \dots, S\}$  do
10:    $t = 1$ 
11:    $e = 1$ 
12:   repeat
13:      $t_{start} = t$ 
14:     Set state  $s_t \leftarrow x_t$  and preprocess  $\phi_t = \phi(s_t)$ 
15:     repeat
16:       Select  $a_t$  according to  $\pi(a_t | \phi_t; \theta)$ 
17:       Execute action  $a_t$  and observe reward  $r_t$  and input  $x_{t+1}$ 
18:       Set new state  $s_{t+1}$  and preprocess  $\phi_{t+1} = \phi(s_{t+1})$ 
19:        $t \leftarrow t + 1$ 
20:     until  $\phi_t$  is terminal or  $t - t_{start} = N$ 
21:     Collect set of partial trajectories  $\mathcal{D}$  on current policy  $\pi$ 
22:     Estimate Advantages  $\hat{A}_t^\pi = \sigma_t + (\gamma\lambda)\sigma_{t+1} + \dots + (\gamma\lambda)^{N-t-1}\sigma_{N-1}$ , where  $\sigma_t = r_t + \gamma V(\phi_{t+1}) - V(\phi_t)$ 
23:      $\theta \leftarrow \operatorname{argmax}_\theta \mathcal{L}_\theta^{CLIP}(\theta)$ 
24:     where  $\mathcal{L}_\theta^{CLIP}(\theta) = \mathbb{E}_{\tau \sim \pi} \left[ \sum_{t=0}^T [\min(r_t(\theta)\hat{A}_t^\pi, \text{clip}(r_t(\theta), 1 - \epsilon, 1 + \epsilon)\hat{A}_t^\pi)] \right]$ 
25:     if  $\phi_t$  is terminal then
26:        $e \leftarrow e + 1$ 
27:     end if
28:     until  $e > e_{max}$ 
29:   end for
    
```

A.5 Additional Hyper-parameter Exploration

Table S1: Experimented Hyper-parameter and network architecture details

Hyper-parameter	Algorithm	Tested Values
Conv ₁ size	DQN, A2C, PPO	(16 × 16) , (64 × 64)
Conv ₂ size	DQN, A2C, PPO	(32 × 32) , (64 × 64)
Conv ₃ size	DQN, A2C, PPO	(32 × 32) , (64 × 64)
Last hidden layer size	DQN, A2C, PPO	{100, 256, 512 }
Number of seeds	DQN, A2C, PPO	150
Kernel size	DQN, A2C, PPO	{ 5 , 4}
Stride	DQN, A2C, PPO	2
Batch size	DQN, A2C, PPO	[5, 128]
Discount factor	DQN, A2C, PPO	{0.85, 0.95, 0.99, 0.999}
Learning rate	DQN	[0.0001, 0.004]
Replay buffer size	DQN	[10, 100000]
Actor-learning rate	A2C, PPO	[0.0001, 0.004]
Critic-learning rate	A2C, PPO	[0.0001, 0.004]
Clipping threshold	PPO	{0.1, 0.2 , 0.3}
Num of epochs	PPO	{ 5 , 8, 10}

* The parameter values jointly chosen for all algorithms are highlighted in bold.

Effect of Batch Size on Deep RL Algorithm Performances:

From a technical standpoint, there exist no foolproof techniques for identifying the ideal hyper-parameter configuration for training deep RL algorithms. In addition, the batch size has an impact on the convergence rate of the prediction network, with smaller batch sizes resulting in faster convergence and well-known degradation in model quality and generalization abilities that can occur with increased batch sizes (Keskar et al., 2016). As such, originally we aimed to select batch sizes that would converge within sample numbers comparable to the training period of biological cultures

while attempting to prioritize computational efficiency, which is a significant area of interest in this study. Hence, opting for large batch sizes may significantly slow down the model convergence and would not confer any benefit to the RL algorithms under investigation.

Figures S3, S4, and S5 investigate the impact of changing batch sizes utilizing the IMAGE INPUT design by incorporating batch sizes of 8, 16, 32, and 64 while keeping the rest of the hyper-parameters in each algorithm fixed at default levels similar to Figure S2 (i.e. *learning rate* = 0.0001, *batch size* = 32, and *replay buffer size* = 10000 for DQN and *actor learning rate* = 0.0001, *batch size* = 32, and *critic learning rate* = 0.001 for A2C and PPO).

In some cases, these results illustrate an unwanted trend in the main metrics of interest when increasing the batch size above certain levels. For instance, an increasing % of aces in the DQN and PPO algorithms, decreasing average rally length in PPO, and decreasing % of long rallies in both A2C and PPO algorithms are observed which may eventually prevent the model from converging to the optima. This suggests that if the comparison were to be extended to a larger number of episodes for all groups, the increase in batch size would not necessarily yield improved performances, as evidenced by the undesirable trend observed in the aforementioned metrics (Extended Data Figures S3, S4, and S5). Notably, this may occur due to the fact that larger batch sizes make larger gradient steps than smaller batch sizes for the same number of samples seen and the update is heavily dependent on the specific samples drawn from the dataset. Conversely, a small batch size leads to updates that are more consistent in size, with the size of the update being only weakly dependent on which particular samples are selected from the dataset. In conclusion, it is possible that in deep neural networks, optimal weight configurations are located far from the initial weights. Hence, averaging the loss function over large batch sizes may not allow the model to explore a large enough space to reach the optimal weight configurations within the same number of training epochs.

Effects of Adding Hidden Layers on DQN Performance:

To evaluate the effect of adding extra hidden layers on the performance of BALL POSITION INPUT and PADDLE&BALL POSITION INPUT designs to the DQN algorithm, we implemented them by adding 2 additional hidden layers before the output layer and incorporating a batch size = 32. Extended Data Figure S6 shows the outcomes of these adjustments.

This further analysis revealed that although certain metrics exhibited qualitative and quantitative changes in their trends, the overall sample efficiency performance remained unaffected and even worsened with the inclusion of additional hidden layers. For example, we noted a degradation and an unwanted decreasing trend in the DQN's performance in the % of long rallies for the PADDLE&BALL POSITION INPUT design. This resulted in the MCC group significantly outperforming DQN PADDLE&BALL POSITION INPUT design in terms of % of long Rallies during the second 15 minutes. The performance of DQN in terms of average rally length was also deteriorated by the addition of these layers. On the other hand, MCC no longer demonstrated a significantly superior performance in terms of % of aces by the addition of hidden layers to the PADDLE&BALL POSITION INPUT design. While some level of improvement was detected in the DQN group with the BALL POSITION INPUT design (specifically in the % of aces achieved) by the addition of the extra layers, overall performance in all 3 metrics was still inferior to those of the biological cultures in all the metrics. Specifically as illustrated in Extended Data Figure S7, the HCC group still demonstrated significant outperformance compared to the DQN PADDLE&BALL POSITION INPUT and BALL POSITION INPUT designs in terms of relative improvement. The relative improvement in both of the PADDLE&BALL POSITION INPUT and BALL POSITION INPUT designs showed a decay compared to the results reported in the main text, where this level of outperformance of MCC over DQN was not observed in the absence of hidden layers.

The observed deteriorated performance in terms of relative improvement in the PADDLE&BALL POSITION INPUT design may be attributed to decreased generalization capabilities and higher variance resulting from the introduction of additional hidden layers. Because, for simpler tasks, a smaller network with fewer hidden layers might be sufficient to achieve good performance, and adding more layers could lead to overfitting. Thereby, this declined performance in the relative improvement as well as the low dimensionality of the input information in these designs combined with the faster computational performance of the algorithm with fewer hidden layers can justify the use of the shallower design for comparison reasons.

A.6 Active Inference Agent

While RL algorithms use back-propagation, it has been argued that this method is likely too inefficient to function within biological systems. Therefore, we attempted to evaluate the sample efficiency of more biologically inspired algorithms, by implementing a counterfactual learning active inference agent (Isomura and Friston, 2020; Isomura et al., 2022). Our preliminary findings show that one can use a generic active inference agent which can then mimic the performance of the DishBrain system depending on additional parameters such as memory.

The active inference framework is a formal way of modelling the behaviour of self-organising systems that interface with the external world and maintain a consistent form over time (Friston et al., 2021; Kaplan and Friston, 2018; Kuchling et al., 2020). The framework assumes that agents embody generative models of the environment they interact with, on which they base their behaviour (Tschantz et al., 2020; Parr and Friston, 2018). A recent active inference scheme is shown to be mathematically equivalent to a particular class of neural networks accompanied by some neuromodulations of synaptic plasticity (Isomura and Friston, 2020; Isomura et al., 2022). It uses counterfactual learning (CL) to accumulate a measure of risk over time based on feedback from the environment. Subsequent work that validates this scheme experimentally using *in vitro* neural networks has also appeared recently (Isomura, 2022). Of particular note, the training schematic for the DishBrain system was inspired by implications from theory on active inference via the Free Energy Principle, making it the most suitable algorithm to compare here (Kagan et al., 2022). Here, we focus on generative models in the form of Partially Observable Markov Decision Processes (POMDPs) for their simplicity and ubiquitous use in the optimal control literature (Lovejoy, 1991; Shani et al., 2013; Kaelbling et al., 1998).

Gameplay performance of these agents with two different memory horizons of 3 (CL(3)) and 7 (CL(7)) is summarised in Figure S8. We see that the CL(7) agents perform at par and in some cases better than the HCC group and are the only group where the HCC has no significant outperformance over them in terms of the relative improvement in time (see Figure S8.h). However, this is not the case for CL(3) agents which have a smaller memory horizon. While further exploring this active inference framework is out of scope for this paper, it does highlight the value of using biologically inspired algorithms in terms of sample efficiency.

Generative model of the pong game environment:

Assuming agents have a discrete representation of their surrounding environment, we turn to the POMDP framework (Kaelbling et al., 1998). POMDPs offer a fairly expressive structure to model discrete state-space environments where parameters can be expressed as tractable categorical distributions. The POMDP-based generative model can be formally defined as a tuple of finite sets $(S, O, U, \mathbb{B}, \mathbb{A})$:

- $s \in S$: S is a set of hidden states (s) causing observations o .
- $o \in O$: O is a set of observations, where $o = s$, in the fully observable setting. In a partially observable setting, $o = f(s)$.
- $u \in U$: U is a set of actions (u). E.g., $U = \{Up, Stay, Down\}$.
- \mathbb{B} : encodes the one-step transition dynamics, $P(s_t | s_{t-1}, u_{t-1})$ i.e., the probability that when action u_{t-1} is taken while being in state s_{t-1} (at time $t - 1$) results in s_t at time t .
- \mathbb{A} : encodes the likelihood mapping, $P(o_\tau | s_\tau)$ for the partially observable setting.
- \mathbb{D} : Encodes the prior of the agent about the hidden state factor s .
- \mathbb{E} : Encodes the prior of the agent about actions u .

In a POMDP, the hidden states (s) generate observations (o) through the likelihood mapping (\mathbb{A}) in the form of a categorical distribution, $P(o_\tau | s_\tau) = \text{Cat}(\mathbb{A} \times s_\tau)$. \mathbb{B} is a collection of square matrices \mathbb{B}_u , where \mathbb{B}_u represents transition dynamics $P(s_t | s_{t-1}, u_{t-1} = u)$: The transition matrix (\mathbb{B}) determines the dynamics of s given the agent’s action u as $P(s_t | s_{t-1}, u_{t-1}) = \text{Cat}(\mathbb{B}_{u_{t-1}} \times s_{t-1})$. In $[\mathbb{A} \times s_\tau]$ and $[\mathbb{B}_{u_\tau} \times s_\tau]$, s_τ is represented as a one-hot vector that is multiplied through regular matrix multiplication⁴. The *Markovianity* of POMDPs means that state transitions are independent of history (i.e. state s_t only depends upon the state-action pair (s_{t-1}, u_{t-1}) and not s_{t-2}, u_{t-2} etc.).

The generative model can be summarised as follows,

$$P(o_{1:t}, s_{1:t}, u_{1:t}) = P(\mathbb{A})P(\mathbb{B})P(\mathbb{D})P(\mathbb{E}) \prod_{\tau=1}^t P(o_\tau | s_\tau, \mathbb{A}) \prod_{\tau=2}^t P(s_\tau | s_{\tau-1}, u_{\tau-1}, \mathbb{B}). \quad (\text{S1})$$

So, from the agent’s perspective, when encountering a stream of observations in time, such as $(o_1, o_2, o_3, \dots, o_t)$, as a consequence of performing a stream of actions $(u_1, u_2, u_3, \dots, u_{t-1})$, the generative model quantitatively couples and quantifies the causal relationship from action to observation through some assumed hidden states of the environment. These are called ‘hidden’ states because, in POMDPs, the agent cannot observe them directly. Based on this representation, an agent can now attempt to optimise its actions to keep receiving preferred observations.

The generative model structure used explicitly for the pong game environment is summarised below:

⁴One-hot is a group of bits among which the legal combinations of values are only those with a single high (1) bit and all the others low (0). Here, the bit (1) is allocated to the state $s = s_\tau$

- **x -axis location of the ball:** Communicated to DishBrain using a stimulation between 4-40 HZ, i.e. 37 states.
- **y -axis location of the ball:** Communicated to DishBrain through 8 sensory electrodes, i.e. 8 states.
- **y -axis location of the paddle:** Assumed to be part of DishBrain’s generative model as control is exerted, i.e. 8 states.
- **Structure:** State Space = $37 * 8 * 8$ states, Action Space = {Up, Down, Stay}

Counterfactual learning algorithm:

In the counterfactual variant of active inference, the agent learns a state-action mapping \mathbb{C}_P . For the exact form of the generative model and free energy, refer to (Isomura and Friston, 2020). This state-action mapping is learned using a ‘Risk’ parameter $\Gamma(t)$ using the update equation as given in (Isomura and Friston, 2020) as:

$$\mathbb{C}_P \leftarrow \mathbb{C}_P + t \langle (1 - 2\Gamma(t)) \langle u_t \otimes s_{t-1} \rangle \rangle. \quad (\text{S2})$$

Here, $\langle \cdot \rangle$ refers to the average over time, and \otimes is the Kronecker-product operator. Given the state-action mapping \mathbb{C}_P , agent samples actions from the distribution,

$$P(u|s)_{CL} = \sigma(\ln \mathbb{C}_P \cdot s_{t-1}). \quad (\text{S3})$$

For the complete model, refer to (Isomura and Friston, 2020). The free parameter in our model is the number of past instances (of state-action pairs) the agent stores in memory use in every time-step to learn \mathbb{C}_P in Eq.S2. In the article, we use active inference agents with memory horizons of 3 and 7.

The functional form of $\Gamma(t)$ used in the simulations of this work is:

$$\Gamma(t)_{prior} = 0.55 \quad (\text{S4})$$

The value of 0.55 corresponds to a bias of “higher risk” in the CL method. An initial value greater than 0.5 is necessary to enable learning.

For updating Γ , we use the equation,

$$\Gamma(t) \leftarrow \Gamma(t) - \frac{1}{T_{goal} - t}. \quad (\text{S5})$$

Here, T_{goal} is when the agent reaches the goal state (received a positive reward from the environment). So, the sooner the agent reaches the goal state, the quicker the $\Gamma(t)$, i.e., risk converges to zero. All the update rules defined in the paper can be derived from the postulate that the agent tries to minimise the (variational) free energy w.r.t the generative model (Paul et al., 2021; Isomura and Friston, 2020).

B Extended Data

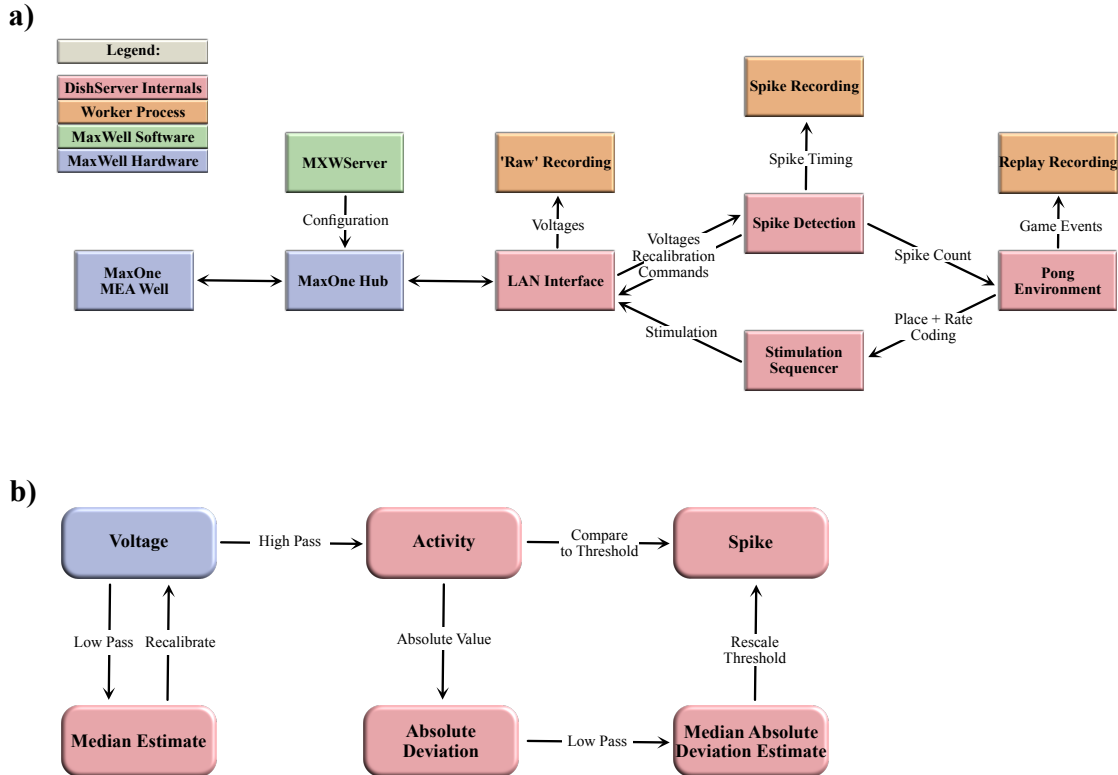


Figure S1: **DishBrain software schematics.** **a)** Software components and data flow in the *DishBrain* closed loop system. Voltage samples flow from the MEA to the ‘Pong’ environment, and sensory information flows from the ‘Pong’ environment back to the MEA, forming a closed loop. The blue rectangles mark proprietary pieces of hardware from MaxWell, including the MEA well which may contain a live culture of neurons. The green MXWServer is a piece of software provided by MaxWell which is used to configure the MEA and Hub, using a private API directly over the network. The red rectangles mark components of the ‘DishServer’ program, a high-performance program consisting of four components designed to run asynchronously, despite being run on a single CPU thread. The ‘LAN Interface’ component stores the network state, for talking to the Hub, and produces arrays of voltage values for processing. Voltage values are passed to the ‘Spike Detection’ component, which stores feedback values and spike counts, and passes recalibration commands back to the LAN Interface. When the pong environment is ready to run, it updates the state of the paddle based on the spike counts, updates the state of the ball based on its velocity and collision conditions, and re-configures the stimulation sequencer based on the relative position of the ball and current state of the game. The stimulation sequencer stores and updates indices and countdowns relating to the stimulations it must produce and converts these into commands each time the corresponding countdown reaches zero, which are finally passed back to the LAN Interface, to send to the MEA system, closing the loop. The procedures associated with each component are run one after the other in a simple loop control flow, but the ‘Pong’ environment only moves forward every 200th update, short-circuiting otherwise. Additionally, up to three worker processes are launched in parallel, depending on which parts of the system need to be recorded. They receive data from the main thread via shared memory and write it to file, allowing the main thread to continue processing data without having to hand control to the operating system and back again. **b)** Numeric operations in the real-time spike detection component of the *DishBrain* closed loop system, including multiple IIR filters. Running a virtual environment in a closed loop imposes strict performance requirements, and digital signal processing is the main bottleneck of this system, with close to 42 MB of data to process every second. Simple sequences of IIR digital filters are applied to incoming data, storing multiple arrays of 1024 feedback values in between each sample. First, spikes on the incoming data are detected by applying a high pass filter to determine the deviation of the activity and comparing that to the MAD, which is itself calculated with a subsequent low pass filter. Then, a low pass filter is applied to the original data to determine whether the MEA hardware needs to be re-calibrated, affecting future samples. This system was able to keep up with the incoming data on a single thread of an Intel Core i7-8809G. Figures adapted from (Kagan et al., 2022).

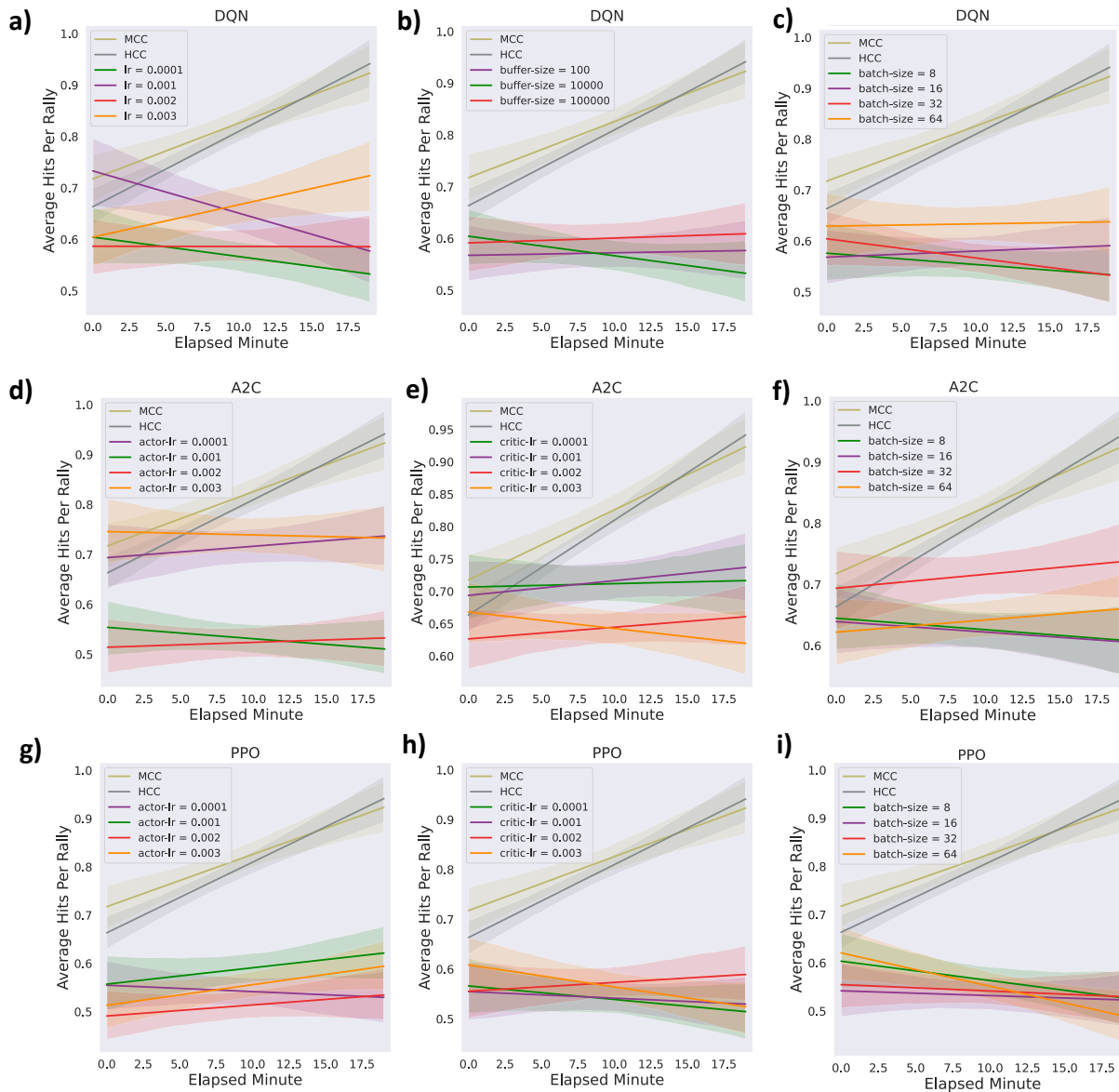


Figure S2: Hyper-parameter exploration of RL algorithms. The changes in average hits-per-rally for each RL algorithm in several sample points of the grid search space. **a)** Effects of changing the learning rate on DQN performance. replay buffer size = 10000 and batch size = 32; **b)** Effects of changing the replay buffer size on DQN performance. learning rate = 0.0001 and batch size = 32; **c)** Effects of changing the batch size on DQN performance. learning rate = 0.0001 and replay buffer size = 10000; **d)** Effects of changing the actor learning rate on A2C performance. critic learning rate = 0.001 and batch size = 32; **e)** Effects of changing the critic learning rate on A2C performance. actor learning rate = 0.0001 and batch size = 32; **f)** Effects of changing the batch size on A2C performance. actor learning rate = 0.0001 and critic learning rate = 0.001; **g)** Effects of changing the actor learning rate on PPO performance. critic learning rate = 0.001 and batch size = 32; **h)** Effects of changing the critic learning rate on PPO performance. actor learning rate = 0.0001 and batch size = 32; **i)** Effects of changing the batch size on PPO performance. actor learning rate = 0.0001 and critic learning rate = 0.001.

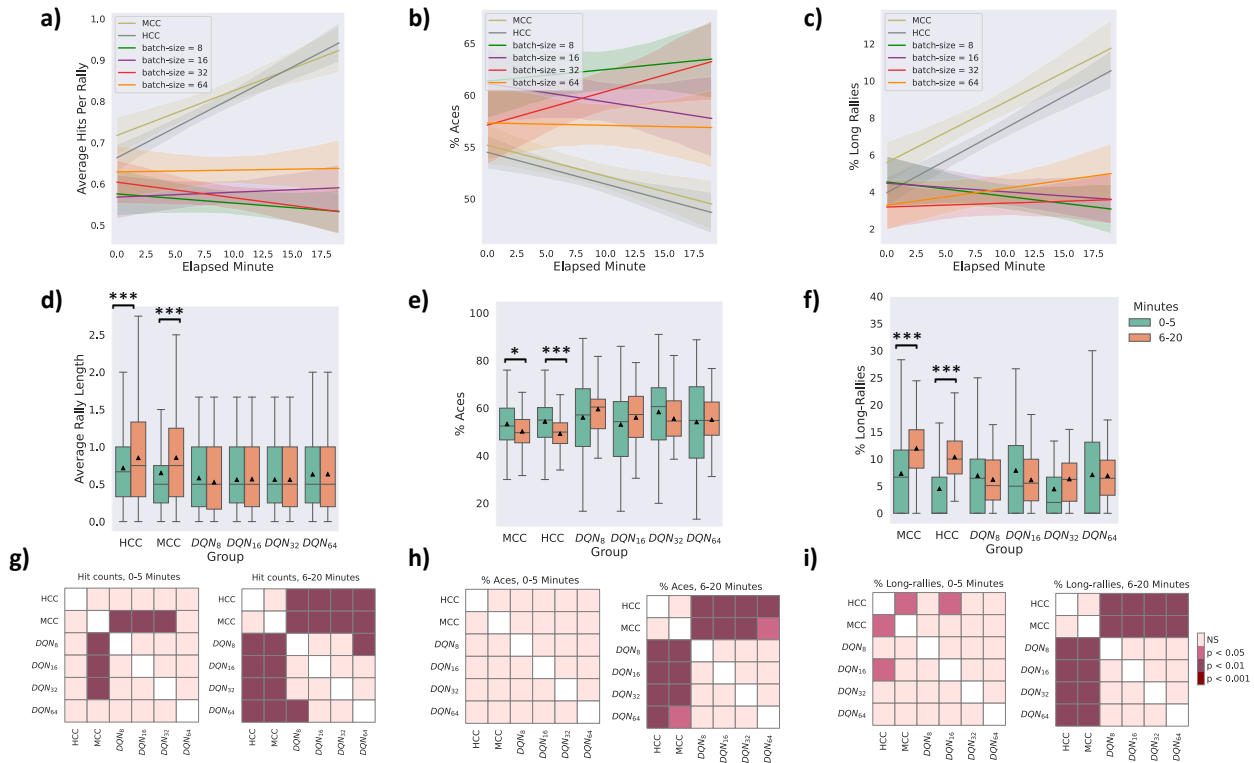


Figure S3: IMAGE INPUT to DQN - Effects of changing the batch size. The Average number of **a)** hits-per-rally, **b)** % of aces, and **c)** % of long rallies over 20 minutes real-time equivalent of training DQN with batch sizes 8, 16, 32, 64, compared to the MCC and HCC cultures. **d)** average rally length over time, **e)** Average % of aces within groups and over time. **f)** Average % of long-rallies (≥ 3) performed in a session. **g,h and i)** Pairwise Tukey's post-hoc test. Box plots show interquartile range, with bars demonstrating 1.5X interquartile range, the line marks the median and the black triangle marks the mean. Error bands = 1 SE.

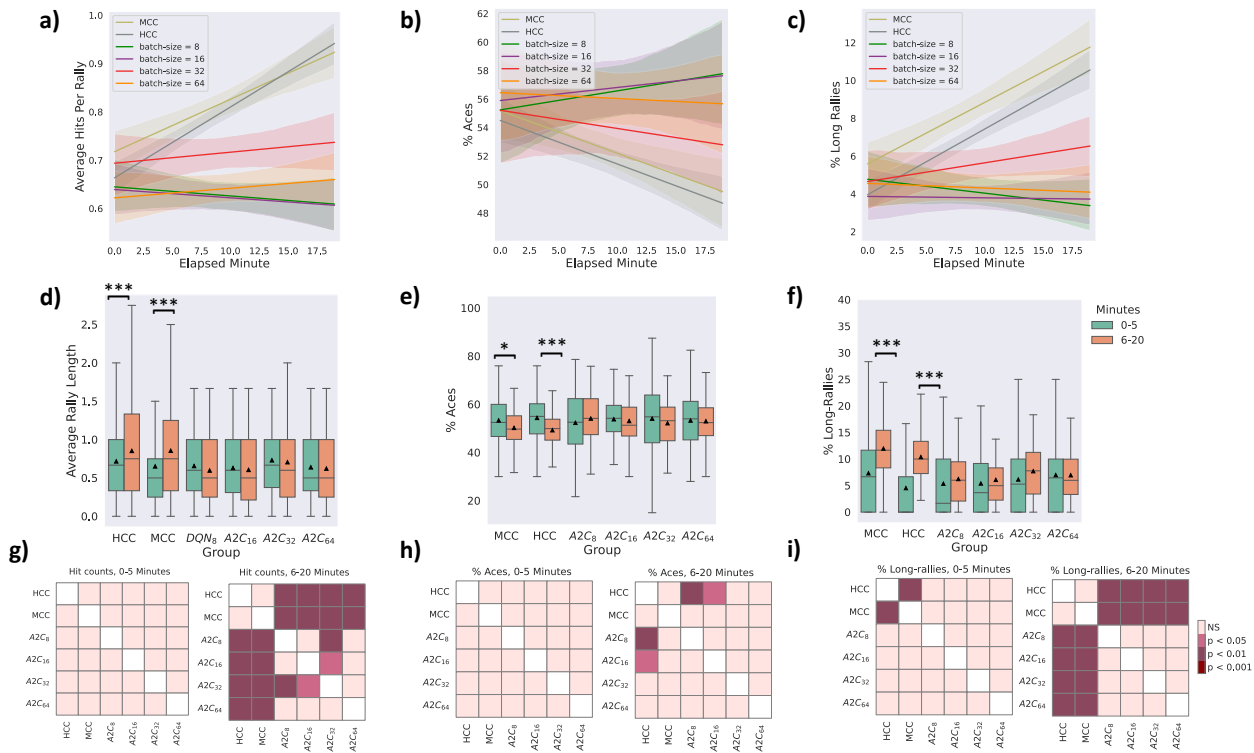


Figure S4: **IMAGE INPUT to A2C - Effects of changing the batch size.** The Average number of **a)** hits-per-rally, **b)** % of aces, and **c)** % of long rallies over 20 minutes real-time equivalent of training A2C with batch sizes 8, 16, 32, 64, compared to the MCC and HCC cultures. **d)** average rally length over time, **e)** Average % of aces within groups and over time. **f)** Average % of long-rallies (≥ 3) performed in a session. **g, h and i)** Pairwise Tukey's post-hoc test. Box plots show interquartile range, with bars demonstrating 1.5X interquartile range, the line marks the median and the black triangle marks the mean. Error bands = 1 SE.

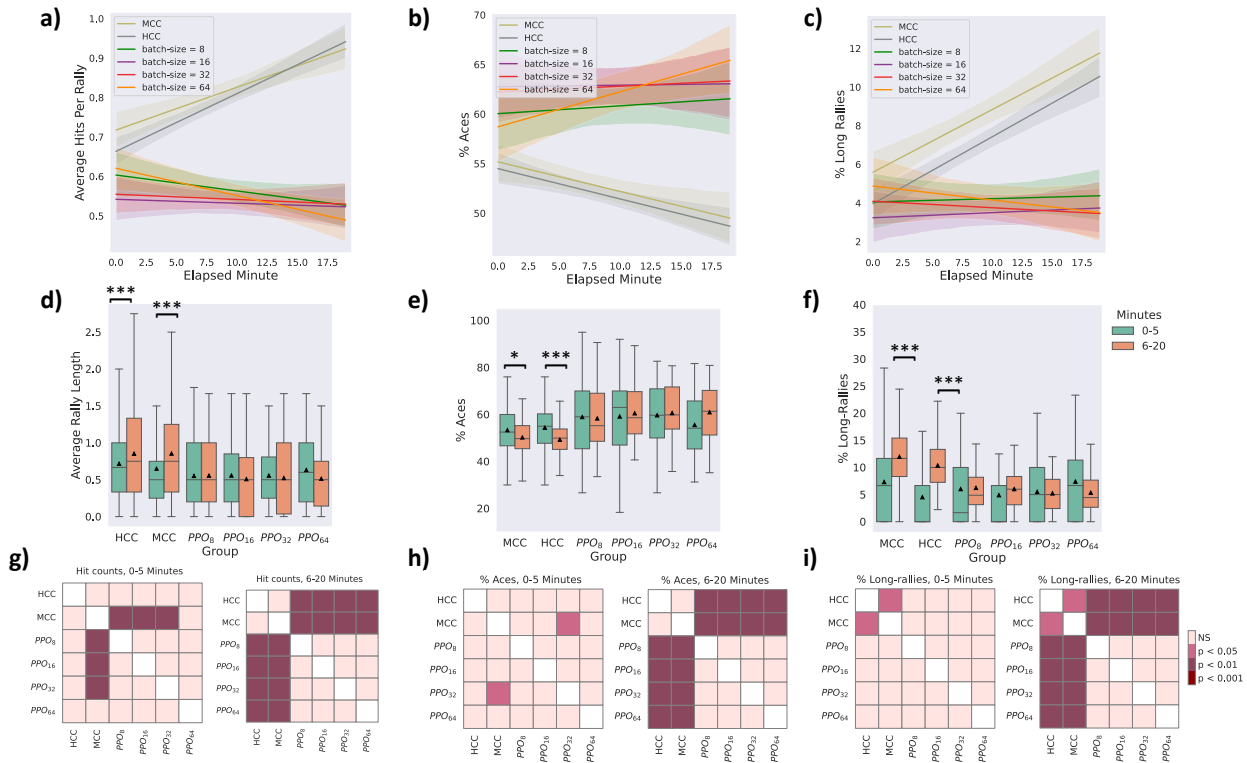


Figure S5: **IMAGE INPUT to PPO - Effects of changing the batch size.** The Average number of **a)** hits-per-rally, **b)** % of aces, and **c)** % of long rallies over 20 minutes real-time equivalent of training PPO with batch sizes 8, 16, 32, 64, compared to the MCC and HCC cultures. **d)** average rally length over time, **e)** Average % of aces within groups and over time. **f)** Average % of long-rallies (≥ 3) performed in a session. **g, h and i)** Pairwise Tukey's post-hoc test. Box plots show interquartile range, with bars demonstrating 1.5X interquartile range, the line marks the median and the black triangle marks the mean. Error bands = 1 SE.

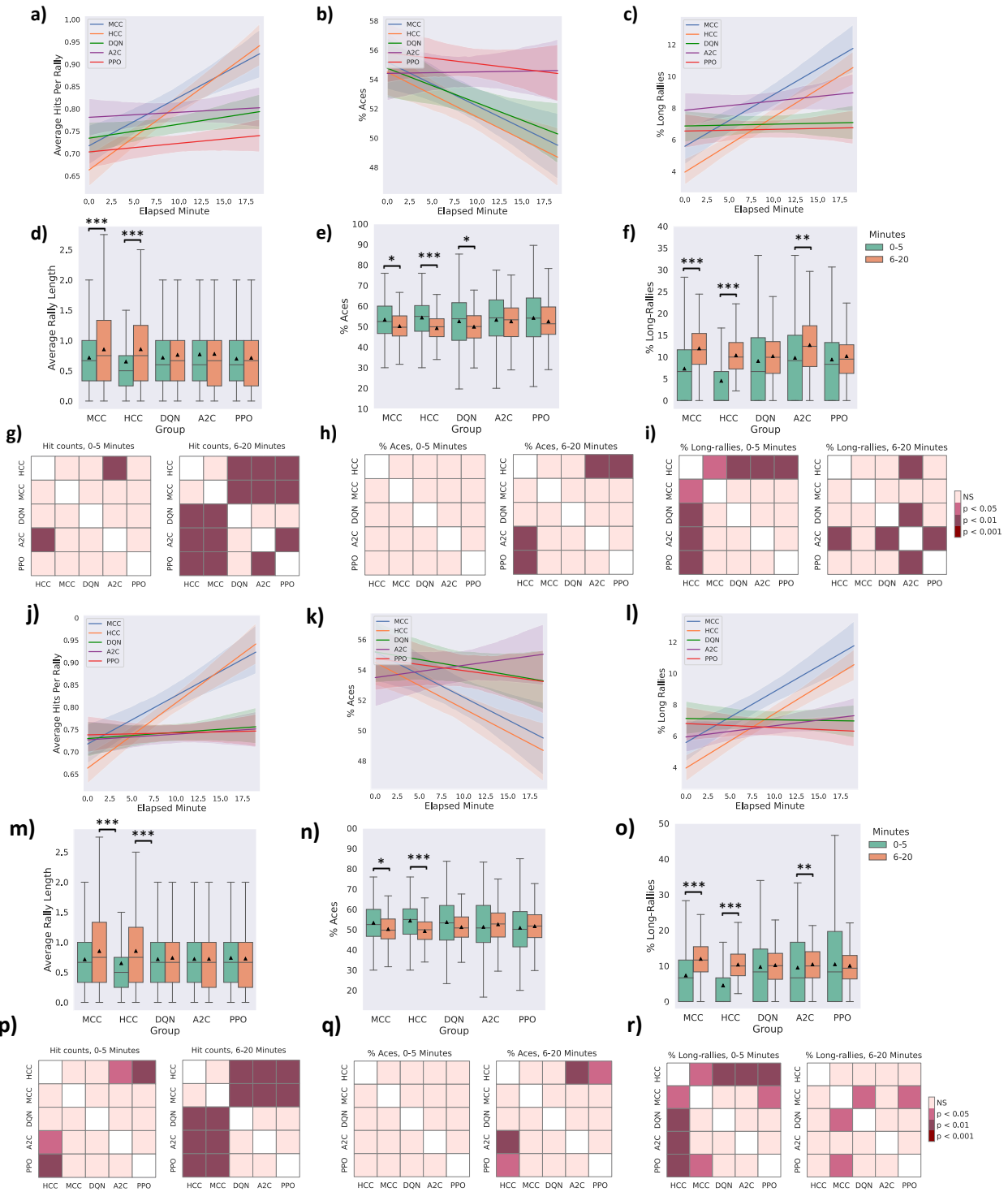


Figure S6: **Additional hidden layers in the DQN algorithm.** BALL POSITION INPUT to the RL Algorithms: The average number of **a)** hits-per-rally, **b)** % of aces, and **c)** % of long rallies over 20 minutes real-time equivalent of training DQN (2 additional hidden layers, batch size = 32), A2C, PPO, and MCC, HCC cultures. **d)** average rally length over time, **e)** Average % of aces within groups and over time. **f)** Average % of long-rallies (≥ 3) performed in a session. **g, h and i)** Pairwise Tukey's post-hoc test. PADDLE&BALL POSITION INPUT to the RL Algorithms: The average number of **j)** hits-per-rally, **k)** % of aces, and **l)** % of long rallies over 20 minutes real-time equivalent of training DQN (2 additional hidden layers, batch size = 32), A2C, PPO, and MCC, HCC cultures. **m)** average rally length over time, **n)** Average % of aces within groups and over time. **o)** Average % of long-rallies (≥ 3) performed in a session. **p, q and r)** Pairwise Tukey's post hoc test. Box plots show interquartile range, with bars demonstrating 1.5X interquartile range, the line marks the median and the black triangle marks the mean. Error bands = 1 SE.

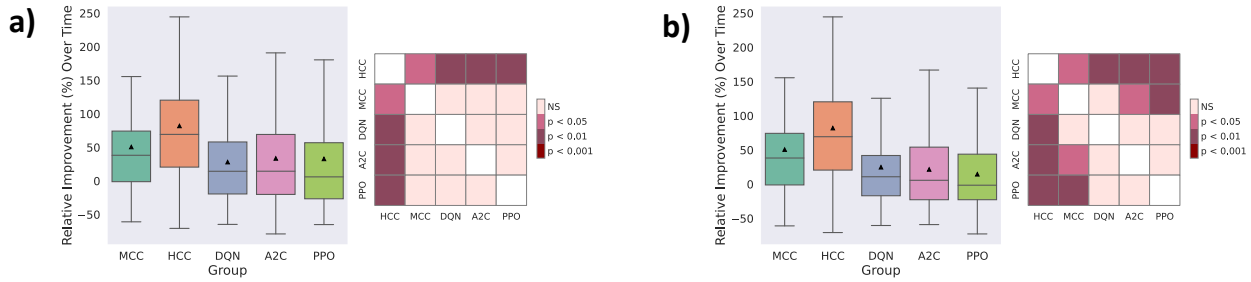


Figure S7: **Relative improvement over time with additional hidden layers in DQN algorithm.** Relative improvement (%) in the average hit counts between the first 5 minutes and the last 15 minutes of all sessions in each separate group for **a)** BALL POSITION INPUT design for DQN with 2 additional hidden layers, **b)** PADDLE&BALL POSITION INPUT design for DQN with 2 additional hidden layers.

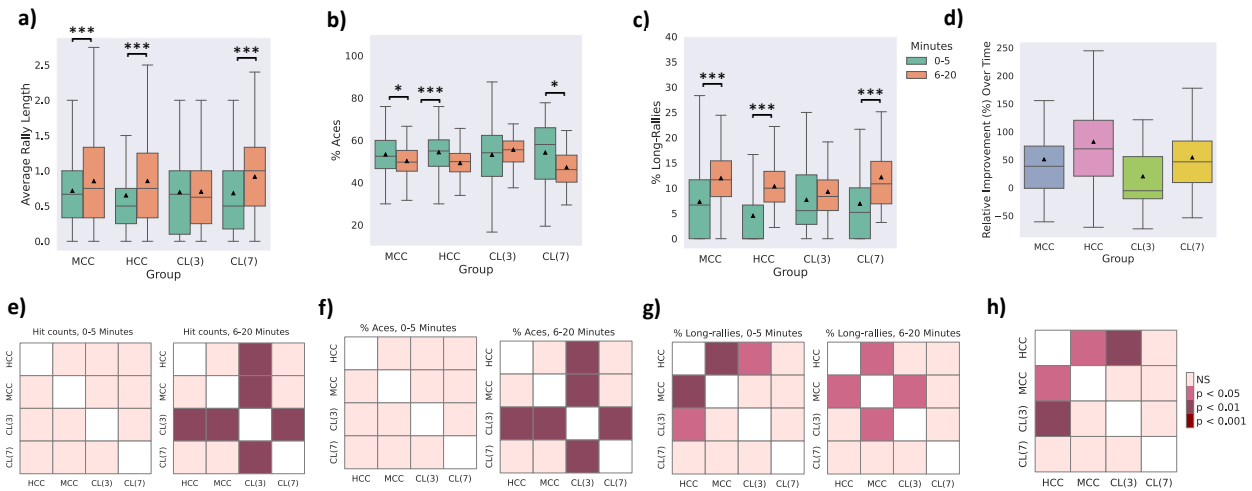


Figure S8: **Comparing Active Inference agent with biological neurons.** **a)** Average rally length over time where this within-group increase was significant for all groups except CL(3) (One-way ANOVA test, $p = 5.854e-6$, $p = 7.936e-17$, $p = 0.873$, and $p = 2.254e-6$, for MCC, HCC, CL(3), and CL(7) respectively). **b)** Average % of aces within groups and over time where this within-group increase was significant only for HCC, MCC, and CL(7) groups (One-way ANOVA test, $p = 0.014$, $p = 2.907e-08$, $p = 0.380$, and $p = 0.016$, for MCC, HCC, CL(3), and CL(7) respectively). **c)** Average % of long-rallies (≥ 3) performed in a session where the increase over time was significant for all groups except CL(3) (One-way ANOVA test, $p = 1.172e-7$, $p = 1.525e-24$, $p = 0.253$, and $p = 8.944e-4$ for MCC, HCC, CL(3), and CL(7), respectively). **d)** Relative improvement (%) in the average hit counts between the first 5 minutes and the last 15 minutes of all sessions in each separate group. **e,f,g and h)** Pairwise post hoc tests. Box plots show interquartile range, with bars demonstrating 1.5X interquartile range, the line marks the median and the black triangle marks the mean. Error bands = 1 SE.

Table S2. Follow up main and supplementary text post-hoc tests for multivariate tests, including means, standard error (SE), t-scores, degree of freedom and exact p-values with hedges.

Figure	Panel	Parameters	Source	A	B	Mean (A)	Mean (B)	diff	se	T	p-val	hedges	Method		
2	h	Hit Counts	0-5 Minutes	A2C	DQN	0.705	0.709	-0.004	0.027	-0.147	0.900	-0.008	Tukey's		
				A2C	HCC	0.705	0.651	0.055	0.025	2.151	0.199	0.110			
				A2C	MCC	0.705	0.716	-0.011	0.029	-0.373	0.900	-0.021			
				A2C	PPO	0.705	0.716	-0.011	0.029	-0.388	0.900	-0.022			
				DQN	HCC	0.709	0.651	0.059	0.025	2.310	0.142	0.117			
				DQN	MCC	0.709	0.716	-0.007	0.029	-0.237	0.900	-0.014			
				DQN	PPO	0.709	0.716	-0.007	0.029	-0.251	0.900	-0.014			
				HCC	MCC	0.651	0.716	-0.065	0.027	-2.386	0.120	-0.131			
				HCC	PPO	0.651	0.716	-0.066	0.027	-2.410	0.113	-0.132			
				MCC	PPO	0.716	0.716	-0.000	0.030	-0.013	0.900	-0.001			
			6-20 Minutes	A2C	DQN	0.738	0.738	0.000	0.018	0.004	0.900	0.000			
				A2C	HCC	0.738	0.854	-0.117	0.017	-6.726	0.001	-0.198			
				A2C	MCC	0.738	0.852	-0.115	0.020	-5.715	0.001	-0.194			
				A2C	PPO	0.738	0.709	0.029	0.019	1.506	0.551	0.049			
				DQN	HCC	0.738	0.854	-0.117	0.017	-6.737	0.001	-0.198			
				DQN	MCC	0.738	0.852	-0.115	0.020	-5.723	0.001	-0.194			
				DQN	PPO	0.738	0.709	0.029	0.019	1.503	0.552	0.049			
				HCC	MCC	0.854	0.852	0.002	0.020	0.101	0.900	0.003			
				HCC	PPO	0.854	0.709	0.146	0.019	7.818	0.001	0.246			
				MCC	PPO	0.852	0.709	0.144	0.021	6.778	0.001	0.243			
	i	% Aces		0-5 Minutes	A2C	DQN	51.842	52.190	-0.347	1.425	-0.244	0.900		-0.028	Tukey's
					A2C	HCC	51.842	54.382	-2.539	1.375	-1.847	0.348		-0.205	
					A2C	MCC	51.842	53.333	-1.490	1.549	-0.962	0.859		-0.120	
					A2C	PPO	51.842	54.731	-2.889	1.425	-2.028	0.254		-0.234	
					DQN	HCC	52.190	54.382	-2.192	1.375	-1.595	0.501		-0.177	
					DQN	MCC	52.190	53.333	-1.143	1.549	-0.738	0.900		-0.092	
					DQN	PPO	52.190	54.731	-2.542	1.425	-1.784	0.385		-0.205	
					HCC	MCC	54.382	53.333	1.049	1.503	0.698	0.900		0.085	
HCC					PPO	54.382	54.731	-0.350	1.375	-0.254	0.900	-0.028			
MCC					PPO	53.333	54.731	-1.399	1.549	-0.903	0.893	-0.113			
6-20 Minutes				A2C	DQN	50.284	50.136	0.148	0.946	0.157	0.900	0.018			
				A2C	HCC	50.284	49.259	1.025	0.912	1.123	0.768	0.125			
				A2C	MCC	50.284	50.232	0.052	1.028	0.051	0.900	0.006			
				A2C	PPO	50.284	53.254	-2.970	0.946	-3.141	0.015	-0.362			
				DQN	HCC	50.136	49.259	0.877	0.912	0.961	0.860	0.107			
				DQN	MCC	50.136	50.232	-0.096	1.028	-0.093	0.900	-0.012			
				DQN	PPO	50.136	53.254	-3.118	0.946	-3.298	0.009	-0.380			
				HCC	MCC	49.259	50.232	-0.973	0.998	-0.975	0.852	-0.118			
				HCC	PPO	49.259	53.254	-3.995	0.912	-4.378	0.001	-0.487			
				MCC	PPO	50.232	53.254	-3.022	1.028	-2.940	0.028	-0.368			

Biological Neurons Vs. Deep Reinforcement Learning

3	j	% Long Rally	0-5 Minute s	A2C	DQN	7.421	9.789	-2.368	0.913	-2.594	0.073	-0.299	Tukey's
				A2C	HCC	7.421	4.523	2.898	0.881	3.290	0.009	0.366	
				A2C	MCC	7.421	7.318	0.103	0.993	0.103	0.900	0.013	
				A2C	PPO	7.421	8.122	-0.701	0.913	-0.767	0.900	-0.088	
				DQN	HCC	9.789	4.523	5.267	0.881	5.978	0.001	0.665	
				DQN	MCC	9.789	7.318	2.471	0.993	2.489	0.094	0.312	
				DQN	PPO	9.789	8.122	1.667	0.913	1.826	0.360	0.210	
				HCC	MCC	4.523	7.318	-2.796	0.963	-2.903	0.031	-0.353	
				HCC	PPO	4.523	8.122	-3.599	0.881	-4.085	0.001	-0.454	
				MCC	PPO	7.318	8.122	-0.803	0.993	-0.809	0.900	-0.101	
			6-20 Minute s	A2C	DQN	10.034	10.248	-0.214	0.623	-0.344	0.900	-0.040	
				A2C	HCC	10.034	10.365	-0.331	0.601	-0.550	0.900	-0.061	
				A2C	MCC	10.034	11.972	-1.938	0.677	-2.863	0.035	-0.358	
				A2C	PPO	10.034	8.506	1.528	0.623	2.454	0.102	0.283	
				DQN	HCC	10.248	10.365	-0.116	0.601	-0.194	0.900	-0.022	
				DQN	MCC	10.248	11.972	-1.724	0.677	-2.547	0.082	-0.319	
				DQN	PPO	10.248	8.506	1.743	0.623	2.798	0.042	0.322	
				HCC	MCC	10.365	11.972	-1.608	0.657	-2.447	0.104	-0.297	
				HCC	PPO	10.365	8.506	1.859	0.601	3.094	0.017	0.344	
				MCC	PPO	11.972	8.506	3.467	0.677	5.121	0.001	0.641	
3	h	Hit Counts	0-5 Minute s	A2C	DQN	0.722	0.713	0.009	0.027	0.325	0.900	0.017	Tukey's
				A2C	HCC	0.722	0.651	0.072	0.026	2.761	0.046	0.141	
				A2C	MCC	0.722	0.716	0.006	0.029	0.216	0.900	0.012	
				A2C	PPO	0.722	0.740	-0.018	0.027	-0.641	0.900	-0.035	
				DQN	HCC	0.713	0.651	0.063	0.026	2.428	0.108	0.123	
				DQN	MCC	0.713	0.716	-0.003	0.029	-0.087	0.900	-0.005	
				DQN	PPO	0.713	0.740	-0.026	0.027	-0.968	0.856	-0.052	
				HCC	MCC	0.651	0.716	-0.065	0.028	-2.335	0.134	-0.128	
				HCC	PPO	0.651	0.740	-0.089	0.026	-3.428	0.006	-0.175	
				MCC	PPO	0.716	0.740	-0.024	0.029	-0.815	0.900	-0.047	
			6-20 Minute s	A2C	DQN	0.724	0.716	0.008	0.018	0.415	0.900	0.013	
				A2C	HCC	0.724	0.854	-0.131	0.018	-7.461	0.001	-0.220	
				A2C	MCC	0.724	0.852	-0.129	0.020	-6.354	0.001	-0.216	
				A2C	PPO	0.724	0.727	-0.004	0.018	-0.217	0.900	-0.007	
				DQN	HCC	0.716	0.854	-0.138	0.017	-7.918	0.001	-0.232	
				DQN	MCC	0.716	0.852	-0.136	0.020	-6.743	0.001	-0.229	
				DQN	PPO	0.716	0.727	-0.011	0.018	-0.633	0.900	-0.019	
				HCC	MCC	0.854	0.852	0.002	0.020	0.100	0.900	0.003	
				HCC	PPO	0.854	0.727	0.127	0.018	7.233	0.001	0.213	
				MCC	PPO	0.852	0.727	0.125	0.020	6.158	0.001	0.210	
3	i	% Aces	0-5 Minute s	A2C	DQN	51.318	54.016	-2.698	1.469	-1.837	0.354	-0.212	Tukey's
				A2C	HCC	51.318	54.382	-3.064	1.417	-2.162	0.196	-0.240	
				A2C	MCC	51.318	53.333	-2.014	1.597	-1.262	0.690	-0.158	
				A2C	PPO	51.318	50.866	0.453	1.469	0.308	0.900	0.035	
				DQN	HCC	54.016	54.382	-0.366	1.417	-0.258	0.900	-0.029	
				DQN	MCC	54.016	53.333	0.683	1.597	0.428	0.900	0.054	

Biological Neurons Vs. Deep Reinforcement Learning

			6-20 Minute s	DQN	PPO	54.016	50.866	3.150	1.469	2.145	0.202	0.247	Tukey's				
				HCC	MCC	54.382	53.333	1.049	1.550	0.677	0.900	0.082					
				HCC	PPO	54.382	50.866	3.516	1.417	2.481	0.096	0.276					
				MCC	PPO	53.333	50.866	2.467	1.597	1.545	0.529	0.193					
				A2C	DQN	52.596	53.001	-0.404	0.919	-0.440	0.900	-0.051					
				A2C	HCC	52.596	49.259	3.337	0.887	3.762	0.002	0.418					
				A2C	MCC	52.596	50.232	2.364	0.999	2.366	0.126	0.296					
				A2C	PPO	52.596	51.658	0.938	0.919	1.020	0.826	0.118					
				DQN	HCC	53.001	49.259	3.741	0.887	4.218	0.001	0.469					
				DQN	MCC	53.001	50.232	2.769	0.999	2.771	0.045	0.347					
				DQN	PPO	53.001	51.658	1.342	0.919	1.460	0.577	0.168					
				HCC	MCC	49.259	50.232	-0.973	0.970	-1.003	0.836	-0.122					
			HCC	PPO	49.259	51.658	-2.399	0.887	-2.705	0.054	-0.301						
			MCC	PPO	50.232	51.658	-1.427	0.999	-1.428	0.595	-0.179						
			j	% Long Rally	0-5 Minute s	A2C	DQN	9.519	10.105	-0.586	0.990	-0.591		0.900	-0.068	Tukey's	
						A2C	HCC	9.519	4.523	4.997	0.955	5.230		0.001	0.581		
						A2C	MCC	9.519	7.318	2.201	1.076	2.045		0.246	0.256		
						A2C	PPO	9.519	10.462	-0.942	0.990	-0.952		0.865	-0.110		
						DQN	HCC	10.105	4.523	5.582	0.955	5.843		0.001	0.650		
						DQN	MCC	10.105	7.318	2.787	1.076	2.589		0.074	0.324		
						DQN	PPO	10.105	10.462	-0.357	0.990	-0.360		0.900	-0.042		
						HCC	MCC	4.523	7.318	-2.796	1.044	-2.677		0.059	-0.325		
						HCC	PPO	4.523	10.462	-5.939	0.955	-6.217		0.001	-0.691		
						MCC	PPO	7.318	10.462	-3.144	1.076	-2.921		0.030	-0.366		
6-20 Minute s	A2C	DQN				10.431	11.238	-0.807	0.616	-1.311	0.661	-0.151					
	A2C	HCC				10.431	10.365	0.066	0.594	0.111	0.900	0.012					
	A2C	MCC			10.431	11.972	-1.541	0.669	-2.303	0.145	-0.288						
	A2C	PPO			10.431	10.049	0.382	0.616	0.620	0.900	0.071						
	DQN	HCC			11.238	10.365	0.873	0.594	1.470	0.571	0.163						
	DQN	MCC			11.238	11.972	-0.734	0.669	-1.097	0.783	-0.137						
	DQN	PPO			11.238	10.049	1.189	0.616	1.931	0.302	0.222						
	HCC	MCC			10.365	11.972	-1.608	0.649	-2.475	0.097	-0.301						
	HCC	PPO			10.365	10.049	0.316	0.594	0.531	0.900	0.059						
	MCC	PPO			11.972	10.049	1.923	0.669	2.873	0.034	0.360						
	4	h			Hit Counts	0-5 Minute s	A2C	DQN	0.771	0.687	0.084	0.028	2.980	0.024	0.159		Tukey's
							A2C	HCC	0.771	0.651	0.121	0.027	4.507	0.001	0.229		
A2C							MCC	0.771	0.716	0.055	0.030	1.826	0.359	0.105			
A2C							PPO	0.771	0.698	0.073	0.028	2.593	0.072	0.139			
DQN			HCC	0.687			0.651	0.037	0.027	1.371	0.628	0.070					
DQN			MCC	0.687			0.716	-0.029	0.030	-0.951	0.866	-0.055					
DQN			PPO	0.687			0.698	-0.011	0.028	-0.375	0.900	-0.020					
HCC			MCC	0.651			0.716	-0.065	0.029	-2.262	0.158	-0.124					
HCC			PPO	0.651			0.698	-0.047	0.027	-1.759	0.399	-0.090					
MCC			PPO	0.716			0.698	0.018	0.030	0.598	0.900	0.034					
6-20 Minute s			A2C	DQN			0.777	0.687	0.090	0.018	4.982	0.001	0.150				
			A2C	HCC			0.777	0.854	-0.077	0.018	-4.348	0.001	-0.128				

Biological Neurons Vs. Deep Reinforcement Learning

				A2C	MCC	0.777	0.852	-0.075	0.020	-3.662	0.002	-0.125		
				A2C	PPO	0.777	0.712	0.065	0.018	3.576	0.003	0.108		
				DQN	HCC	0.687	0.854	-0.167	0.018	-9.521	0.001	-0.278		
				DQN	MCC	0.687	0.852	-0.165	0.020	-8.119	0.001	-0.275		
				DQN	PPO	0.687	0.712	-0.025	0.018	-1.389	0.617	-0.042		
				HCC	MCC	0.854	0.852	0.002	0.020	0.099	0.900	0.003		
				HCC	PPO	0.854	0.712	0.142	0.018	8.044	0.001	0.236		
				MCC	PPO	0.852	0.712	0.140	0.020	6.854	0.001	0.233		
i	% Aces	0-5 Minute s	A2C	DQN	53.293	55.443	-2.150	1.473	-1.459	0.577	-0.168	Tukey's		
			A2C	HCC	53.293	54.382	-1.089	1.422	-0.766	0.900	-0.085			
			A2C	MCC	53.293	53.333	-0.040	1.602	-0.025	0.900	-0.003			
			A2C	PPO	53.293	54.248	-0.956	1.473	-0.649	0.900	-0.075			
			DQN	HCC	55.443	54.382	1.061	1.422	0.746	0.900	0.083			
			DQN	MCC	55.443	53.333	2.110	1.602	1.317	0.658	0.165			
			DQN	PPO	55.443	54.248	1.194	1.473	0.811	0.900	0.093			
			HCC	MCC	54.382	53.333	1.049	1.554	0.675	0.900	0.082			
			HCC	PPO	54.382	54.248	0.133	1.422	0.094	0.900	0.010			
			MCC	PPO	53.333	54.248	-0.916	1.602	-0.572	0.900	-0.072			
				6-20 Minute s	A2C	DQN	52.530	53.879	-1.349	0.966	-1.397		0.613	-0.161
					A2C	HCC	52.530	49.259	3.270	0.932	3.508		0.004	0.390
					A2C	MCC	52.530	50.232	2.298	1.050	2.188		0.185	0.274
					A2C	PPO	52.530	52.511	0.018	0.966	0.019		0.900	0.002
					DQN	HCC	53.879	49.259	4.620	0.932	4.955		0.001	0.551
					DQN	MCC	53.879	50.232	3.647	1.050	3.472		0.005	0.435
					DQN	PPO	53.879	52.511	1.368	0.966	1.415		0.602	0.163
					HCC	MCC	49.259	50.232	-0.973	1.019	-0.954		0.864	-0.116
					HCC	PPO	49.259	52.511	-3.252	0.932	-3.488		0.005	-0.388
					MCC	PPO	50.232	52.511	-2.280	1.050	-2.170		0.192	-0.272
j	% Long Rally	0-5 Minute s	A2C	DQN	9.810	9.554	0.256	0.935	0.274	0.900	0.032	Tukey's		
			A2C	HCC	9.810	4.523	5.288	0.902	5.861	0.001	0.652			
			A2C	MCC	9.810	7.318	2.492	1.016	2.452	0.103	0.307			
			A2C	PPO	9.810	9.403	0.408	0.935	0.436	0.900	0.050			
			DQN	HCC	9.554	4.523	5.032	0.902	5.577	0.001	0.620			
			DQN	MCC	9.554	7.318	2.236	1.016	2.200	0.181	0.275			
			DQN	PPO	9.554	9.403	0.151	0.935	0.162	0.900	0.019			
			HCC	MCC	4.523	7.318	-2.796	0.986	-2.834	0.038	-0.344			
			HCC	PPO	4.523	9.403	-4.880	0.902	-5.410	0.001	-0.601			
			MCC	PPO	7.318	9.403	-2.085	1.016	-2.051	0.243	-0.257			
				6-20 Minute s	A2C	DQN	12.722	9.511	3.211	0.632	5.083		0.001	0.585
					A2C	HCC	12.722	10.365	2.357	0.610	3.868		0.001	0.430
					A2C	MCC	12.722	11.972	0.750	0.687	1.092		0.786	0.137
					A2C	PPO	12.722	10.183	2.540	0.632	4.020		0.001	0.463
					DQN	HCC	9.511	10.365	-0.854	0.610	-1.401		0.611	-0.156
					DQN	MCC	9.511	11.972	-2.461	0.687	-3.584		0.003	-0.449
					DQN	PPO	9.511	10.183	-0.672	0.632	-1.063		0.802	-0.122
					HCC	MCC	10.365	11.972	-1.608	0.666	-2.412		0.113	-0.293

Biological Neurons Vs. Deep Reinforcement Learning

5	a	Average Paddle Movement	HCC	PPO	10.365	10.183	0.182	0.610	0.299	0.900	0.033	Tukey's
			MCC	PPO	11.972	10.183	1.790	0.687	2.606	0.070	0.326	
			A2C	DQN	71606.154	75257.436	-3651.282	4997.725	-0.731	0.900	-0.164	
			A2C	HCC	71606.154	52000.427	19605.727	3783.228	5.182	0.001	0.886	
			A2C	MCC	71606.154	50007.504	21598.650	4190.720	5.154	0.001	0.973	
			A2C	PPO	71606.154	72712.500	-1106.346	4966.391	-0.223	0.900	-0.050	
			DQN	HCC	75257.436	52000.427	23257.009	3783.228	6.147	0.001	1.051	
			DQN	MCC	75257.436	50007.504	25249.932	4190.720	6.025	0.001	1.138	
			DQN	PPO	75257.436	72712.500	2544.936	4966.391	0.512	0.900	0.114	
			HCC	MCC	52000.427	50007.504	1992.923	2626.345	0.759	0.900	0.090	
HCC	PPO	52000.427	72712.500	-20712.073	3741.737	-5.535	0.001	-0.936				
MCC	PPO	50007.504	72712.500	-22704.996	4153.302	-5.467	0.001	-1.023				
b	Relative improvement (%) in the average hit counts	A2C	DQN	29.919	24.634	5.285	7.934	288.957	0.900	0.077	Games Howell	
		A2C	HCC	29.919	82.147	-52.227	9.623	316.974	0.001	-0.603		
		A2C	MCC	29.919	50.755	-20.836	9.830	223.464	0.215	-0.265		
		A2C	PPO	29.919	21.602	8.318	7.665	279.006	0.789	0.125		
		DQN	HCC	24.634	82.147	-57.512	9.026	296.959	0.001	-0.708		
		DQN	MCC	24.634	50.755	-26.121	9.246	197.121	0.041	-0.354		
		DQN	PPO	24.634	21.602	3.033	6.900	295.706	0.900	0.051		
		HCC	MCC	82.147	50.755	31.391	10.731	262.994	0.030	0.355		
		HCC	PPO	82.147	21.602	60.545	8.791	284.214	0.001	0.766		
		MCC	PPO	50.755	21.602	29.154	9.016	184.940	0.012	0.405		
c	Average Paddle Movement	A2C	DQN	78719.250	83859.000	-5139.750	4264.838	-1.205	0.722	-0.267	Tukey's	
		A2C	HCC	78719.250	52000.427	26718.823	3233.710	8.263	0.001	1.397		
		A2C	MCC	78719.250	50007.504	28711.746	3589.396	7.999	0.001	1.497		
		A2C	PPO	78719.250	75665.500	3053.750	4264.838	0.716	0.900	0.159		
		DQN	HCC	83859.000	52000.427	31858.573	3233.710	9.852	0.001	1.666		
		DQN	MCC	83859.000	50007.504	33851.496	3589.396	9.431	0.001	1.765		
		DQN	PPO	83859.000	75665.500	8193.500	4264.838	1.921	0.307	0.425		
		HCC	MCC	52000.427	50007.504	1992.923	2269.758	0.878	0.900	0.104		

Biological Neurons Vs. Deep Reinforcement Learning

			HCC	PPO	52000.4 27	75665.5 00	- 23665 .073	3233. 710	-7.318	0.001	-1.238	
			MCC	PPO	50007.5 04	75665.5 00	- 25657 .996	3589. 396	-7.148	0.001	-1.338	
d	Relative improvement (%) in the average hit counts- Paddle&Ball Position Input		A2C	DQN	21.717	36.623	- 14.90 6	10.28 6	245.4 47	0.584	-0.167	Games Howell
			A2C	HCC	21.717	82.147	- 60.42 9	9.165	303.1 51	0.001	-0.733	
			A2C	MCC	21.717	50.755	- 29.03 8	9.381	203.8 60	0.019	-0.387	
			A2C	PPO	21.717	14.690	7.027	7.082	292.7 73	0.842	0.114	
			DQN	HCC	36.623	82.147	- 45.52 3	11.53 1	304.5 65	0.001	-0.439	
			DQN	MCC	36.623	50.755	- 14.13 2	11.70 3	257.8 34	0.720	-0.151	
			DQN	PPO	36.623	14.690	21.93 3	9.955	226.5 46	0.182	0.254	
			HCC	MCC	82.147	50.755	31.39 1	10.73 1	262.9 94	0.030	0.355	
			HCC	PPO	82.147	14.690	67.45 6	8.792	284.2 59	0.001	0.853	
			MCC	PPO	50.755	14.690	36.06 5	9.017	184.9 81	0.001	0.501	
e	Average Paddle Movement		A2C	DQN	67718.7 50	75019.2 50	- 7300. 500	4333. 263	-1.685	0.446	-0.373	Tukey's
			A2C	HCC	67718.7 50	52000.4 27	15718 .323	3285. 592	4.784	0.001	0.809	
			A2C	MCC	67718.7 50	50007.5 04	17711 .246	3646. 984	4.856	0.001	0.909	
			A2C	PPO	67718.7 50	73952.2 50	- 6233. 500	4333. 263	-1.439	0.589	-0.319	
			DQN	HCC	75019.2 50	52000.4 27	23018 .823	3285. 592	7.006	0.001	1.185	
			DQN	MCC	75019.2 50	50007.5 04	25011 .746	3646. 984	6.858	0.001	1.283	
			DQN	PPO	75019.2 50	73952.2 50	1067. 000	4333. 263	0.246	0.900	0.055	
			HCC	MCC	52000.4 27	50007.5 04	1992. 923	2306. 174	0.864	0.900	0.103	
			HCC	PPO	52000.4 27	73952.2 50	- 21951 .823	3285. 592	-6.681	0.001	-1.130	
			MCC	PPO	50007.5 04	73952.2 50	- 23944 .746	3646. 984	-6.566	0.001	-1.229	
f	Relative improvement (%) in the average hit counts- Ball Position Input		A2C	DQN	33.724	29.397	4.327	9.789	297.5 13	0.900	0.051	Games Howell
			A2C	HCC	33.724	82.147	- 48.42 3	10.07 7	321.8 71	0.001	-0.534	
			A2C	MCC	33.724	50.755	- 17.03 1	10.27 4	238.3 11	0.464	-0.207	
			A2C	PPO	33.724	33.016	0.709	10.30 1	292.7 92	0.900	0.008	
			DQN	HCC	29.397	82.147	- 52.74 9	10.26 8	321.8 66	0.001	-0.571	

Biological Neurons Vs. Deep Reinforcement Learning

				DQN	MCC	29.397	50.755	-21.358	10.461	243.172	0.249	-0.256		
				DQN	PPO	29.397	33.016	-3.618	10.487	295.423	0.900	-0.040		
				HCC	MCC	82.147	50.755	31.391	10.731	262.994	0.030	0.355		
				HCC	PPO	82.147	33.016	49.131	10.756	317.852	0.001	0.508		
				MCC	PPO	50.755	33.016	17.740	10.941	252.147	0.486	0.203		
6	a	Relative improvement (%) in the average hit counts – DQN		<i>DQN_16</i>	<i>DQN_32</i>	6.400	43.207	-36.806	17.554	75.733	0.300	-0.416	Games Howell	
				<i>DQN_16</i>	<i>DQN_64</i>	6.400	22.119	-15.719	13.194	94.597	0.820	-0.236		
				<i>DQN_16</i>	<i>DQN_8</i>	6.400	12.525	-6.124	12.502	97.075	0.900	-0.097		
				<i>DQN_16</i>	HCC	6.400	82.147	-75.746	11.229	133.216	0.001	-1.079		
				<i>DQN_16</i>	MCC	6.400	50.755	-44.355	11.407	126.260	0.002	-0.660		
				<i>DQN_32</i>	<i>DQN_64</i>	43.207	22.119	21.088	18.470	84.890	0.848	0.227		
				<i>DQN_32</i>	<i>DQN_8</i>	43.207	12.525	30.682	17.983	80.300	0.527	0.339		
				<i>DQN_32</i>	HCC	43.207	82.147	-38.940	17.122	73.462	0.218	-0.364		
				<i>DQN_32</i>	MCC	43.207	50.755	-7.549	17.239	74.550	0.900	-0.074		
				<i>DQN_64</i>	<i>DQN_8</i>	22.119	12.525	9.594	13.759	97.145	0.900	0.138		
	<i>DQN_64</i>	HCC	22.119	82.147	-60.027	12.614	106.983	0.001	-0.761					
	<i>DQN_64</i>	MCC	22.119	50.755	-28.636	12.772	105.863	0.228	-0.381					
	<i>DQN_8</i>	HCC	12.525	82.147	-69.622	11.889	118.917	0.001	-0.936					
	<i>DQN_8</i>	MCC	12.525	50.755	-38.231	12.057	115.635	0.023	-0.538					
					HCC	MCC	82.147	50.755	31.391	10.731	262.994	0.043	0.355	
	b	Relative improvement (%) in the average hit counts – A2C			<i>A2C_16</i>	<i>A2C_32</i>	18.203	23.304	-5.101	11.700	97.985	0.900	-0.087	Games Howell
					<i>A2C_16</i>	<i>A2C_64</i>	18.203	23.700	-5.497	13.380	92.457	0.900	-0.082	
					<i>A2C_16</i>	<i>A2C_8</i>	18.203	13.710	4.493	10.929	96.325	0.900	0.082	
					<i>A2C_16</i>	HCC	18.203	82.147	-63.944	11.098	136.551	0.001	-0.921	
					<i>A2C_16</i>	MCC	18.203	50.755	-32.552	11.277	128.559	0.051	-0.490	
<i>A2C_32</i>					<i>A2C_64</i>	23.304	23.700	-0.396	13.444	92.951	0.900	-0.006		
<i>A2C_32</i>					<i>A2C_8</i>	23.304	13.710	9.594	11.007	96.006	0.900	0.173		

Biological Neurons Vs. Deep Reinforcement Learning

				A2C_32	HCC	23.304	82.147	-58.843	11.175	134.580	0.001	-0.842	
				A2C_32	MCC	23.304	50.755	-27.452	11.353	127.209	0.158	-0.410	
				A2C_64	A2C_8	23.700	13.710	9.990	12.778	86.482	0.900	0.155	
				A2C_64	HCC	23.700	82.147	-58.446	12.923	102.820	0.001	-0.723	
				A2C_64	MCC	23.700	50.755	-27.055	13.077	102.271	0.312	-0.351	
				A2C_8	HCC	13.710	82.147	-68.436	10.364	158.702	0.001	-1.056	
				A2C_8	MCC	13.710	50.755	-37.045	10.556	142.025	0.008	-0.596	
				HCC	MCC	82.147	50.755	31.391	10.731	262.994	0.043	0.355	
c		Relative improvement (%) in the average hit counts – PPO		PPO_16	PPO_32	24.036	11.686	12.350	14.077	81.194	0.900	0.174	Games Howell
				PPO_16	PPO_64	24.036	-1.291	25.326	14.037	80.683	0.470	0.358	
				PPO_16	PPO_8	24.036	49.866	-25.830	25.190	75.516	0.900	-0.204	
				PPO_16	HCC	24.036	82.147	-58.111	14.132	90.262	0.001	-0.658	
				PPO_16	MCC	24.036	50.755	-26.720	14.274	90.898	0.428	-0.318	
				PPO_32	PPO_64	11.686	-1.291	12.977	10.338	97.989	0.783	0.249	
				PPO_32	PPO_64	11.686	49.866	-38.180	23.333	59.662	0.568	-0.325	
				PPO_32	HCC	11.686	82.147	-70.461	10.468	155.189	0.001	-1.076	
				PPO_32	MCC	11.686	50.755	-39.070	10.658	140.107	0.005	-0.622	
				PPO_64	PPO_8	-1.291	49.866	-51.157	23.308	59.445	0.256	-0.436	
				PPO_64	HCC	-1.291	82.147	-83.437	10.414	157.004	0.001	-1.281	
				PPO_64	MCC	-1.291	50.755	-52.046	10.605	141.109	0.001	-0.833	
				PPO_8	HCC	49.866	82.147	-32.280	23.366	60.514	0.712	-0.221	
				PPO_8	MCC	49.866	50.755	-0.889	23.452	61.224	0.900	-0.006	
				HCC	MCC	82.147	50.755	31.391	10.731	262.994	0.043	0.355	
S3	g	Hit Counts	0-5 Minutes	DQN_16	DQN_32	0.560	0.562	-0.002	0.045	-0.054	0.900	-0.005	
				DQN_16	DQN_64	0.560	0.632	-0.072	0.046	-1.567	0.604	-0.150	
				DQN_16	DQN_8	0.560	0.582	-0.022	0.046	-0.472	0.900	-0.045	
				DQN_16	HCC	0.560	0.651	-0.091	0.037	-2.457	0.137	-0.190	

Biological Neurons Vs. Deep Reinforcement Learning

				<i>DQN_16</i>	MCC	0.560	0.716	-0.156	0.039	-3.998	0.001	-0.326	
				<i>DQN_32</i>	<i>DQN_64</i>	0.562	0.632	-0.069	0.044	-1.566	0.605	-0.145	
				<i>DQN_32</i>	<i>DQN_8</i>	0.562	0.582	-0.019	0.045	-0.433	0.900	-0.040	
				<i>DQN_32</i>	HCC	0.562	0.651	-0.088	0.035	-2.522	0.118	-0.184	
				<i>DQN_32</i>	MCC	0.562	0.716	-0.154	0.037	-4.127	0.001	-0.321	
				<i>DQN_64</i>	<i>DQN_8</i>	0.632	0.582	0.050	0.045	1.111	0.867	0.105	
				<i>DQN_64</i>	HCC	0.632	0.651	-0.019	0.036	-0.525	0.900	-0.039	
				<i>DQN_64</i>	MCC	0.632	0.716	-0.084	0.038	-2.220	0.229	-0.176	
				<i>DQN_8</i>	HCC	0.582	0.651	-0.069	0.036	-1.916	0.394	-0.144	
				<i>DQN_8</i>	MCC	0.582	0.716	-0.134	0.038	-3.521	0.006	-0.281	
				HCC	MCC	0.651	0.716	-0.065	0.026	-2.490	0.127	-0.137	
			6-20 Minute s	<i>DQN_16</i>	<i>DQN_32</i>	0.567	0.560	0.007	0.031	0.232	0.900	0.012	
				<i>DQN_16</i>	<i>DQN_64</i>	0.567	0.634	-0.067	0.030	-2.207	0.235	-0.116	
				<i>DQN_16</i>	<i>DQN_8</i>	0.567	0.526	0.041	0.031	1.326	0.743	0.070	
				<i>DQN_16</i>	HCC	0.567	0.854	-0.288	0.025	-11.616	0.001	-0.495	
				<i>DQN_16</i>	MCC	0.567	0.852	-0.286	0.027	-10.708	0.001	-0.492	
				<i>DQN_32</i>	<i>DQN_64</i>	0.560	0.634	-0.074	0.030	-2.442	0.142	-0.128	
				<i>DQN_32</i>	<i>DQN_8</i>	0.560	0.526	0.034	0.031	1.093	0.878	0.058	
				<i>DQN_32</i>	HCC	0.560	0.854	-0.295	0.025	-11.906	0.001	-0.508	
				<i>DQN_32</i>	MCC	0.560	0.852	-0.293	0.027	-10.977	0.001	-0.504	
				<i>DQN_64</i>	<i>DQN_8</i>	0.634	0.526	0.108	0.030	3.555	0.005	0.186	
				<i>DQN_64</i>	HCC	0.634	0.854	-0.220	0.024	-9.087	0.001	-0.380	
				<i>DQN_64</i>	MCC	0.634	0.852	-0.218	0.026	-8.335	0.001	-0.376	
				<i>DQN_8</i>	HCC	0.526	0.854	-0.328	0.025	-13.309	0.001	-0.566	
				<i>DQN_8</i>	MCC	0.526	0.852	-0.326	0.027	-12.274	0.001	-0.562	
				HCC	MCC	0.854	0.852	0.002	0.019	0.103	0.900	0.003	
	h	% Aces	0-5 Minute s	<i>DQN_16</i>	<i>DQN_32</i>	53.103	58.358	-5.255	2.638	-1.992	0.349	-0.395	Tukey's
				<i>DQN_16</i>	<i>DQN_64</i>	53.103	54.163	-1.061	2.638	-0.402	0.900	-0.080	
				<i>DQN_16</i>	<i>DQN_8</i>	53.103	56.084	-2.981	2.638	-1.130	0.856	-0.224	
				<i>DQN_16</i>	HCC	53.103	54.382	-1.279	2.117	-0.604	0.900	-0.097	

Biological Neurons Vs. Deep Reinforcement Learning

				<i>DQN_16</i>	MCC	53.103	53.333	-0.230	2.250	-0.102	0.900	-0.017	
				<i>DQN_32</i>	<i>DQN_64</i>	58.358	54.163	4.194	2.638	1.590	0.591	0.316	
				<i>DQN_32</i>	<i>DQN_8</i>	58.358	56.084	2.274	2.638	0.862	0.900	0.171	
				<i>DQN_32</i>	HCC	58.358	54.382	3.976	2.117	1.879	0.419	0.300	
				<i>DQN_32</i>	MCC	58.358	53.333	5.025	2.250	2.234	0.224	0.379	
				<i>DQN_64</i>	<i>DQN_8</i>	54.163	56.084	-1.921	2.638	-0.728	0.900	-0.145	
				<i>DQN_64</i>	HCC	54.163	54.382	-0.219	2.117	-0.103	0.900	-0.017	
				<i>DQN_64</i>	MCC	54.163	53.333	0.831	2.250	0.369	0.900	0.063	
				<i>DQN_8</i>	HCC	56.084	54.382	1.702	2.117	0.804	0.900	0.129	
				<i>DQN_8</i>	MCC	56.084	53.333	2.751	2.250	1.223	0.802	0.208	
					HCC	MCC	54.382	53.333	1.049	1.607	0.653	0.900	0.079
			6-20 Minute s	<i>DQN_16</i>	<i>DQN_32</i>	56.069	55.545	0.524	1.744	0.300	0.900	0.060	
				<i>DQN_16</i>	<i>DQN_64</i>	56.069	55.105	0.964	1.744	0.553	0.900	0.110	
				<i>DQN_16</i>	<i>DQN_8</i>	56.069	59.565	-3.496	1.744	-2.004	0.341	-0.398	
				<i>DQN_16</i>	HCC	56.069	49.259	6.810	1.399	4.866	0.001	0.778	
				<i>DQN_16</i>	MCC	56.069	50.232	5.837	1.488	3.924	0.001	0.666	
				<i>DQN_32</i>	<i>DQN_64</i>	55.545	55.105	0.440	1.744	0.252	0.900	0.050	
				<i>DQN_32</i>	<i>DQN_8</i>	55.545	59.565	-4.020	1.744	-2.305	0.194	-0.457	
				<i>DQN_32</i>	HCC	55.545	49.259	6.286	1.399	4.491	0.001	0.718	
				<i>DQN_32</i>	MCC	55.545	50.232	5.313	1.488	3.572	0.005	0.606	
				<i>DQN_64</i>	<i>DQN_8</i>	55.105	59.565	-4.460	1.744	-2.557	0.110	-0.507	
				<i>DQN_64</i>	HCC	55.105	49.259	5.846	1.399	4.177	0.001	0.668	
				<i>DQN_64</i>	MCC	55.105	50.232	4.873	1.488	3.276	0.014	0.556	
				<i>DQN_8</i>	HCC	59.565	49.259	10.306	1.399	7.364	0.001	1.178	
				<i>DQN_8</i>	MCC	59.565	50.232	9.334	1.488	6.274	0.001	1.065	
					HCC	MCC	49.259	50.232	-0.973	1.062	-0.915	0.900	-0.111
i	% Long Rally		0-5 Minute s	<i>DQN_16</i>	<i>DQN_32</i>	7.882	4.460	3.422	1.409	2.428	0.148	0.482	Tukey's
				<i>DQN_16</i>	<i>DQN_64</i>	7.882	7.083	0.798	1.409	0.567	0.900	0.112	
				<i>DQN_16</i>	<i>DQN_8</i>	7.882	6.948	0.933	1.409	0.662	0.900	0.131	
				<i>DQN_16</i>	HCC	7.882	4.523	3.359	1.130	2.972	0.037	0.475	
				<i>DQN_16</i>	MCC	7.882	7.318	0.563	1.202	0.469	0.900	0.080	
				<i>DQN_32</i>	<i>DQN_64</i>	4.460	7.083	-2.623	1.409	-1.862	0.429	-0.370	
				<i>DQN_32</i>	<i>DQN_8</i>	4.460	6.948	-2.488	1.409	-1.766	0.489	-0.350	
				<i>DQN_32</i>	HCC	4.460	4.523	-0.063	1.130	-0.055	0.900	-0.009	
				<i>DQN_32</i>	MCC	4.460	7.318	-2.858	1.202	-2.379	0.166	-0.404	
				<i>DQN_64</i>	<i>DQN_8</i>	7.083	6.948	0.135	1.409	0.096	0.900	0.019	

Biological Neurons Vs. Deep Reinforcement Learning

				<i>DQN_64</i>	HCC	7.083	4.523	2.561	1.130	2.265	0.210	0.362	
				<i>DQN_64</i>	MCC	7.083	7.318	-0.235	1.202	-0.195	0.900	-0.033	
				<i>DQN_8</i>	HCC	6.948	4.523	2.426	1.130	2.146	0.266	0.343	
				<i>DQN_8</i>	MCC	6.948	7.318	-0.370	1.202	-0.308	0.900	-0.052	
				HCC	MCC	4.523	7.318	-2.796	0.858	-3.258	0.015	-0.396	
			6-20 Minute s	<i>DQN_16</i>	<i>DQN_32</i>	6.138	6.310	-0.172	0.929	-0.185	0.900	-0.037	
				<i>DQN_16</i>	<i>DQN_64</i>	6.138	6.916	-0.777	0.929	-0.837	0.900	-0.166	
				<i>DQN_16</i>	<i>DQN_8</i>	6.138	6.221	-0.083	0.929	-0.089	0.900	-0.018	
				<i>DQN_16</i>	HCC	6.138	10.365	-4.226	0.746	-5.668	0.001	-0.906	
				<i>DQN_16</i>	MCC	6.138	11.972	-5.834	0.793	-7.361	0.001	-1.250	
				<i>DQN_32</i>	<i>DQN_64</i>	6.310	6.916	-0.605	0.929	-0.651	0.900	-0.129	
				<i>DQN_32</i>	<i>DQN_8</i>	6.310	6.221	0.090	0.929	0.096	0.900	0.019	
				<i>DQN_32</i>	HCC	6.310	10.365	-4.054	0.746	-5.438	0.001	-0.870	
				<i>DQN_32</i>	MCC	6.310	11.972	-5.662	0.793	-7.144	0.001	-1.213	
				<i>DQN_64</i>	<i>DQN_8</i>	6.916	6.221	0.695	0.929	0.748	0.900	0.148	
				<i>DQN_64</i>	HCC	6.916	10.365	-3.449	0.746	-4.626	0.001	-0.740	
				<i>DQN_64</i>	MCC	6.916	11.972	-5.057	0.793	-6.380	0.001	-1.083	
				<i>DQN_8</i>	HCC	6.221	10.365	-4.144	0.746	-5.558	0.001	-0.889	
				<i>DQN_8</i>	MCC	6.221	11.972	-5.751	0.793	-7.257	0.001	-1.232	
				S4	g	Hit Counts	0-5 Minute s	<i>A2C_16</i>	<i>A2C_32</i>	0.629	0.730	-0.101	
<i>A2C_16</i>	<i>A2C_64</i>	0.629	0.638					-0.009	0.044	-0.208	0.900	-0.019	
<i>A2C_16</i>	<i>A2C_8</i>	0.629	0.655					-0.026	0.044	-0.594	0.900	-0.056	
<i>A2C_16</i>	HCC	0.629	0.651					-0.021	0.035	-0.611	0.900	-0.045	
<i>A2C_16</i>	MCC	0.629	0.716					-0.087	0.037	-2.326	0.184	-0.184	
<i>A2C_32</i>	<i>A2C_64</i>	0.730	0.638					0.092	0.043	2.115	0.280	0.195	
<i>A2C_32</i>	<i>A2C_8</i>	0.730	0.655					0.075	0.044	1.710	0.521	0.158	
<i>A2C_32</i>	HCC	0.730	0.651					0.080	0.035	2.302	0.193	0.169	
<i>A2C_32</i>	MCC	0.730	0.716					0.014	0.037	0.386	0.900	0.030	
<i>A2C_64</i>	<i>A2C_8</i>	0.638	0.655					-0.017	0.044	-0.390	0.900	-0.036	
<i>A2C_64</i>	HCC	0.638	0.651					-0.012	0.035	-0.355	0.900	-0.026	
<i>A2C_64</i>	MCC	0.638	0.716					-0.078	0.037	-2.104	0.286	-0.165	
<i>A2C_8</i>	HCC	0.655	0.651					0.005	0.035	0.136	0.900	0.010	
<i>A2C_8</i>	MCC	0.655	0.716					-0.061	0.037	-1.626	0.570	-0.128	
HCC	MCC	0.651	0.716					-0.065	0.026	-2.523	0.118	-0.139	
<i>A2C_16</i>	<i>A2C_32</i>	0.605	0.705					-0.100	0.031	-3.254	0.015	-0.173	

Biological Neurons Vs. Deep Reinforcement Learning

		6-20 Minute s	A2C_16	A2C_64	0.605	0.622	-0.017	0.031	-0.541	0.900	-0.029	
			A2C_16	A2C_8	0.605	0.597	0.008	0.031	0.256	0.900	0.014	
			A2C_16	HCC	0.605	0.854	-0.250	0.025	-9.962	0.001	-0.430	
			A2C_16	MCC	0.605	0.852	-0.248	0.027	-9.188	0.001	-0.426	
			A2C_32	A2C_64	0.705	0.622	0.083	0.031	2.735	0.069	0.144	
			A2C_32	A2C_8	0.705	0.597	0.108	0.031	3.526	0.006	0.186	
			A2C_32	HCC	0.705	0.854	-0.149	0.024	-6.122	0.001	-0.257	
			A2C_32	MCC	0.705	0.852	-0.147	0.026	-5.595	0.001	-0.254	
			A2C_64	A2C_8	0.622	0.597	0.025	0.031	0.801	0.900	0.043	
			A2C_64	HCC	0.622	0.854	-0.233	0.025	-9.427	0.001	-0.401	
			A2C_64	MCC	0.622	0.852	-0.231	0.027	-8.673	0.001	-0.397	
			A2C_8	HCC	0.597	0.854	-0.258	0.025	-10.339	0.001	-0.444	
			A2C_8	MCC	0.597	0.852	-0.256	0.027	-9.531	0.001	-0.440	
			HCC	MCC	0.854	0.852	0.002	0.019	0.103	0.900	0.003	
h	% Aces	0-5 Minute s	A2C_16	A2C_32	53.810	54.083	-0.272	2.370	-0.115	0.900	-0.023	Tukey's
			A2C_16	A2C_64	53.810	53.299	0.511	2.370	0.216	0.900	0.043	
			A2C_16	A2C_8	53.810	52.332	1.478	2.370	0.624	0.900	0.124	
			A2C_16	HCC	53.810	54.382	-0.571	1.901	-0.301	0.900	-0.048	
			A2C_16	MCC	53.810	53.333	0.478	2.021	0.236	0.900	0.040	
			A2C_32	A2C_64	54.083	53.299	0.783	2.370	0.331	0.900	0.066	
			A2C_32	A2C_8	54.083	52.332	1.750	2.370	0.738	0.900	0.147	
			A2C_32	HCC	54.083	54.382	-0.299	1.901	-0.157	0.900	-0.025	
			A2C_32	MCC	54.083	53.333	0.750	2.021	0.371	0.900	0.063	
			A2C_64	A2C_8	53.299	52.332	0.967	2.370	0.408	0.900	0.081	
			A2C_64	HCC	53.299	54.382	-1.083	1.901	-0.569	0.900	-0.091	
			A2C_64	MCC	53.299	53.333	-0.034	2.021	-0.017	0.900	-0.003	
			A2C_8	HCC	52.332	54.382	-2.049	1.901	-1.078	0.886	-0.172	
			A2C_8	MCC	52.332	53.333	-1.000	2.021	-0.495	0.900	-0.084	
		HCC	MCC	54.382	53.333	1.049	1.443	0.727	0.900	0.088		
		6-20 Minute s	A2C_16	A2C_32	53.076	52.170	0.906	1.627	0.557	0.900	0.110	
			A2C_16	A2C_64	53.076	52.981	0.094	1.627	0.058	0.900	0.012	
			A2C_16	A2C_8	53.076	54.117	-1.042	1.627	-0.640	0.900	-0.127	
			A2C_16	HCC	53.076	49.259	3.816	1.305	2.924	0.042	0.468	
			A2C_16	MCC	53.076	50.232	2.844	1.388	2.049	0.316	0.348	
			A2C_32	A2C_64	52.170	52.981	-0.811	1.627	-0.499	0.900	-0.099	
			A2C_32	A2C_8	52.170	54.117	-1.947	1.627	-1.197	0.817	-0.238	
A2C_32	HCC		52.170	49.259	2.911	1.305	2.230	0.226	0.357			
A2C_32	MCC		52.170	50.232	1.938	1.388	1.397	0.702	0.237			
A2C_64	A2C_8		52.981	54.117	-1.136	1.627	-0.698	0.900	-0.139			

Biological Neurons Vs. Deep Reinforcement Learning

				A2C_64	HCC	52.981	49.259	3.722	1.305	2.851	0.051	0.456				
				A2C_64	MCC	52.981	50.232	2.749	1.388	1.981	0.355	0.336				
				A2C_8	HCC	54.117	49.259	4.858	1.305	3.721	0.003	0.595				
				A2C_8	MCC	54.117	50.232	3.885	1.388	2.800	0.059	0.475				
				HCC	MCC	49.259	50.232	-0.973	0.991	-0.981	0.900	-0.119				
i	% Long Rally	0-5 Minute s	A2C_16	A2C_32	5.395	6.147	-0.752	1.314	-0.572	0.900	-0.114		Tukey's			
			A2C_16	A2C_64	5.395	6.973	-1.578	1.314	-1.201	0.815	-0.238					
			A2C_16	A2C_8	5.395	5.357	0.038	1.314	0.029	0.900	0.006					
			A2C_16	HCC	5.395	4.523	0.872	1.054	0.828	0.900	0.132					
			A2C_16	MCC	5.395	7.318	-1.923	1.120	-1.717	0.518	-0.291					
			A2C_32	A2C_64	6.147	6.973	-0.826	1.314	-0.629	0.900	-0.125					
			A2C_32	A2C_8	6.147	5.357	0.790	1.314	0.602	0.900	0.119					
			A2C_32	HCC	6.147	4.523	1.624	1.054	1.541	0.619	0.246					
			A2C_32	MCC	6.147	7.318	-1.171	1.120	-1.045	0.900	-0.177					
			A2C_64	A2C_8	6.973	5.357	1.617	1.314	1.231	0.798	0.244					
			A2C_64	HCC	6.973	4.523	2.451	1.054	2.325	0.186	0.372					
			A2C_64	MCC	6.973	7.318	-0.345	1.120	-0.308	0.900	-0.052					
			A2C_8	HCC	5.357	4.523	0.834	1.054	0.791	0.900	0.127					
			A2C_8	MCC	5.357	7.318	-1.962	1.120	-1.751	0.498	-0.297					
			HCC	MCC	4.523	7.318	-2.796	0.800	-3.494	0.007	-0.424					
					6-20 Minute s	A2C_16	A2C_32	6.077	7.705	-1.628	0.942	-1.727		0.512	-0.343	
						A2C_16	A2C_64	6.077	6.942	-0.865	0.942	-0.917		0.900	-0.182	
						A2C_16	A2C_8	6.077	6.231	-0.154	0.942	-0.163		0.900	-0.032	
				A2C_16		HCC	6.077	10.365	-4.287	0.756	-5.671	0.001		-0.907		
				A2C_16		MCC	6.077	11.972	-5.895	0.804	-7.336	0.001		-1.245		
				A2C_32		A2C_64	7.705	6.942	0.763	0.942	0.810	0.900		0.161		
				A2C_32		A2C_8	7.705	6.231	1.474	0.942	1.564	0.606		0.310		
				A2C_32		HCC	7.705	10.365	-2.660	0.756	-3.518	0.006		-0.563		
				A2C_32		MCC	7.705	11.972	-4.267	0.804	-5.310	0.001		-0.901		
				A2C_64		A2C_8	6.942	6.231	0.711	0.942	0.754	0.900		0.150		
				A2C_64	HCC	6.942	10.365	-3.423	0.756	-4.528	0.001	-0.724				
		A2C_64	MCC	6.942	11.972	-5.030	0.804	-6.260	0.001	-1.063						
		A2C_8	HCC	6.231	10.365	-4.134	0.756	-5.468	0.001	-0.874						
		A2C_8	MCC	6.231	11.972	-5.741	0.804	-7.144	0.001	-1.213						
		HCC	MCC	10.365	11.972	-1.608	0.574	-2.801	0.059	-0.340						

Biological Neurons Vs. Deep Reinforcement Learning

S5	g	Hit Counts	0-5 Minute s	<i>PPO_16</i>	<i>PPO_32</i>	0.557	0.555	0.002	0.044	0.035	0.900	0.003	Tukey's
				<i>PPO_16</i>	<i>PPO_64</i>	0.557	0.632	-0.075	0.044	-1.684	0.537	-0.159	
				<i>PPO_16</i>	<i>PPO_8</i>	0.557	0.552	0.005	0.045	0.121	0.900	0.011	
				<i>PPO_16</i>	HCC	0.557	0.651	-0.094	0.035	-2.639	0.088	-0.199	
				<i>PPO_16</i>	MCC	0.557	0.716	-0.159	0.038	-4.227	0.001	-0.338	
				<i>PPO_32</i>	<i>PPO_64</i>	0.555	0.632	-0.076	0.044	-1.734	0.508	-0.162	
				<i>PPO_32</i>	<i>PPO_64</i>	0.555	0.552	0.004	0.044	0.088	0.900	0.008	
				<i>PPO_32</i>	HCC	0.555	0.651	-0.095	0.035	-2.720	0.072	-0.202	
				<i>PPO_32</i>	MCC	0.555	0.716	-0.161	0.037	-4.322	0.001	-0.341	
				<i>PPO_64</i>	<i>PPO_8</i>	0.632	0.552	0.080	0.044	1.816	0.457	0.171	
				<i>PPO_64</i>	HCC	0.632	0.651	-0.019	0.035	-0.536	0.900	-0.040	
				<i>PPO_64</i>	MCC	0.632	0.716	-0.084	0.037	-2.262	0.210	-0.179	
				<i>PPO_8</i>	HCC	0.552	0.651	-0.099	0.035	-2.816	0.055	-0.211	
				<i>PPO_8</i>	MCC	0.552	0.716	-0.164	0.037	-4.405	0.001	-0.350	
				HCC	MCC	0.651	0.716	-0.065	0.026	-2.532	0.115	-0.139	
			6-20 Minute s	<i>PPO_16</i>	<i>PPO_32</i>	0.508	0.523	-0.015	0.030	-0.486	0.900	-0.026	
				<i>PPO_16</i>	<i>PPO_64</i>	0.508	0.513	-0.005	0.030	-0.160	0.900	-0.008	
				<i>PPO_16</i>	<i>PPO_8</i>	0.508	0.556	-0.048	0.030	-1.579	0.597	-0.083	
				<i>PPO_16</i>	HCC	0.508	0.854	-0.347	0.024	-14.206	0.001	-0.607	
				<i>PPO_16</i>	MCC	0.508	0.852	-0.345	0.026	-13.114	0.001	-0.603	
				<i>PPO_32</i>	<i>PPO_64</i>	0.523	0.513	0.010	0.030	0.328	0.900	0.017	
				<i>PPO_32</i>	<i>PPO_64</i>	0.523	0.556	-0.033	0.030	-1.090	0.880	-0.058	
				<i>PPO_32</i>	HCC	0.523	0.854	-0.332	0.024	-13.615	0.001	-0.581	
				<i>PPO_32</i>	MCC	0.523	0.852	-0.330	0.026	-12.563	0.001	-0.577	
				<i>PPO_64</i>	<i>PPO_8</i>	0.513	0.556	-0.043	0.030	-1.424	0.687	-0.075	
				<i>PPO_64</i>	HCC	0.513	0.854	-0.342	0.024	-14.092	0.001	-0.598	
				<i>PPO_64</i>	MCC	0.513	0.852	-0.340	0.026	-12.997	0.001	-0.595	
				<i>PPO_8</i>	HCC	0.556	0.854	-0.299	0.024	-12.406	0.001	-0.523	
				<i>PPO_8</i>	MCC	0.556	0.852	-0.297	0.026	-11.422	0.001	-0.520	

Biological Neurons Vs. Deep Reinforcement Learning

			HCC	MCC	0.854	0.852	0.002	0.019	0.104	0.900	0.003	
h	% Aces	0-5 Minutes	PPO_16	PPO_32	59.143	59.654	-0.511	2.553	-0.200	0.900	-0.040	Tukey's
			PPO_16	PPO_64	59.143	55.534	3.610	2.553	1.414	0.692	0.281	
			PPO_16	PPO_8	59.143	58.904	0.239	2.553	0.094	0.900	0.019	
			PPO_16	HCC	59.143	54.382	4.762	2.048	2.325	0.186	0.372	
			PPO_16	MCC	59.143	53.333	5.811	2.177	2.669	0.084	0.453	
			PPO_32	PPO_64	59.654	55.534	4.120	2.553	1.614	0.577	0.320	
			PPO_32	PPO_64	59.654	58.904	0.750	2.553	0.294	0.900	0.058	
			PPO_32	HCC	59.654	54.382	5.273	2.048	2.575	0.106	0.412	
			PPO_32	MCC	59.654	53.333	6.322	2.177	2.904	0.044	0.493	
			PPO_64	PPO_8	55.534	58.904	-3.370	2.553	-1.320	0.746	-0.262	
			PPO_64	HCC	55.534	54.382	1.152	2.048	0.563	0.900	0.090	
			PPO_64	MCC	55.534	53.333	2.201	2.177	1.011	0.900	0.172	
			PPO_8	HCC	58.904	54.382	4.522	2.048	2.208	0.236	0.353	
			PPO_8	MCC	58.904	53.333	5.571	2.177	2.559	0.110	0.434	
		HCC	MCC	54.382	53.333	1.049	1.555	0.675	0.900	0.082		
		6-20 Minutes	PPO_16	PPO_32	60.504	60.595	-0.091	1.900	-0.048	0.900	-0.010	
			PPO_16	PPO_64	60.504	60.941	-0.438	1.900	-0.230	0.900	-0.046	
			PPO_16	PPO_8	60.504	58.316	2.187	1.900	1.151	0.844	0.228	
			PPO_16	HCC	60.504	49.259	11.24 4	1.524	7.376	0.001	1.180	
			PPO_16	MCC	60.504	50.232	10.27 2	1.620	6.339	0.001	1.076	
			PPO_32	PPO_64	60.595	60.941	-0.347	1.900	-0.182	0.900	-0.036	
			PPO_32	PPO_64	60.595	58.316	2.279	1.900	1.199	0.816	0.238	
			PPO_32	HCC	60.595	49.259	11.33 5	1.524	7.436	0.001	1.189	
			PPO_32	MCC	60.595	50.232	10.36 3	1.620	6.395	0.001	1.086	
			PPO_64	PPO_8	60.941	58.316	2.625	1.900	1.382	0.711	0.274	
			PPO_64	HCC	60.941	49.259	11.68 2	1.524	7.663	0.001	1.225	
PPO_64	MCC		60.941	50.232	10.70 9	1.620	6.609	0.001	1.122			
PPO_8	HCC	58.316	49.259	9.057	1.524	5.941	0.001	0.950				
PPO_8	MCC	58.316	50.232	8.084	1.620	4.989	0.001	0.847				
HCC	MCC	49.259	50.232	-0.973	1.157	-0.840	0.900	-0.102				
i	% Long Rally	0-5 Minutes	PPO_16	PPO_32	4.885	5.501	-0.616	1.359	-0.453	0.900	-0.090	Tukey's
			PPO_16	PPO_64	4.885	7.393	-2.508	1.359	-1.845	0.439	-0.366	
			PPO_16	PPO_8	4.885	6.020	-1.135	1.359	-0.835	0.900	-0.166	
			PPO_16	HCC	4.885	4.523	0.362	1.090	0.332	0.900	0.053	

Biological Neurons Vs. Deep Reinforcement Learning

				PPO_16	MCC	4.885	7.318	-2.433	1.159	-2.099	0.290	-0.356
				PPO_32	PPO_64	5.501	7.393	-1.892	1.359	-1.392	0.705	-0.276
				PPO_32	PPO_64	5.501	6.020	-0.519	1.359	-0.382	0.900	-0.076
				PPO_32	HCC	5.501	4.523	0.979	1.090	0.897	0.900	0.144
				PPO_32	MCC	5.501	7.318	-1.817	1.159	-1.568	0.604	-0.266
				PPO_64	PPO_8	7.393	6.020	1.373	1.359	1.010	0.900	0.201
				PPO_64	HCC	7.393	4.523	2.871	1.090	2.633	0.091	0.421
				PPO_64	MCC	7.393	7.318	0.075	1.159	0.065	0.900	0.011
				PPO_8	HCC	6.020	4.523	1.497	1.090	1.373	0.716	0.220
				PPO_8	MCC	6.020	7.318	-1.298	1.159	-1.120	0.862	-0.190
				HCC	MCC	4.523	7.318	-2.796	0.828	-3.377	0.010	-0.410
			6-20 Minute s	PPO_16	PPO_32	6.008	5.224	0.784	0.871	0.900	0.900	0.179
				PPO_16	PPO_64	6.008	5.339	0.669	0.871	0.769	0.900	0.153
				PPO_16	PPO_8	6.008	6.234	-0.226	0.871	-0.260	0.900	-0.052
				PPO_16	HCC	6.008	10.365	-4.357	0.699	-6.237	0.001	-0.997
				PPO_16	MCC	6.008	11.972	-5.964	0.743	-8.032	0.001	-1.363
				PPO_32	PPO_64	5.224	5.339	-0.114	0.871	-0.131	0.900	-0.026
				PPO_32	PPO_64	5.224	6.234	-1.010	0.871	-1.160	0.839	-0.230
				PPO_32	HCC	5.224	10.365	-5.140	0.699	-7.358	0.001	-1.177
				PPO_32	MCC	5.224	11.972	-6.748	0.743	-9.088	0.001	-1.543
				PPO_64	PPO_8	5.339	6.234	-0.896	0.871	-1.029	0.900	-0.204
				PPO_64	HCC	5.339	10.365	-5.026	0.699	-7.195	0.001	-1.151
				PPO_64	MCC	5.339	11.972	-6.634	0.743	-8.934	0.001	-1.517
				PPO_8	HCC	6.234	10.365	-4.130	0.699	-5.913	0.001	-0.946
				PPO_8	MCC	6.234	11.972	-5.738	0.743	-7.728	0.001	-1.312
				HCC	MCC	10.365	11.972	-1.608	0.530	-3.031	0.031	-0.368
S6	g	Hit Counts	0-5 Minute s	A2C	DQN	0.771	0.717	0.054	0.028	1.937	0.298	0.103
				A2C	HCC	0.771	0.651	0.121	0.027	4.508	0.001	0.229
				A2C	MCC	0.771	0.716	0.055	0.030	1.827	0.359	0.105
				A2C	PPO	0.771	0.698	0.073	0.028	2.594	0.072	0.139
				DQN	HCC	0.717	0.651	0.066	0.027	2.476	0.096	0.126
				DQN	MCC	0.717	0.716	0.001	0.030	0.025	0.900	0.001
				DQN	PPO	0.717	0.698	0.019	0.028	0.668	0.900	0.036
				HCC	MCC	0.651	0.716	-0.065	0.029	-2.263	0.157	-0.124
				HCC	PPO	0.651	0.698	-0.047	0.027	-1.760	0.399	-0.090
				MCC	PPO	0.716	0.698	0.018	0.030	0.598	0.900	0.034
			6-20 Minute s	A2C	DQN	0.777	0.762	0.016	0.018	0.866	0.900	0.026
				A2C	HCC	0.777	0.854	-0.077	0.018	-4.329	0.001	-0.127
				A2C	MCC	0.777	0.852	-0.075	0.021	-3.647	0.002	-0.124
				A2C	PPO	0.777	0.712	0.065	0.018	3.561	0.003	0.108
												Tukey's

Biological Neurons Vs. Deep Reinforcement Learning

				DQN	HCC	0.762	0.854	-0.093	0.018	-5.262	0.001	-0.153	
				DQN	MCC	0.762	0.852	-0.091	0.020	-4.442	0.001	-0.150	
				DQN	PPO	0.762	0.712	0.049	0.018	2.723	0.051	0.082	
				HCC	MCC	0.854	0.852	0.002	0.020	0.099	0.900	0.003	
				HCC	PPO	0.854	0.712	0.142	0.018	8.009	0.001	0.235	
				MCC	PPO	0.852	0.712	0.140	0.021	6.825	0.001	0.232	
h	% Aces	0-5 Minute s	A2C	DQN	53.293	52.579	0.714	1.455	0.491	0.900	0.057	Tukey's	
			A2C	HCC	53.293	54.382	-1.089	1.404	-0.776	0.900	-0.086		
			A2C	MCC	53.293	53.333	-0.040	1.582	-0.025	0.900	-0.003		
			A2C	PPO	53.293	54.248	-0.956	1.455	-0.657	0.900	-0.076		
			DQN	HCC	52.579	54.382	-1.803	1.404	-1.284	0.677	-0.143		
			DQN	MCC	52.579	53.333	-0.754	1.582	-0.477	0.900	-0.060		
			DQN	PPO	52.579	54.248	-1.670	1.455	-1.147	0.754	-0.132		
			HCC	MCC	54.382	53.333	1.049	1.535	0.683	0.900	0.083		
			HCC	PPO	54.382	54.248	0.133	1.404	0.095	0.900	0.011		
			MCC	PPO	53.333	54.248	-0.916	1.582	-0.579	0.900	-0.072		
		6-20 Minute s	A2C	DQN	52.530	49.935	2.595	0.959	2.706	0.054	0.312		
			A2C	HCC	52.530	49.259	3.270	0.925	3.535	0.004	0.393		
			A2C	MCC	52.530	50.232	2.298	1.042	2.205	0.179	0.276		
			A2C	PPO	52.530	52.511	0.018	0.959	0.019	0.900	0.002		
			DQN	HCC	49.935	49.259	0.676	0.925	0.730	0.900	0.081		
			DQN	MCC	49.935	50.232	-0.297	1.042	-0.285	0.900	-0.036		
			DQN	PPO	49.935	52.511	-2.576	0.959	-2.687	0.057	-0.310		
			HCC	MCC	49.259	50.232	-0.973	1.011	-0.962	0.860	-0.117		
			HCC	PPO	49.259	52.511	-3.252	0.925	-3.515	0.004	-0.391		
			MCC	PPO	50.232	52.511	-2.280	1.042	-2.187	0.186	-0.274		
i	% Long Rally	0-5 Minute s	A2C	DQN	12.722	10.195	2.527	0.631	4.004	0.001	0.461	Tukey's	
			A2C	HCC	12.722	10.365	2.357	0.609	3.871	0.001	0.430		
			A2C	MCC	12.722	11.972	0.750	0.686	1.093	0.785	0.137		
			A2C	PPO	12.722	10.183	2.540	0.631	4.024	0.001	0.463		
			DQN	HCC	10.195	10.365	-0.169	0.609	-0.278	0.900	-0.031		
			DQN	MCC	10.195	11.972	-1.777	0.686	-2.590	0.073	-0.324		
			DQN	PPO	10.195	10.183	0.013	0.631	0.020	0.900	0.002		
			HCC	MCC	10.365	11.972	-1.608	0.666	-2.415	0.113	-0.293		
			HCC	PPO	10.365	10.183	0.182	0.609	0.299	0.900	0.033		
			MCC	PPO	11.972	10.183	1.790	0.686	2.609	0.070	0.327		
		6-20 Minute s	A2C	DQN	11.266	9.629	1.637	0.589	2.777	0.044	0.226		
			A2C	HCC	11.266	7.444	3.823	0.569	6.721	0.001	0.529		
			A2C	MCC	11.266	9.645	1.621	0.641	2.530	0.085	0.224		
			A2C	PPO	11.266	9.793	1.474	0.589	2.500	0.091	0.204		
			DQN	HCC	9.629	7.444	2.186	0.569	3.843	0.001	0.302		
			DQN	MCC	9.629	9.645	-0.016	0.641	-0.025	0.900	-0.002		
			DQN	PPO	9.629	9.793	-0.163	0.589	-0.277	0.900	-0.023		
			HCC	MCC	7.444	9.645	-2.202	0.622	-3.540	0.004	-0.305		
			HCC	PPO	7.444	9.793	-2.349	0.569	-4.130	0.001	-0.325		

Biological Neurons Vs. Deep Reinforcement Learning

p	Hit Counts	0-5 Minutes	MCC	PPO	9.645	9.793	-0.147	0.641	-0.230	0.900	-0.020	Tukey's	
			A2C	DQN	0.722	0.719	0.003	0.027	0.124	0.900	0.007		
			A2C	HCC	0.722	0.651	0.072	0.026	2.773	0.044	0.141		
			A2C	MCC	0.722	0.716	0.006	0.029	0.217	0.900	0.012		
			A2C	PPO	0.722	0.740	-0.018	0.027	-0.644	0.900	-0.035		
			DQN	HCC	0.719	0.651	0.068	0.026	2.648	0.062	0.135		
			DQN	MCC	0.719	0.716	0.003	0.029	0.101	0.900	0.006		
			DQN	PPO	0.719	0.740	-0.021	0.027	-0.769	0.900	-0.041		
			HCC	MCC	0.651	0.716	-0.065	0.028	-2.346	0.131	-0.129		
			HCC	PPO	0.651	0.740	-0.089	0.026	-3.444	0.005	-0.176		
		MCC	PPO	0.716	0.740	-0.024	0.029	-0.819	0.900	-0.047			
		6-20 Minutes	A2C	DQN	0.724	0.741	-0.017	0.018	-0.947	0.868	-0.029		
			A2C	HCC	0.724	0.854	-0.131	0.017	-7.488	0.001	-0.220		
			A2C	MCC	0.724	0.852	-0.129	0.020	-6.378	0.001	-0.217		
			A2C	PPO	0.724	0.727	-0.004	0.018	-0.218	0.900	-0.007		
			DQN	HCC	0.741	0.854	-0.114	0.017	-6.567	0.001	-0.192		
			DQN	MCC	0.741	0.852	-0.112	0.020	-5.570	0.001	-0.189		
			DQN	PPO	0.741	0.727	0.013	0.018	0.727	0.900	0.022		
			HCC	MCC	0.854	0.852	0.002	0.020	0.100	0.900	0.003		
			HCC	PPO	0.854	0.727	0.127	0.017	7.259	0.001	0.214		
MCC	PPO		0.852	0.727	0.125	0.020	6.181	0.001	0.211				
q	% Aces	0-5 Minutes	A2C	DQN	51.318	53.675	-2.356	1.437	-1.640	0.473	-0.189	Tukey's	
			A2C	HCC	51.318	54.382	-3.064	1.387	-2.209	0.177	-0.246		
			A2C	MCC	51.318	53.333	-2.014	1.562	-1.289	0.674	-0.161		
			A2C	PPO	51.318	50.866	0.453	1.437	0.315	0.900	0.036		
			DQN	HCC	53.675	54.382	-0.707	1.387	-0.510	0.900	-0.057		
			DQN	MCC	53.675	53.333	0.342	1.562	0.219	0.900	0.027		
			DQN	PPO	53.675	50.866	2.809	1.437	1.955	0.290	0.225		
			HCC	MCC	54.382	53.333	1.049	1.516	0.692	0.900	0.084		
			HCC	PPO	54.382	50.866	3.516	1.387	2.536	0.084	0.282		
			MCC	PPO	53.333	50.866	2.467	1.562	1.579	0.510	0.198		
		6-20 Minutes	A2C	DQN	52.596	51.199	1.397	0.907	1.540	0.532	0.177		
			A2C	HCC	52.596	49.259	3.337	0.875	3.813	0.001	0.424		
			A2C	MCC	52.596	50.232	2.364	0.986	2.398	0.117	0.300		
			A2C	PPO	52.596	51.658	0.938	0.907	1.034	0.818	0.119		
			DQN	HCC	51.199	49.259	1.940	0.875	2.217	0.175	0.246		
			DQN	MCC	51.199	50.232	0.968	0.986	0.981	0.848	0.123		
			DQN	PPO	51.199	51.658	-0.459	0.907	-0.506	0.900	-0.058		
			HCC	MCC	49.259	50.232	-0.973	0.957	-1.017	0.828	-0.124		
			HCC	PPO	49.259	51.658	-2.399	0.875	-2.742	0.049	-0.305		
			MCC	PPO	50.232	51.658	-1.427	0.986	-1.447	0.584	-0.181		
r	% Long Rally	0-5 Minutes	A2C	DQN	9.519	9.710	-0.191	0.965	-0.198	0.900	-0.023	Tukey's	
			A2C	HCC	9.519	4.523	4.997	0.931	5.366	0.001	0.596		
			A2C	MCC	9.519	7.318	2.201	1.049	2.098	0.222	0.263		
			A2C	PPO	9.519	10.462	-0.942	0.965	-0.976	0.851	-0.112		

Biological Neurons Vs. Deep Reinforcement Learning

				DQN	HCC	9.710	4.523	5.188	0.931	5.571	0.001	0.619							
				DQN	MCC	9.710	7.318	2.392	1.049	2.280	0.153	0.285							
				DQN	PPO	9.710	10.462	-0.752	0.965	-0.779	0.900	-0.090							
				HCC	MCC	4.523	7.318	-2.796	1.018	-2.746	0.048	-0.334							
				HCC	PPO	4.523	10.462	-5.939	0.931	-6.378	0.001	-0.709							
				MCC	PPO	7.318	10.462	-3.144	1.049	-2.996	0.024	-0.375							
				6-20 Minute s	A2C	DQN	10.431	10.187	0.244	0.591	0.413	0.900		0.048					
					A2C	HCC	10.431	10.365	0.066	0.570	0.116	0.900		0.013					
					A2C	MCC	10.431	11.972	-1.541	0.642	-2.400	0.117		-0.300					
					A2C	PPO	10.431	10.049	0.382	0.591	0.646	0.900		0.074					
					DQN	HCC	10.187	10.365	-0.178	0.570	-0.312	0.900		-0.035					
					DQN	MCC	10.187	11.972	-1.785	0.642	-2.780	0.044		-0.348					
					DQN	PPO	10.187	10.049	0.138	0.591	0.233	0.900		0.027					
					HCC	MCC	10.365	11.972	-1.608	0.623	-2.579	0.075		-0.313					
					HCC	PPO	10.365	10.049	0.316	0.570	0.554	0.900		0.062					
					MCC	PPO	11.972	10.049	1.923	0.642	2.994	0.024		0.375					
					S7	a	Relative improvement (%) in the average hit counts – Ball Position Input		A2C	DQN	33.724	28.251		5.473	8.669	283.8 06	0.900	0.073	Games Howell
									A2C	HCC	33.724	82.147		-48.42 3	10.07 7	321.8 71	0.001	-0.534	
				A2C					MCC	33.724	50.755	-17.03 1		10.27 4	238.3 11	0.464	-0.207		
A2C	PPO	33.724	33.016	0.709					10.30 1	292.7 92	0.900	0.008							
DQN	HCC	28.251	82.147	-53.89 6					9.206	304.7 84	0.001	-0.651							
DQN	MCC	28.251	50.755	-22.50 5					9.421	205.7 71	0.123	-0.299							
DQN	PPO	28.251	33.016	-4.765					9.450	266.0 29	0.900	-0.058							
HCC	MCC	82.147	50.755	31.39 1					10.73 1	262.9 94	0.030	0.355							
HCC	PPO	82.147	33.016	49.13 1					10.75 6	317.8 52	0.001	0.508							
MCC	PPO	50.755	33.016	17.74 0					10.94 1	252.1 47	0.486	0.203							
b	Relative improvement (%) in the average hit counts – Paddle&Ball Position Input			A2C		DQN	21.717	24.949	-3.232	8.194	291.1 51	0.900	-0.045	Games Howell					
				A2C		HCC	21.717	82.147	-60.42 9	9.165	303.1 51	0.001	-0.733						
				A2C		MCC	21.717	50.755	-29.03 8	9.381	203.8 60	0.019	-0.387						
				A2C		PPO	21.717	14.690	7.027	7.082	292.7 73	0.842	0.114						
				DQN		HCC	24.949	82.147	-57.19 7	9.711	318.5 26	0.001	-0.655						
				DQN		MCC	24.949	50.755	-25.80 6	9.915	226.6 75	0.073	-0.326						
				DQN		PPO	24.949	14.690	10.25 9	7.775	276.1 59	0.657	0.152						
				HCC		MCC	82.147	50.755	31.39 1	10.73 1	262.9 94	0.030	0.355						

Biological Neurons Vs. Deep Reinforcement Learning

				HCC	PPO	82.147	14.690	67.456	8.792	284.259	0.001	0.853	
				MCC	PPO	50.755	14.690	36.065	9.017	184.981	0.001	0.501	
S8	e	Hit Counts	0-5 Minutes	CL(3)	CL(7)	0.696	0.682	0.014	0.050	0.281	0.900	0.027	Tuckey's
				CL(3)	HCC	0.696	0.651	0.045	0.039	1.147	0.641	0.088	
				CL(3)	MCC	0.696	0.716	-0.020	0.042	-0.484	0.900	-0.039	
				CL(7)	HCC	0.682	0.651	0.031	0.039	0.804	0.834	0.061	
				CL(7)	MCC	0.682	0.716	-0.034	0.041	-0.827	0.821	-0.066	
				HCC	MCC	0.651	0.716	-0.065	0.028	-2.318	0.094	-0.127	
			6-20 Minutes	CL(3)	CL(7)	0.703	0.916	-0.213	0.039	-5.439	0.001	-0.336	
				CL(3)	HCC	0.703	0.854	-0.151	0.030	-4.972	0.001	-0.239	
				CL(3)	MCC	0.703	0.852	-0.149	0.032	-4.624	0.001	-0.236	
				CL(7)	HCC	0.916	0.854	0.061	0.030	2.017	0.182	0.097	
				CL(7)	MCC	0.916	0.852	0.063	0.032	1.962	0.203	0.100	
				HCC	MCC	0.854	0.852	0.002	0.021	0.094	0.900	0.003	
	f	%Aces	0-5 Minutes	CL(3)	CL(7)	53.140	54.239	-1.099	2.560	-0.429	0.900	-0.095	
				CL(3)	HCC	53.140	54.382	-1.242	2.008	-0.618	0.900	-0.108	
				CL(3)	MCC	53.140	53.333	-0.192	2.114	-0.091	0.900	-0.017	
				CL(7)	HCC	54.239	54.382	-0.143	2.008	-0.071	0.900	-0.012	
				CL(7)	MCC	54.239	53.333	0.906	2.114	0.429	0.900	0.079	
				HCC	MCC	54.382	53.333	1.049	1.395	0.752	0.863	0.091	
			6-20 Minutes	CL(3)	CL(7)	55.605	47.256	8.349	1.712	4.876	0.001	1.080	
				CL(3)	HCC	55.605	49.259	6.346	1.343	4.726	0.001	0.826	
				CL(3)	MCC	55.605	50.232	5.373	1.414	3.800	0.001	0.698	
				CL(7)	HCC	47.256	49.259	-2.003	1.343	-1.492	0.445	-0.261	
				CL(7)	MCC	47.256	50.232	-2.976	1.414	-2.105	0.154	-0.387	
				HCC	MCC	49.259	50.232	-0.973	0.933	-1.043	0.700	-0.127	
g	%Long Rally	0-5 Minutes	CL(3)	CL(7)	7.692	6.923	0.769	1.432	0.537	0.900	0.119		
			CL(3)	HCC	7.692	4.523	3.170	1.123	2.822	0.026	0.493		
			CL(3)	MCC	7.692	7.318	0.374	1.183	0.316	0.900	0.058		
			CL(7)	HCC	6.923	4.523	2.401	1.123	2.138	0.143	0.373		
			CL(7)	MCC	6.923	7.318	-0.395	1.183	-0.334	0.900	-0.061		
			HCC	MCC	4.523	7.318	-2.796	0.780	-3.583	0.002	-0.435		
		6-20 Minutes	CL(3)	CL(7)	9.292	12.160	-2.868	1.111	-2.582	0.050	-0.572		
			CL(3)	HCC	9.292	10.365	-1.073	0.871	-1.232	0.594	-0.215		
			CL(3)	MCC	9.292	11.972	-2.680	0.917	-2.923	0.019	-0.537		
			CL(7)	HCC	12.160	10.365	1.795	0.871	2.061	0.168	0.360		
			CL(7)	MCC	12.160	11.972	0.187	0.917	0.204	0.900	0.038		
			HCC	MCC	10.365	11.972	-1.608	0.605	-2.657	0.041	-0.323		
h	Relative improvement (%) in the average hit counts – Active Inference		CL(3)	CL(7)	20.341	54.109	-33.768	15.953	-2.117	0.157	-0.469	Games Howell	
			CL(3)	HCC	20.341	82.147	-61.806	14.023	-4.407	0.001	-0.770		
			CL(3)	MCC	20.341	50.755	-30.414	14.165	-2.147	0.148	-0.394		
			CL(7)	HCC	54.109	82.147	-28.038	13.000	-2.157	0.144	-0.377		

				CL(7)	MCC	54.109	50.755	3.353	13.15 4	0.255	0.900	0.047	
				HCC	MCC	82.147	50.755	31.39 1	10.73 1	2.925	0.019	0.355	

Table S3. Multivariate statistical tests and all results for tests done.

Figure	Panel	Parameters	Source	DF1	DF2	MS	F	p-value	np2	Method
2	e	Average Rally Length	Group - all	4	729	0.185	1.021	0.395	0.006	Mixed ANOVA
			Time Interval - all	1	729	2.134	-21.944	1.000	-0.031	
			Interaction - all	4	729	0.575	-5.909	1.000	-0.034	
	f	% Aces	Group - all	4	729	0.044	1.014	0.399	0.006	Mixed ANOVA
			Time Interval - all	1	729	0.124	-5.589	1.000	-0.008	
			Interaction - all	4	729	0.015	-0.685	1.000	-0.004	
	g	% Long Rally	Group - all	4	729	0.019	1.749	0.137	0.010	Mixed ANOVA
			Time Interval - all	1	729	0.063	-11.125	1.000	-0.015	
			Interaction - all	4	729	0.039	-6.931	1.000	-0.040	
3	e	Average Rally Length	Group - all	4	729	0.170	0.926	0.448	0.005	Mixed ANOVA
			Time Intervals - all	1	729	1.488	-15.161	1.000	-0.021	
			Interaction - all	4	729	0.704	-7.170	1.000	-0.041	
	f	% Aces	Group - all	4	729	0.061	1.332	0.256	0.007	Mixed ANOVA
			Time Intervals - all	1	729	0.022	-0.957	1.000	-0.001	
			Interaction - all	4	729	0.041	-1.745	1.000	-0.010	
	g	% Long Rally	Group - all	4	729	0.011	0.886	0.472	0.005	Mixed ANOVA
			Time Intervals - all	1	729	0.073	-11.249	1.000	-0.016	
			Interaction - all	4	729	0.033	-5.038	1.000	-0.028	
4	e	Average Rally Length	Group - all	4	729	0.499	2.589	0.036	0.014	Mixed ANOVA
			Time Intervals- all	1	729	1.934	-18.645	1.000	-0.026	
			Interaction - all	4	729	0.599	-5.774	1.000	-0.033	
	f	% Aces	Group - all	4	729	0.111	2.331	0.055	0.013	Mixed ANOVA
			Time Intervals- all	1	729	0.111	-4.583	1.000	-0.006	
			Interaction - all	4	729	0.021	-0.871	1.000	-0.005	
	g	% Long Rally	Group - all	4	729	0.018	1.523	0.194	0.008	Mixed ANOVA
			Time Intervals - all	1	729	0.081	-12.847	1.000	-0.018	
			Interaction - all	4	729	0.032	-5.057	1.000	-0.029	
S3	d	Average Rally Length	Group - all	5	478	1.645	8.293	0.0	0.080	Mixed ANOVA
			Time Intervals - all	1	478	2.153	-18.414	1.0	-0.040	
			Interaction - all	5	478	0.443	-3.787	1.0	-0.041	
	e	% Aces	Group - all	5	478	0.259	5.194	0.0	0.052	Mixed ANOVA
			Time Intervals - all	1	478	0.059	-2.212	1.0	-0.005	
			Interaction - all	5	478	0.027	-1.008	1.0	-0.011	

Biological Neurons Vs. Deep Reinforcement Learning

S4	f	% Long Rally	Group - all	5	478	0.049	4.611	0.0	0.046	Mixed ANOVA
			Time Intervals - all	1	478	0.113	-18.808	1.0	-0.041	
			Interaction - all	5	478	0.019	-3.197	1.0	-0.035	
	d	Average Rally Length	Group - all	5	478	0.765	4.206	0.001	0.042	Mixed ANOVA
			Time Intervals - all	1	478	1.873	-17.980	1.000	-0.039	
			Interaction - all	5	478	0.502	-4.819	1.000	-0.053	
	e	% Aces	Group - all	5	478	0.060	1.410	0.219	0.015	Mixed ANOVA
			Time Intervals - all	1	478	0.050	-2.277	1.000	-0.005	
			Interaction - all	5	478	0.029	-1.306	1.000	-0.014	
f	% Long Rally	Group - all	5	478	0.032	2.926	0.013	0.030	Mixed ANOVA	
		Time Intervals - all	1	478	0.081	-13.550	1.000	-0.029		
		Interaction - all	5	478	0.026	-4.281	1.000	-0.047		
S5	d	Average Rally Length	Group - all	5	478	2.177	10.721	0.0	0.101	Mixed ANOVA
			Time Intervals - all	1	478	1.503	-12.236	1.0	-0.026	
			Interaction - all	5	478	0.645	-5.254	1.0	-0.058	
	e	% Aces	Group - all	5	478	0.421	7.738	0.0	0.075	Mixed ANOVA
			Time Intervals - all	1	478	0.029	-0.970	1.0	-0.002	
			Interaction - all	5	478	0.046	-1.526	1.0	-0.016	
	f	% Long Rally	Group - all	5	478	0.046	4.651	0.0	0.046	Mixed ANOVA
			Time Intervals - all	1	478	0.095	-16.734	1.0	-0.036	
			Interaction - all	5	478	0.025	-4.406	1.0	-0.048	
S6	d	Average Rally Length	Group - all	4	729	0.260	1.372	0.242	0.007	Mixed ANOVA
			Time Intervals - all	1	729	2.355	-23.160	1.000	-0.033	
			Interaction - all	4	729	0.525	-5.161	1.000	-0.029	
	e	% Aces	Group - all	4	729	0.066	1.445	0.217	0.008	Mixed ANOVA
			Time Intervals - all	1	729	0.141	-5.986	1.000	-0.008	
			Interaction - all	4	729	0.021	-0.897	1.000	-0.005	
	f	% Long Rally	Group - all	4	729	0.017	1.370	0.243	0.007	Mixed ANOVA
			Time Intervals - all	1	729	0.113	-17.552	1.000	-0.025	
			Interaction - all	4	729	0.024	-3.684	1.000	-0.021	
	p	Average Rally Length	Group - all	4	729	0.136	0.756	0.554	0.004	Mixed ANOVA
			Time Intervals - all	1	729	1.690	-17.577	1.000	-0.025	
			Interaction - all	4	729	0.663	-6.889	1.000	-0.039	
	q	% Aces	Group - all	4	729	0.032	0.712	0.584	0.004	Mixed ANOVA
			Time Intervals - all	1	729	0.054	-2.376	1.000	-0.003	
			Interaction - all	4	729	0.042	-1.838	1.000	-0.010	
	r	% Long Rally	Group - all	4	729	0.009	0.763	0.55	0.004	Mixed ANOVA
			Time Intervals - all	1	729	0.073	-11.682	1.00	-0.016	

S8	a	Average Rally Length	Interaction - all	4	729	0.032	-5.152	1.00	-0.029	Mixed ANOVA
			Group - all	3	360	0.160	0.792	0.499	0.007	
			Time Intervals - all	1	360	4.486	-38.506	1.000	-0.120	
	b	% Aces	Group - all	3	360	0.033	0.844	0.471	0.007	Mixed ANOVA
			Time Intervals - all	1	360	0.162	-7.936	1.000	-0.023	
			Interaction - all	3	360	0.031	-1.503	1.000	-0.013	
	c	% Long Rally	Group - all	3	360	0.012	1.004	0.391	0.008	Mixed ANOVA
			Time Intervals - all	1	360	0.234	-36.162	1.000	-0.112	
			Interaction - all	3	360	0.003	-0.517	1.000	-0.004	

Table S4. Multivariate statistical tests and all results for tests done.

Figure	Panel	Parameters	Source	DF	MS	F	p-value	np2	Method
5	a	Average Paddle Movement	Group - all	4	1.064e+10	21.837	0.0	0.155	ANOVA
	b	Relative improvement (%) in the average hit counts	Group - all	4	104528.369	17.807	0.0	0.089	ANOVA
	c	Average Paddle Movement	Group - all	4	1.801e+10	49.523	0.0	0.293	ANOVA
	d	Relative improvement (%) in the average hit counts	Group - all	4	116698.296	16.243	0.0	0.082	ANOVA
	e	Average Paddle Movement	Group - all	4	1.009e+10	26.881	0.0	0.184	ANOVA
	f	Relative improvement (%) in the average hit counts	Group - all	4	79671.720	9.889	0.0	0.051	ANOVA
6	a	Relative improvement (%) in the average hit counts - DQN	Group - all	5	77257.903	10.241	0.0	0.097	ANOVA
	b	Relative improvement (%) in the average hit counts - A2C	Group - all	5	73239.513	11.211	0.0	0.105	ANOVA
	c	Relative improvement (%) in the average hit counts - PPO	Group - all	5	83698.926	9.517	0.0	0.091	ANOVA
S7	a	Relative improvement (%) in the average hit counts - Ball Position Input	Group - all	4	81200.989	10.941	0.0	0.057	ANOVA
	b	Relative improvement (%) in the average hit counts -	Group - all	4	125476.158	20.915	0.0	0.103	ANOVA

Biological Neurons Vs. Deep Reinforcement Learning

		Paddle&Ball Position Input							
S8	d	Relative improvement (%) in the average hit counts – Active Inference	Group - all	3	52072.238	6.733	0.0	0.053	ANOVA